

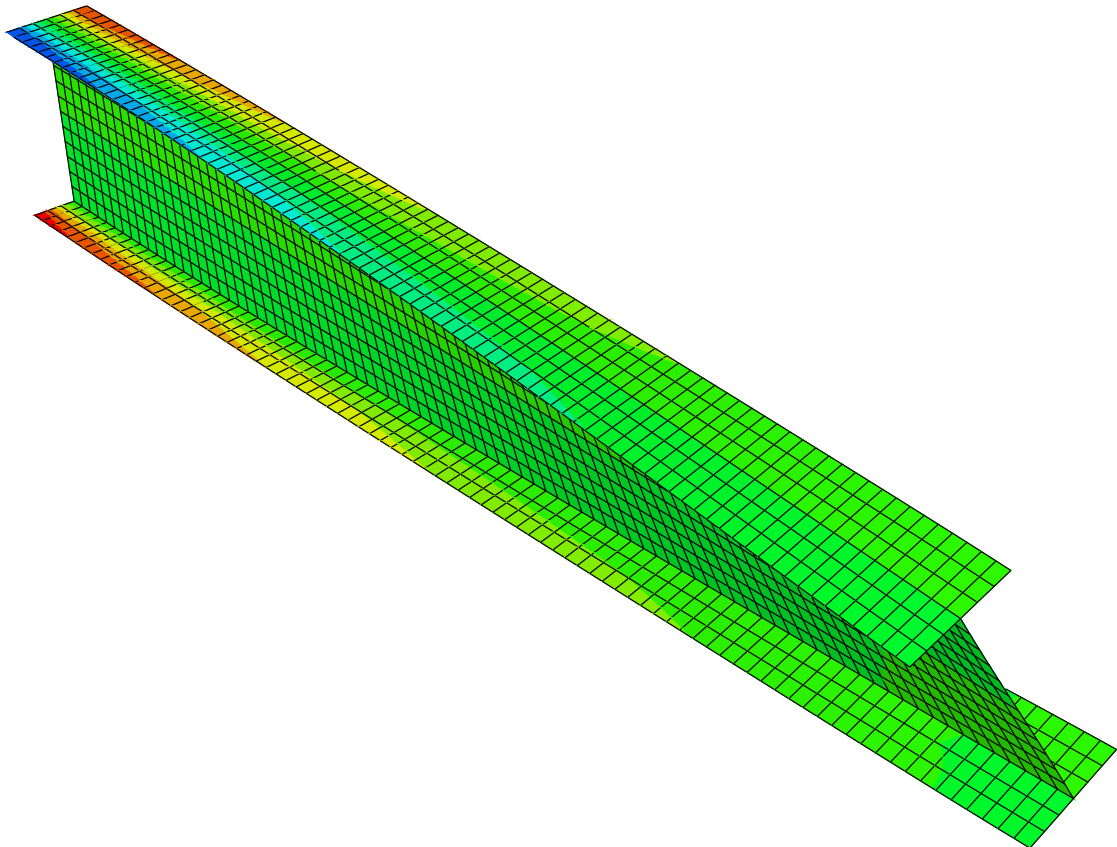
AALBORG UNIVERSITY

---

**WARPING TORSION  
IN  
3D BEAM FINITE ELEMENTS**

---

MASTER'S THESIS, M.Sc. IN STRUCTURAL AND CIVIL ENGINEERING



---

DENNIS N. OLSEN

LYNGE U. ANDERSEN

SCHOOL OF ENGINEERING AND SCIENCE

2015

---

© Aalborg University, spring 2015

Dennis Nedergaard Olsen and Lynge Udengaard Andersen

The content of this report is freely accessible, however publication  
(with source references) is only allowed upon agreement with the authors

This report is typeset in New TX and New TX Math, 11pt  
Layout and typography by the authors using L<sup>A</sup>T<sub>E</sub>X

---



**AALBORG UNIVERSITY**  
STUDENT REPORT

**Master's Thesis, Master of Science**  
**School of Engineering and Science**  
**Study Board of Civil Engineering**

Fibigerstræde 10  
9220 Aalborg East  
<http://www.en.ses.aau.dk/>

**Title:**

Warping Torsion in 3D Beam Finite Elements

**Project period:**

4<sup>th</sup> semester M.Sc, spring 2015

**Supervisor:**

Johan Clausen

**Page numbers:** 56

**Appendix numbers:** 4

**Handed in:** The 10<sup>th</sup> of June 2015

**Synopsis:**

This project deals with torsion both analytically and numerically. The report starts by presenting analytical derivations of spatial beam theory from which everything originates. Torsion can be looked at in two ways, which depend on the support and load condition. Both scenarios, homogeneous torsion and non-homogeneous, are investigated analytically. Furthermore non-homogeneous torsion is analysed numerically in a home-made MATLAB code and compared with results from an advanced numerical commercial software program ABAQUS.

**Participants:**

---

Dennis N. Olsen

---

Lynge U. Andersen



# Preface

---

This report presents the master's thesis of Dennis Nedergaard Olsen and Lyng Udengaard Andersen from the 4<sup>th</sup> semester master program in *Structural and Civil Engineering* at Aalborg University. The main subject is “*Warping Torsion in 3D Beam Finite Elements*” with focus on documentation of beam theory, formulation of torsion, both homogeneous and non-homogeneous, and inclusion of the 7<sup>th</sup> degree of freedom in the beam finite element formulation. Finally a comparison between a home made finite element code in MATLAB and the advanced numerical software program ABAQUS is made in order to verify the correctness of the finite element code.

The project was made during spring semester and delivered on 10.06.2015. Guidance was achieved from supervisor, Associate Professor Johan Clausen, which we are truly grateful for. We would also like to thank the lecturers Jesper W. Stærdahl, Johan Clausen and Lars Andersen for a start-up finite element program, which we were able to build further on to include non-homogeneous torsion.

## Reading Guidelines

The project starts with an introduction, which starts by outlining previous knowledge about the field of torsion followed by a brief research documentation of the problem's severity when looking at I/H-profiles. The introduction concludes by converging into specific areas of interest mentioned above. A theoretical basis is established within the spatial beam theory chapter, presenting analytical solutions for both St. Venant and Vlasov torsion. A basis for the finite element code is presented in the basics of the finite element method chapter. Numerical results of the home-made finite element code in MATLAB and the numerical analysis in the software program ABAQUS are presented in chapter 4 which rounds off the master's thesis along with the conclusion.

References throughout the report are collected in a bibliography at the back of the report, where all the sources of knowledge are mentioned with the needed data. Sources are presented using the Harvard Method, presenting a reference as: [Author, Year].

Tables, pictures and equations are given reference numbers, starting with the number of the chapter. If needed, commentary text is added below figures/tables presenting a more user friendly readable report.



# Contents

---

<b>Preface</b>	<b>iii</b>
Reading Guidelines . . . . .	iii
<b>Notation list</b>	<b>vii</b>
<b>1 Introduction</b>	<b>1</b>
1.1 Objective and scope . . . . .	8
<b>2 Spatial Beam Theory</b>	<b>9</b>
2.1 Equations of Equilibrium . . . . .	9
2.2 Uncoupled System of Equations . . . . .	10
2.3 Internal Forces, Moments and Stresses . . . . .	12
2.4 Deformation, Kinematic and Constitutive Relations . . . . .	12
2.5 Homogeneous Torsion . . . . .	14
2.6 Non-homogeneous Torsion of Open Thin-Walled Cross-Sections . . . . .	21
2.7 Shear stresses due to Bending in Open Thin-Walled Cross-sections . . . . .	24
2.8 Generalised Internal Forces and Stresses . . . . .	25
2.9 Differential Equations . . . . .	29
<b>3 Basics of the Finite Element Method</b>	<b>35</b>
3.1 The Principle of Virtual Displacements . . . . .	35
3.2 Basic Deformation and Shape Functions . . . . .	36
3.3 Stiffness Matrix for a Beam Element . . . . .	38
3.4 System of Equations . . . . .	42
3.5 Coordinate Transformation . . . . .	43
<b>4 Numerical Results and Comparison</b>	<b>45</b>
4.1 ABAQUS Comparison . . . . .	49
<b>5 Conclusion</b>	<b>53</b>
<b>Bibliography</b>	<b>55</b>
<b>Appendix</b>	<b>59</b>
<b>A Analysis of torsional behaviour of I/H-profiles</b>	<b>59</b>
<b>B Shell- and solid model comparison</b>	<b>79</b>
<b>C von Mises Criterion</b>	<b>81</b>

<b>D Exact Non-Homogeneous Shape Functions</b>	<b>83</b>
--	-----------

# Nomenclature

---

$A$	Cross-sectional area	$\mathbf{n}$	Unit normal vector
$b$	Width	$Q$	Shear force
$B$	Bending centre, bimoment	$q$	Uniform distributed load
$B_0$	Concentrated bimoment	$\mathbf{q}$	Vector of uniform distributed loads
$E$	Young's modulus	$r$	Radii of curvature, moment arm
$\mathbf{F}$	Vector of internal forces	$\mathbf{r}$	Vector of internal reaction forces
$G$	Shear modulus	$s$	Arc-length coordinate
$H$	Shear force per unit length	$\mathbf{s}$	Unit tangential vector
$h$	Height	$S$	Shear centre, Prandtl's stress function, statical moment
$\hat{i}$	Unit vector in $x$ -direction	$t$	Thickness
$I$	Moment of inertia	$\mathbf{T}$	Transformation matrix
$\hat{j}$	Unit vector in $y$ -direction	$u$	Displacement
$\mathbf{K}$	Stiffness matrix	$\mathbf{u}$	Vector of displacement field
$\hat{k}$	Unit vector in $z$ -direction	$\mathbf{v}$	Direction vector
$L$	Profile length	$w$	Displacement
$M$	Moment	$\mathbf{w}$	Vector of displacements
$m$	Uniform distributed moment	$W$	Work
$\mathbf{M}$	Vector of internal moments	$x$	$x$ -axis
$\mathbf{m}$	Vector of uniform distributed moments	$y$	$y$ -axis
$M_0$	Concentrated torsional moment	$y_S$	$y$ -distance to shear centre
$N$	Normal force	$z$	$z$ -axis
$n$	Normal arc-length coordinate	$z_S$	$z$ -distance to shear centre

$\alpha_T$	Value contained in hyperbolic stiffness matrix	$\theta$	Rotation
$\beta_T$	Values contained in hyperbolic stiffness matrix	$\boldsymbol{\theta}$	Vector of rotations
$\Gamma$	Closed boundary curve	$\kappa$	Curvature
$\gamma_T$	Values contained in hyperbolic stiffness matrix	$\phi$	Shape function
$\delta$	Virtual	$\Phi$	Matrix containing shape functions
$\delta_T$	Values contained in hyperbolic stiffness matrix	$\sigma$	Stress
$\varepsilon$	Strain	$\tau$	Maximum shear stress
		$\omega$	Warping function, work per unit length
		$\Omega$	Open boundary curve

### Notation and Indices

$(\cdot)_i$	External	$(\cdot)_s$	St. Venant, with respect to the $s$ -direction
$(\cdot)_e$	Element	$(\cdot)_v$	Vlasov
$(\cdot)_f$	Flange	$(\cdot)_w$	Web
$(\cdot)_f$	Free degrees of freedom	$(\cdot)_\omega$	With respect to $\omega_n$
$(\cdot)_i$	Internal	$(\cdot)_x$	With respect to the $x$ -axis
$(\cdot)_n$	Normalized	$(\cdot)_y$	With respect to the $y$ -axis
$(\cdot)_f$	Prescribed degrees of freedom	$(\cdot)_z$	With respect to the $z$ -axis

# 1 Introduction

---

Torsion can be divided into two parts, namely homogeneous and non-homogeneous torsion. The support condition and load scenario clarifies what should be accounted for with respect to the two torsional phenomena.

The finite element method is a calculation tool used in bearing structural elements worldwide, where complicated systems of beam elements can be set up and solved numerically. A standard beam element consists of two nodes, each containing a set of degrees of freedom, which in the two-dimensional situation consists of two translations and one rotation. The analysis is often used when dealing with simple load situations, where torsion and rotation of the beam's second axis is negligible. When dealing with more advanced structures in three dimensions, the load exposure can result in magnitudes, where the mentioned factors can no longer be neglected, which is why beams with six degrees of freedom per node are utilized (three translations and three rotations). A good understanding of the torsional behaviour of beams is therefore crucial when dealing with three-dimensional frame structures.

A lot of standard implementations of three-dimensional beam elements only accounts for one contribution to torsion, namely the first correct analysis of torsion in beams and this analysis was given by St. Venant (1855). The rate of change of rotation about the  $x$ -axis was thought as constant, meaning the warping in all cross-sections becomes identical, this was the underlying assumption by St. Venant, see figure 1.1. As a result of this, the axial strain from torsion disappeared and the distribution of the shear strains were identical in all sections. This gave rise to another reference name than St. Venant torsion known as homogeneous torsion.

In additional situations, specifically when dealing with open cross-sections as I/H-profiles, a big underestimation of the deformation is happening when omitting the other contribution to torsion originated from warping of the cross-section, under the assumption of fixed support conditions. The rate of twist can no longer be thought as constant as a



**Figure 1.1:** St. Venant/Homogeneous torsion

function of  $x$ , when warping or the twist of the cross-section is prevented at one or more cross-sections, see figure 1.2. Axial strains are now developed, and as a consequence of this, with respect to the constitutive condition, axial stresses arise and the shear strains and shear stresses are varying along the beam. Vlasov in 1961 systematically analysed these phenomena for thin-walled beams and for this reason Vlasov torsion is often referred to as non-homogeneous torsion.



**Figure 1.2:** Vlasov/Non-homogeneous torsion

Not every analytical calculation takes into account the non-homogeneous torsion phenomena and practical commercial software like FEM-design, [Strusoft, 2015] and Autodesk Robot Structural Analysis Professional, [Autodesk, 2015a] is therefore investigated as done in the following problem severity investigation:

#### Problem severity research document

I/H-profiles are commonly used within the construction industry and these profiles are particularly critical with respect to torsion as they fall under the category open thin-walled profiles. On the basis of the previous, a research of the problem severity with respect to the deviations of the utilization percentage, in a wide variety of I/H-profiles when comparing St. Venant and Vlasov torsion, is presented in the following.

Both investigated commercial software uses eurocodes to evaluate the utilization. The steel eurocode points out, non-homogeneous torsion must be evaluated if present. The steel eurocode states:

“(4) The following stresses due to torsion should be taken into account:

- The shear stress  $\sigma_{xs}$  due to St. Venant torsion  $M_{x,s}$
- The direct stresses  $\sigma_{xx}$  due to bimoment  $B$  and shear stresses  $\sigma_{xs}$  due to warping torsion  $M_{x,v}$

(5) For the elastic verification the yield criterion in 6.2.1(5) may be applied.”

[Eurocode 3, 2007, Section 6.2.7 Torsion]

Most commercial software (Autodesk robot, FEM-design etc.), used in consulting engineering companies, uses the steel eurocode, as previous mentioned, to check

the bearing capacity but only accounts for St. Venant torsion even though having boundary conditions as fixed at the ends of a beam. This gives rise to some significant deviations worthy of announcing.

In situations, when having a fixed beam subjected to a torsional moment, non-homogeneous torsion should be investigated, as listed in the statement above. A case with a fixed support in one end is a cantilever beam which is investigated further. The boundary and load condition are shown below:

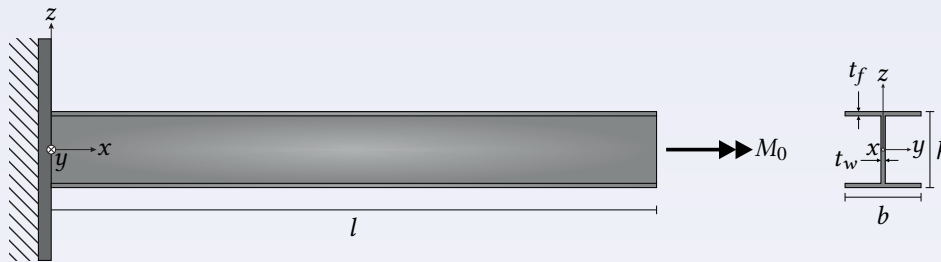


**Figure 1.3:** Boundary- and load condition for a cantilever beam.

The theory and equations used to find the St. Venant torsion in I/H steel profiles are shown in section 2.5.2, see (2.45) and the utilization is found with respect to Von Mises, see (C.3), whereas for Vlasov torsion it can be found in section 2.6, where the normal stress is estimated from (2.62) and the shear stress from (2.69), as both the contribution from St. Venant and Vlasov is included in *Grashof's formula*. The utilization with respect to Vlasov torsion is also checked by means of Von Mises. The critical deviations in utilization between exposure of St. Venant- and Vlasov torsion are especially clear when looking at the utilization of a IPE 450 steel profile, see figure 1.4.

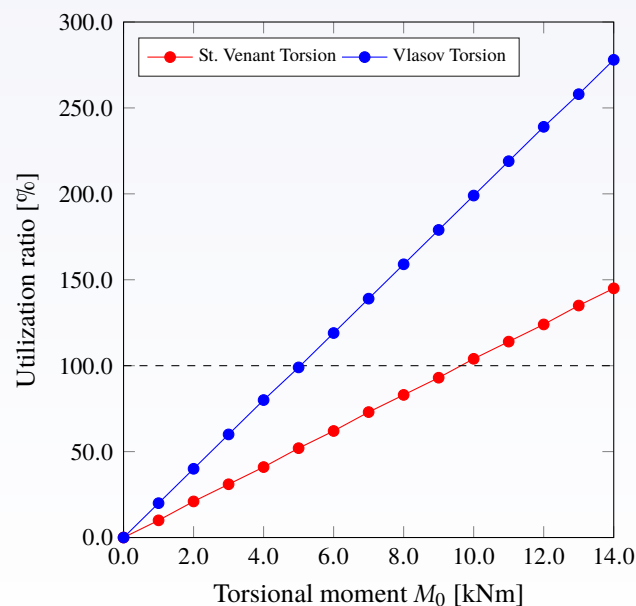


**Figure 1.4:** Utilization of a IPE 450 steel profile.

The dots on each line presents data points. St. Venant torsion is increasing linearly with increasing torsional moment, similar is the non-homogeneous torsion but with twice the slope of St. Venant torsion. already from torsional moments of magnitude 1 kNm, St. Venant torsion starts underestimating the utilization of the IPE 450 steel profile due to the gentler slope, presented with a red dotted line in figure 1.4. A substantial error is therefore made, when using commercial software, like Autodesk Robot Structural Analysis Professional and FEM-design, to design structures in situations where torsional exposure is occurring.

Looking at the steel profile types HEM, the following utilizations are found:

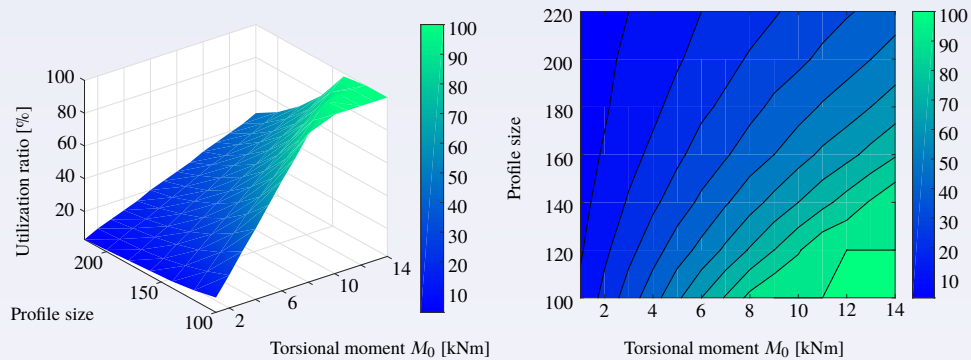


**Figure 1.5:** The left picture shows utilization in a 3D surface plot and the right picture shows utilization in a contour plot, when HEM profiles are exposed to St. Venant torsion.

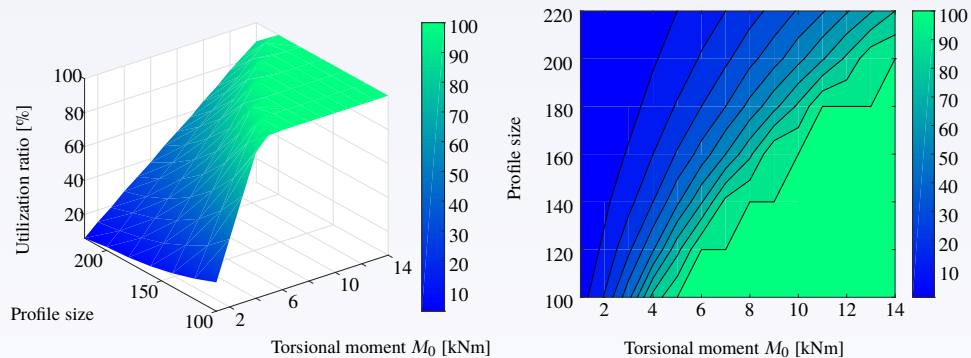
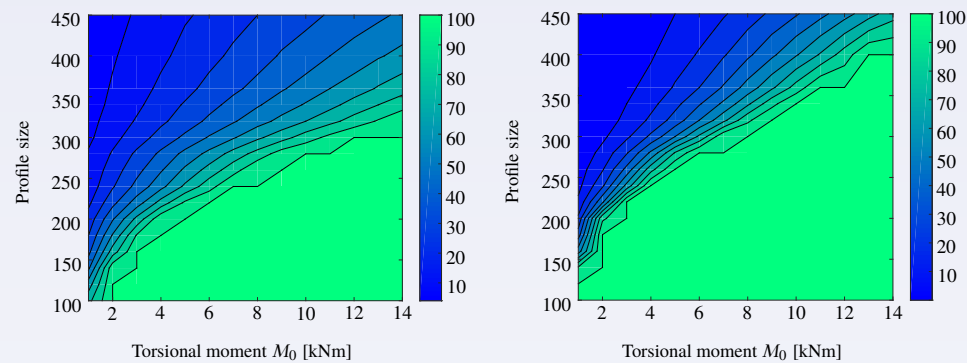


**Figure 1.6:** The left picture shows utilization in a 3D surface plot and the right picture shows utilization in a contour plot, when HEM steel profiles are exposed to Vlasov torsion.

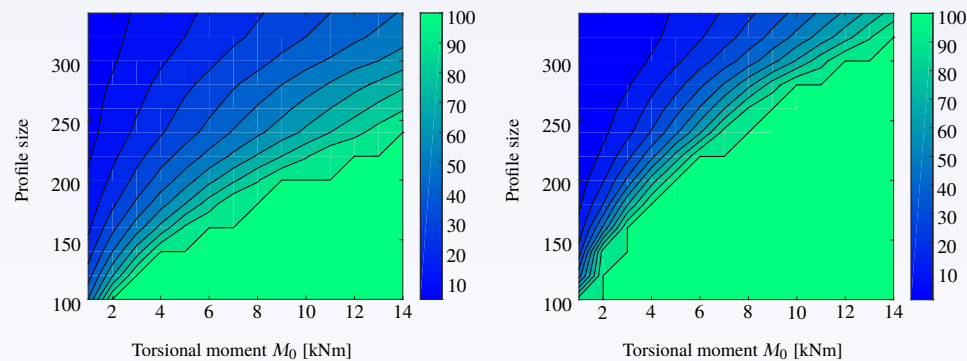
The steeper slope for Vlasov torsion can clearly be seen in the 3D surface plot of figure 1.5 and stating, that the behaviour in figure 1.4 is present in all sizes of the HEM profiles. The behaviour can also be seen in the contour plot of figure 1.6, as the contour lines are more compact and therefore showing a drastically increase in utilization contradictory to 1.5. It can furthermore also be concluded from the contour plot in figure 1.5, a rather small area is covered with light green and therefore only a small interval of the HEM profiles is fully utilized within the presented torsional moment interval when having St. Venant torsion. The torsional moments have to be very high in order to fully utilize the profiles, which is very contradictory compared to the Vlasov torsion case, see the contour plot of

figure 1.6, where a much larger area is covered with light green and profiles up to size HE200M are fully utilized within the higher end of the torsional moment interval. It can clearly be stated, the discrepancies are present in all steel profile types, when comparing the results of HEM, HEA, HEB, INP and IPE profiles. Surface plot combined with a contour plot visualizations of every I/H-shaped steel profile types are presented in appendix A.

Identical deviations are present for all types of H-profiles as seen in figure 1.7 and 1.8 below.



**Figure 1.7:** The left picture shows utilization when exposed to St. Venant torsion and the right picture shows utilization when exposed to Vlasov torsion in HEA profiles, displayed in a contour plot.



**Figure 1.8:** The left picture shows utilization when exposed to St. Venant torsion and the right picture shows utilization when exposed to Vlasov torsion in HEB profiles, displayed in a contour plot.

When comparing the two figures in 1.7 it can be seen, when looking at e.g. a torsional moment of 8 kNm and St. Venant torsion a HE260A is required as this profile is not 100% utilized, but a HE320A is required in order to keep the utilization below 100% when dealing with Vlasov torsion. This phenomena is more or less present throughout all the profile sizes which is also why the light green area in the Vlasov torsion case is larger compared to St. Venant, see figure 1.7. The same deviations are occurring when looking at HEB profiles in figure 1.8 where a HE200B is needed when having the same a torsional moment(8 kNm) and St. Venant torsion, whereas a HE260B is required when having a non-homogeneous torsional case. Notice the HEB profiles require a

smaller profile size in order to withstand the same torsional moment compared to the HEA profiles meaning HEB profiles are better suited to obtain torsional moments but still weaker compared to HEM profiles, see figure 1.5 and 1.6. Similar deviations are equally present for I-profiles as shown in figure 1.9 and 1.10 below.

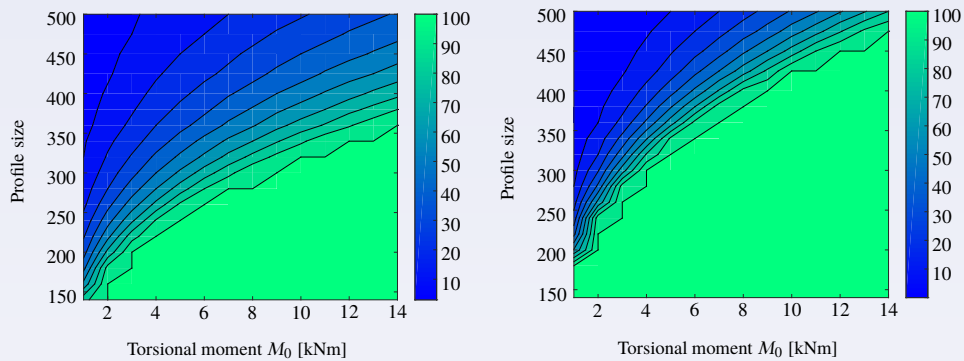


**Figure 1.9:** The left picture shows utilization when exposed to St. Venant torsion and the right picture shows utilization when exposed to Vlasov torsion in INP profiles, displayed in a contour plot.

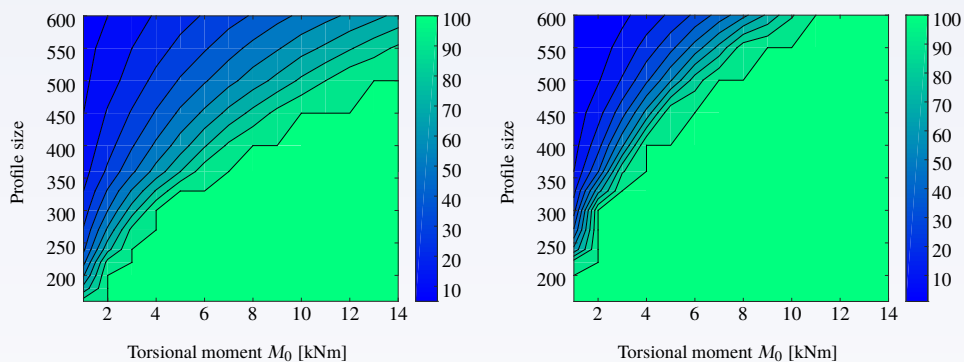


**Figure 1.10:** The left picture shows utilization when exposed to St. Venant torsion and the right picture shows utilization when exposed to Vlasov torsion in IPE profiles, displayed in a contour plot.

The same characteristics are present in the INP profiles when looking at a torsional moment of 8 kNm, here St. Venant torsion requires a INP 300 profile, whereas a INP 400 profile is needed when having non-homogeneous torsion. The same deviation between St. Venant- and non-homogeneous torsion is present for IPE profiles where a IPE 450 profile is needed when the beam is exposed to St. Venant torsion and a IPE 550 profile is required for Vlasov torsion, which is a significant deviation in profile size. This is why a significantly larger light green area is seen, when looking at the Vlasov torsion in figure 1.9 and 1.10 compared to the St. Venant torsion for both profiles. It should again be noticed a difference between the profile types INP and IPE is occurring, showing INP profiles are stronger against torsional exposure as a smaller profile size is required when subjected to the same torsional moment as for IPE profiles.

It can furthermore be stated, HEM profiles would be a wise choice of profile in areas, where the structure is subjected to torsional moments, as small profiles can accumulate a high torsional moment which is very different from IPE profiles, see figure 1.5 and St. Venant torsion of figure 1.10.

In order to verify the correlation between the analytical solutions, presented in section 2.5.2, 2.6 and 2.8, and the commercial software programs, the procedure of the analysis is investigated within the software programs. The same results are obtained in both models (simply supported and fixed) in the programs and utilization ratio is the same compared to the analytical solution for St. Venant torsion (when adding partial coefficients), furthermore see quotation below, which is presenting a statement directly from the feature: “troubleshooting” at the homepage of Autodesk:

“Issue:

Are both torsional effects in the analysis of one-dimensional members: St Venant torsion (uniform) and warping torsion (non-uniform) supported?

Answer:

Since in Robot one-dimensional members, e.g. beams and columns, are modelled with six degrees-of-freedom only St Venant torsion is accounted for and warping torsion is neglected.”

[Autodesk, 2015b]

Results from the commercial software can be seen in appendix A, where the results from a simply supported beam subjected to torsion is compared to a fixed supported beam and the results are as previous mentioned revealing identical results in the two support scenarios, meaning non-homogeneous torsion is not accounted for in programs like Autodesk Robot Structural Analysis Professional and FEM-Design, as the results are identical to the analytical results for St. Venant torsion.

Practical calculations, performed in consulting engineering companies, of torsion in steel members, in most cases, follow the codes and guidelines presented in the steel eurocode, meaning the codes and guidelines needs to have credibility. As previous displayed in the problem severity research document, the steel eurocode states [Eurocode 3, 2007, Section 6.2.7 Torsion], the following stresses due to torsion should be taken into account. Firstly the shear stresses due to St. Venant torsion, secondly the direct stress due to bimoment and shear stress from warping torsion, here introducing one more degree of freedom in the finite element perspective, making it a total of seven degrees of freedom per node. Numerical calculations in a home-made MATLAB program [Mathworks, 2015] are compared with an advanced commercial software program ABAQUS [SIMULIA, 2015], in order to evaluate possible deviations in estimating the stresses due to non-homogeneous torsion.

The primary advantage of Vlasov torsion theory, seen from an engineering point of view, is the way the theory explains that restraining the beam and therefore preventing warping leads to much stiffer structural elements than achieved in the case of homogeneous warping, i.e. a given torsional moment will induce a smaller twist, which is one

of the basic features of beams.

By the inclusion of a thick plate orthogonal to the beam axis and welded to the flanges and the web, warping of the cross-section can be counteracted, as the profile in these cross-sections is seen as a rectangle instead of an open profile. The prevention of torsion in this way is particularly useful in the case of slender beams with open thin-walled cross-sections, which are prone to coupled flexural–torsional buckling. Obviously, Vlasov torsion theory needs to be applied for the analysis of such problems, and it is therefore of deep interest to investigate Vlasov torsion further both analytically as well as numerically.

## 1.1 Objective and scope

With the presented deviations in the problem severity research text box above, non-homogeneous torsion should be thought as crucial and worthy of investigating in more advanced software programs like `MATLAB` and `ABAQUS` using finite element method, which will be issued as a main objective in this report.

How can non-homogeneous torsion be taken into account in a finite element code and how large a deviation in stress magnitudes and displacement from non-homogeneous torsion is actually present, between analytical solutions, a home-made numerical program in `MATLAB` and an advanced numerical software program `ABAQUS`?

Only numerical results for an open I/H profiles is investigated, as these profiles are commonly used in the industry and problems can occur with respect to non-homogeneous torsion situations. As I/H profiles is most commonly fabricated with steel as material, material properties for steel is used only. The case of pure torsion is only investigated, as this case is sought to be adequate, due to torsion being the main focus area. Profile IPE 450 is one of the profiles with the largest deviation in utilization when looking at St. Venant and Vlasov torsional exposure and numerical results from the `MATLAB` code and `ABAQUS` is only generated with respect to this profile.

## 2 Spatial Beam Theory

---

The following chapter derives the general differential equations for spatial beams based on Euler-Bernoulli beam theory with an additional component due to twisting of the beam. This includes axial, bending and torsional deformations. The described theory is greatly inspired by [Andersen and Nielsen, 2008] and [Nielsen and Hansen, 1978].

As the theory is based on first order theory the following assumptions are basis:

- The material behaves lineary elastic which means, that Hooke's law is valid without any restrictions.
- The displacements are so small that the equilibrium conditions may be formulated in the undeformed state and kinematic relations may be linearised.
- In biaxial bending with axial force, Bernoulli's hypothesis is assumed, which states that cross-sections remain plane and orthogonal to the beam axis.

Firstly, the equations of equilibrium are presented.

### 2.1 Equations of Equilibrium

In a referential right-handed  $(x, y, z)$ -coordinate system an initially straight beam is considered as shown on figure 2.1. The beam has a length  $l$  with an arbitrary cross-section, that everywhere is identical and whose normal is parallel to the  $x$ -axis throughout the beam length.

The beam is loaded by a distributed load per unit length defined as  $\mathbf{q} = \mathbf{q}(x)$  and distributed moment load per unit length  $\mathbf{m} = \mathbf{m}(x)$  as

$$\mathbf{q} = \begin{bmatrix} q_x \\ q_y \\ q_z \end{bmatrix}, \quad \mathbf{m} = \begin{bmatrix} m_x \\ m_y \\ m_z \end{bmatrix}. \quad (2.1a-b)$$

As shown on figure 2.1 an infinitesimal segment of the beam is considered with a length  $dx$  and loaded by the external force vector  $\mathbf{q}dx$  and external moment vector  $\mathbf{m}dx$ .

These external loads deforms the beam into a current state where the external loads are balanced by internal sectional forces  $\mathbf{F} = \mathbf{F}(x)$  and internal sectional moments  $\mathbf{M} = \mathbf{M}(x)$ . The components of these vectors are

$$\mathbf{F} = \begin{bmatrix} N \\ Q_y \\ Q_z \end{bmatrix}, \quad \mathbf{M} = \begin{bmatrix} M_x \\ M_y \\ M_z \end{bmatrix}, \quad (2.2a-b)$$

where  $N$  is the axial force,  $Q_y$  and  $Q_z$  are signified as the shear force components in the  $y$ - and  $z$ -direction, respectively.  $M_x$  is the torsional moment and the components  $M_y$  and  $M_z$

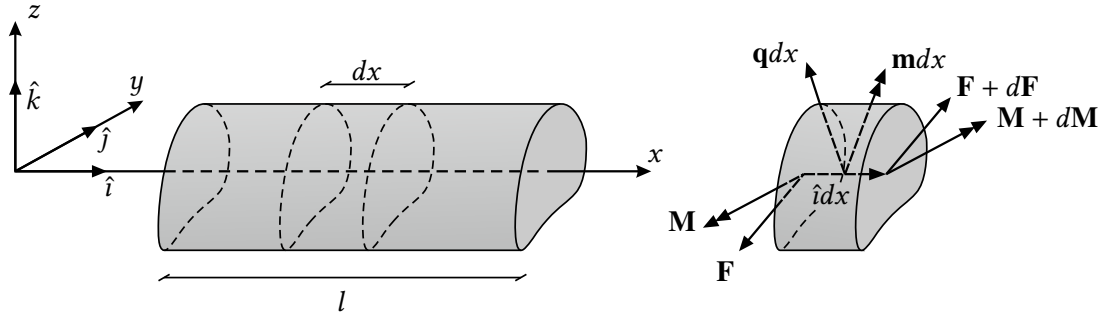


**Figure 2.1:** Beam in referential state.

are the bending moments in the  $y$ - and  $z$ -direction causing normal bending and buckling. The vectors act on the cross-section with the base unit vector  $\hat{i}$  as an outward directed normal vector. In the left end of the beam segment the section forces and moment acting are  $\mathbf{F}$  and  $\mathbf{M}$  and in the right end these are changed differentially into  $\mathbf{F} + d\mathbf{F}$  and  $\mathbf{M} + d\mathbf{M}$ . Here  $d(\cdot)$  are increments and may fully be written as,  $d(\cdot) = (d(\cdot)/dx)dx$ .

Force and moment equilibrium can be formulated as:

$$-\mathbf{F} + \mathbf{F} + d\mathbf{F} + \mathbf{q}dx = 0 \quad \Rightarrow \quad \frac{d\mathbf{F}}{dx} + \mathbf{q} = 0, \quad (2.3a)$$

$$-\mathbf{M} + \mathbf{M} + d\mathbf{M} + \hat{i}dx \times (\mathbf{F} + d\mathbf{F}) + \mathbf{m}dx = 0 \quad \Rightarrow \quad \frac{d\mathbf{M}}{dx} + \hat{i} \times \mathbf{F} + \mathbf{m} = 0. \quad (2.3b)$$

Here  $\times$  is the cross-product between two vectors. Also, second order terms have been disregarded due to  $dx \rightarrow 0$  and the equivalent component relations are:

$$\begin{aligned} \frac{dN}{dx} + q_x &= 0, & \frac{dM_x}{dx} + m_x &= 0, \\ \frac{dQ_y}{dx} + q_y &= 0, & \frac{dM_y}{dx} - Q_z + m_y &= 0, \\ \frac{dQ_z}{dx} + q_z &= 0, & \frac{dM_z}{dx} + Q_y + m_z &= 0. \end{aligned} \quad (2.4a-f)$$

## 2.2 Uncoupled System of Equations

By choosing a coordinate system in a smart way, coupled deformation variables from the axial force ( $N$ ) and bending moments ( $M_y, M_z$ ) are avoided. The origin  $B$  called the *bending centre* only induces an uniform axial displacement over the cross-section from the axial force; otherwise the point of attack of an axial force would produce a bending moment as well. Furthermore the axes of  $y$  and  $z$  are determined to be *principal axes* of the beam cross-section. These ensure that a bending moment around the axes will neither produce an axial force nor flexural displacement in the other direction. The positive direction of moment and rotation are defined as illustrated on figure 2.2, commonly referred to as the *right-hand rule*.



**Figure 2.2:** Right-hand rule applied to define the positive moment and rotation directions.

Another important reference point in the cross-section is the *shear centre*, presented as the point  $S$ , which is positioned the distance  $(y_S, z_S)$  from  $B$ . If the line loads  $(q_y, q_z)$  and shear forces  $(Q_y, Q_z)$  acts in this point of application, uncoupling between bending and torsional deformation are utilized and the torsion caused is solely produced by the moment load  $m_x$  (this includes contributions from the translation of  $q_y$  and  $q_z$  to  $S$ ).

By having both axial, bending, and torsional deformations uncoupled the different situations can be dealt with separately and superpositioned to give the total response of the beam. The differential equations of the beam are presented in section 2.9.

On figure 2.3 the point of application and sign convention are shown for the deformation, load, internal force and moment, and stress variables. The deformation variables apply to the bending centre, which are the displacements  $u_x, u_y, u_z$  in the  $x, y, z$  direction, respectively. The cross-sectional bending moments  $M_y, M_z$  and associated rotation  $\theta_y, \theta_z$  components also apply here, where the index indicates on which axis the rotation is about. The loads per unit length  $q_x, m_y, m_z$  also act in the bending centre while  $m_x, q_y, q_z$  are positioned at the shear centre. Lastly, the internal axial force  $N$  acts at the bending centre and shear forces  $Q_y, Q_z$  and the torsional moment  $M_x$  are applied at the shear centre.

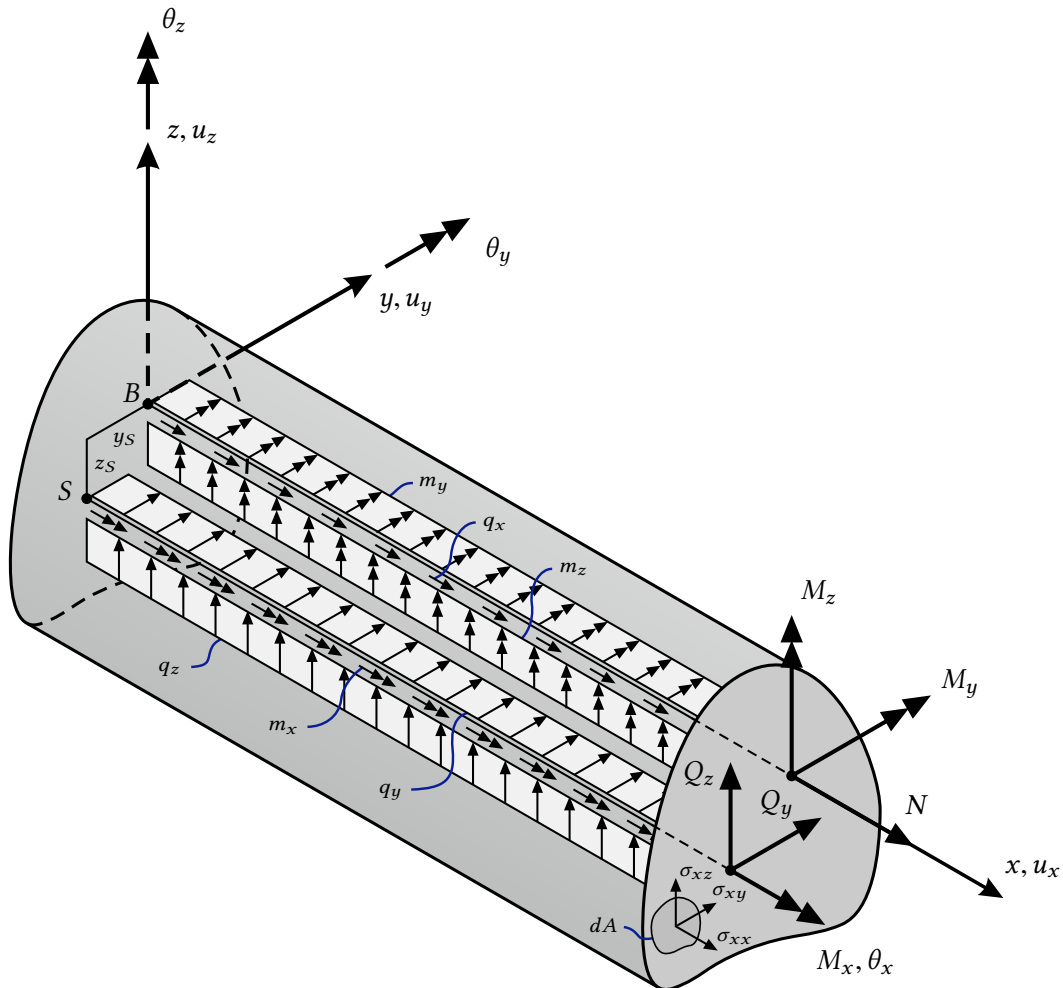


**Figure 2.3:** Variables in local beam  $(x, y, z)$ -coordinate system and definition of positive sign convention.

### 2.3 Internal Forces, Moments and Stresses

As seen on figure 2.3 the normal stress  $\sigma_{xx}$  and the shear stresses  $\sigma_{xy}$  and  $\sigma_{xz}$  act on the cross-section over an area  $dA$ . These stresses must be a resultant of the force vector  $\mathbf{F}$  and moment vector  $\mathbf{M}$  and must be statically equivalent as the following relations:

$$\begin{aligned} N &= \int_A \sigma_{xx} dA, & M_x &= \int_A (\sigma_{xz}(y - y_S) - \sigma_{xy}(z - z_S)) dA, \\ Q_y &= \int_A \sigma_{xy} dA, & M_y &= \int_A \sigma_{xx} z dA, \\ Q_z &= \int_A \sigma_{xz} dA, & M_z &= - \int_A \sigma_{xx} y dA. \end{aligned} \quad (2.5a-f)$$

### 2.4 Deformation, Kinematic and Constitutive Relations

As stated before the basic assumption in Euler-Bernoulli beam theory is, that the cross-section remains plane and orthogonal to the  $x$ -axis. In other words, the cross-section translates and rotates as a rigid body.

As seen on figure 2.4 the deformed position of a cross-section throughout the beam can be described by the position vector  $\mathbf{w} = \mathbf{w}(x)$  and the rotation vector  $\boldsymbol{\theta} = \boldsymbol{\theta}(x)$  with the following components:

$$\mathbf{w} = \begin{bmatrix} w_x \\ w_y \\ w_z \end{bmatrix}, \quad \boldsymbol{\theta} = \begin{bmatrix} \theta_x \\ \theta_y \\ \theta_z \end{bmatrix}. \quad (2.6a-b)$$

Here, the longitudinal displacement  $w_x$  refers to the bending centre  $B$  while the displacements  $w_y$  and  $w_z$  describes the displacement of the shear centre  $S$ .

Furthermore, due to the displacement components all being small compared to the beam length together with the rotation components also being small, the kinematic relations can be linearised, which means that  $\sin \theta \simeq \tan \theta \simeq \theta$ . From figure 2.4 the entire displacement field can be expressed as:

$$u_x(x, y, z) = w_x(x) + z\theta_y(x) - y\theta_z(x) + \omega(y, z) \frac{d\theta_x(x)}{dx} \quad (2.7a)$$

$$u_y(x, y, z) = w_y(x) - (z - z_S) \theta_x(x) \quad (2.7b)$$

$$u_z(x, y, z) = w_z(x) + (y - y_S) \theta_x(x) \quad (2.7c)$$

In all cross-sections except circular ones, the torsional moment  $M_x$  will induce an additional non-planar displacement in the  $x$ -axis seen in (2.7a), where  $\omega(y, z)$  is called the *warping function*. A more explained derivation of the displacement field and warping due to torsion in thin-walled cross-sections are presented in section 2.5.2.

The kinematic constraint that involves the beam to be orthogonal to its normal, the rotation of the cross-section in  $y$ - and  $z$ -direction is directly equivalent to the change of the transverse displacement with respect to the longitudinal direction, thus

$$\theta_y = -\frac{dw_z}{dx}, \quad \theta_z = \frac{dw_y}{dx}. \quad (2.8a-b)$$

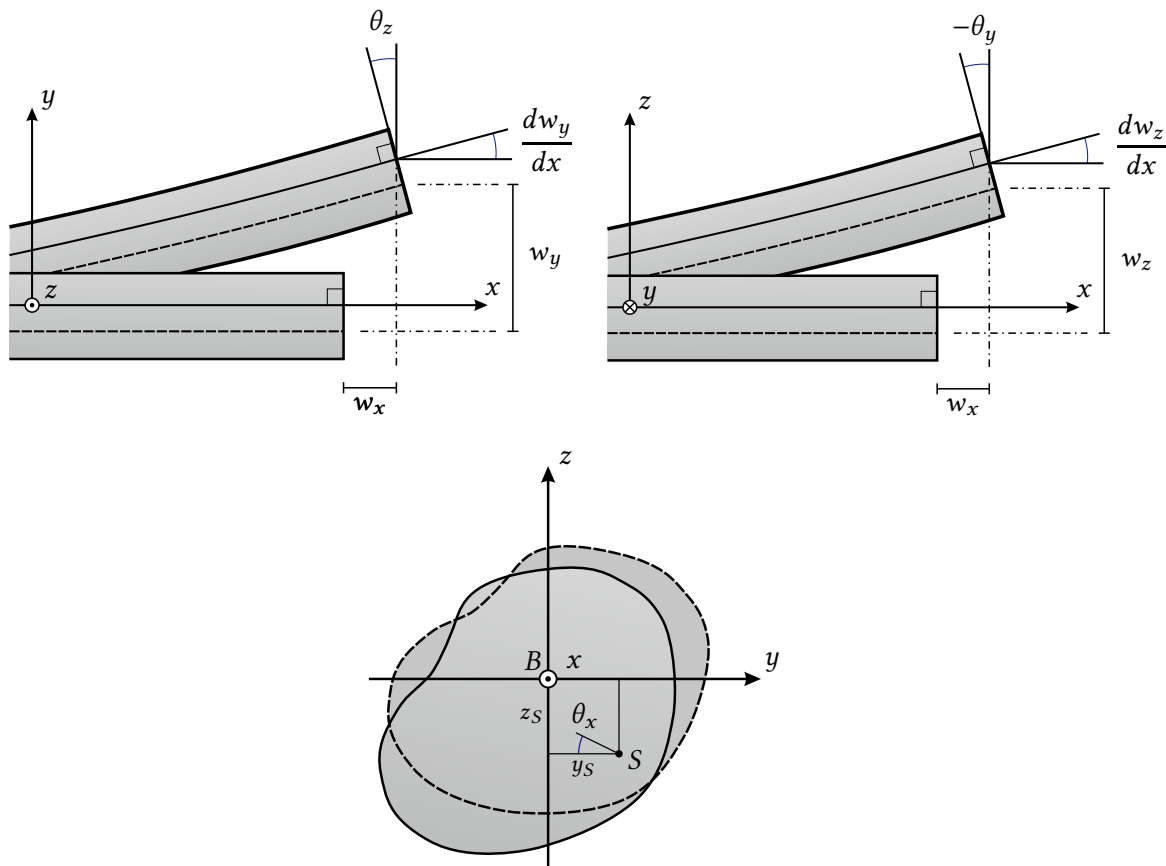


**Figure 2.4:** Deformation components in beam theory.

These are merely caused by bending components and are related to the curvature of the beam. The radii of curvatures  $r_y$  and  $r_z$  are related to the rotation increments  $d\theta_z$  and  $-d\theta_y$  over a differential beam element with length  $dx$  as:

$$\left. \begin{array}{l} r_y d\theta_z \simeq dx \\ \kappa_z = \frac{1}{r_y} \end{array} \right\} \kappa_z = \frac{d\theta_z}{dx} = \frac{d^2 w_y}{dx^2} \quad (2.9a)$$

$$\left. \begin{array}{l} -r_z d\theta_y \simeq dx \\ \kappa_y = -\frac{1}{r_z} \end{array} \right\} \kappa_y = \frac{d\theta_y}{dx} = -\frac{d^2 w_z}{dx^2} \quad (2.9b)$$

Going back to (2.7a) an additional component is now added to the displacement. This is because of non-planar displacements from warping due to torsion. The warping function is dependent on the geometry of the cross-section and it is part of finding the solution to the torsion problem. An exact solution is seldom possible and one must resort to numerical procedures to obtain an expression to solve the equations. An approximate solution for thin-walled cross-section are given in section 2.5.2.

The strains of the displacement field can be found as:

$$\varepsilon_{xx} = \frac{\partial u_x}{\partial x} = \frac{dw_x}{dx} + z \frac{d\theta_y}{dx} - y \frac{d\theta_z}{dx} + \omega \frac{d^2\theta_x}{dx^2}, \quad (2.10a)$$

$$\varepsilon_{yy} = \frac{\partial u_y}{\partial x} = 0, \quad \varepsilon_{zz} = \frac{\partial u_z}{\partial x} = 0, \quad (2.10b-c)$$

$$\gamma_{xy} = \frac{\partial u_x}{\partial y} + \frac{\partial u_y}{\partial x} = \left[ \frac{\partial \omega}{\partial y} - (z - z_S) \right] \frac{d\theta_x}{dx}, \quad (2.10d)$$

$$\gamma_{xz} = \frac{\partial u_x}{\partial z} + \frac{\partial u_z}{\partial x} = \left[ \frac{\partial \omega}{\partial z} + (y - y_S) \right] \frac{d\theta_x}{dx}, \quad (2.10e)$$

$$\gamma_{yz} = \frac{\partial u_y}{\partial z} + \frac{\partial u_z}{\partial y} = -\theta_x + \theta_x = 0. \quad (2.10f)$$

Similarly, the stresses are:

$$\sigma_{xx} = E\varepsilon_{xx} = E \left( \frac{du_x}{dx} + z \frac{d\theta_y}{dx} - y \frac{d\theta_z}{dx} + \omega \frac{d^2\theta_x}{dx^2} \right), \quad (2.11a)$$

$$\sigma_{xy} = G\gamma_{xy} = G \left[ \frac{\partial \omega}{\partial y} - (z - z_S) \right] \frac{d\theta_x}{dx}, \quad (2.11b)$$

$$\sigma_{xz} = G\gamma_{xz} = G \left[ \frac{\partial \omega}{\partial z} + (y - y_S) \right] \frac{d\theta_x}{dx}. \quad (2.11c)$$

## 2.5 Homogeneous Torsion

The simplest form of torsion (also referred to as homogeneous torsion or St. Venant torsion) is dealt with in this section. Figure 2.5 shows a cross-section of a prismatic beam subjected to a statically equivalent twisting moment  $M_{x,s}$  at both ends. It is assumed that there is *no* restraint with respect to axial displacements at the ends and the torsional moment  $M_{x,s}$  remains unchanged along the beam.

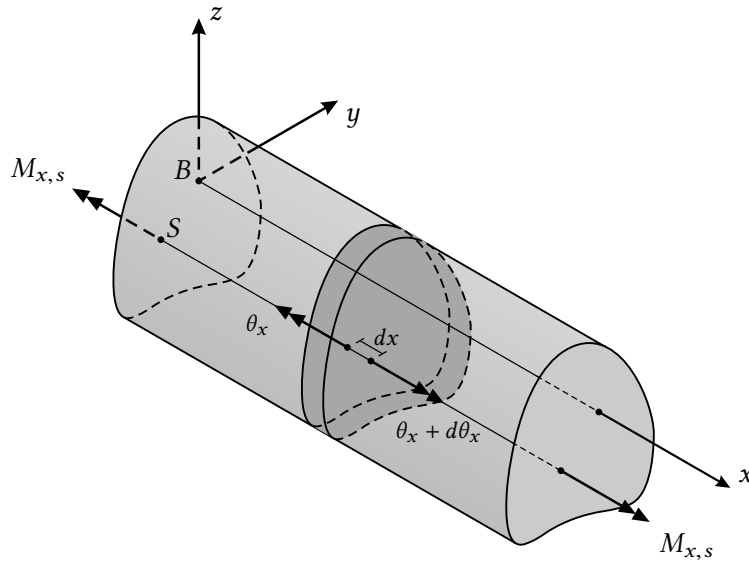


**Figure 2.5:** Differential beam subjected to homogeneous torsion.

The displacement components from (2.7) reduces to:

$$u_x = \omega \frac{d\theta_x}{dx}, \quad u_y = -(z - z_S) \theta_x, \quad u_z = (y - y_S) \theta_x. \quad (2.12a-c)$$

The corresponding strains must be independent of  $x$  since each cross-section is subjected to the same moment, meaning that the incremental twist per unit length  $d\theta_x/dx$  must be constant. Thus, the axial displacement (warping) must be the same in all cross-sections,  $u_x = u_x(y, z)$  and implies that warping in homogeneous torsion does not induce normal strains, nor normal stresses

$$\varepsilon_{xx} = \frac{\partial u_x}{\partial x} = 0, \quad \sigma_{xx} = E\varepsilon_{xx} = 0. \quad (2.13a-b)$$

Hence, only shear stresses  $\sigma_{xy}$  and  $\sigma_{xz}$  are present and expressed by (2.11b) and (2.11c). The shear stresses must be statically equivalent to the shear forces  $Q_y = Q_z = 0$  and the torsional moment  $M_{x,s}$ . The torsional moment  $M_{x,s}$  around  $S$  is expressed in (2.5) and can be reduced to

$$M_{x,s} = \int_A (\sigma_{xz} y - \sigma_{xy} z) dA. \quad (2.14)$$

Here it has been used that  $\int_A \sigma_{xy} dA = \int_A \sigma_{xz} dA = 0$ .

(2.14) can be expressed by substituting the shear stresses and one obtains:

$$\begin{aligned} M_{x,s} &= \int_A \left( G \left[ \frac{\partial \omega}{\partial y} - (z - z_S) \right] \frac{d\theta_x}{dx} y - G \left[ \frac{\partial \omega}{\partial z} + (y - y_S) \right] \frac{d\theta_x}{dx} z \right) dA \\ &= GI_x \frac{d\theta_x}{dx}, \end{aligned} \quad (2.15)$$

where it has been used that  $\int_A z dA = \int_A y dA = 0$  and

$$I_x = \int_A \left( y^2 + z^2 + y \frac{\partial \omega}{\partial z} - z \frac{\partial \omega}{\partial y} \right) dA. \quad (2.16)$$

$I_x$  is denoted the *torsional constant*. From (2.15) it can be seen that torsional moment depends linearly on  $d\theta_x/dx$ .

### 2.5.1 Solution to Homogeneous Torsion

An often used solution to the homogeneous torsion problem is based on the formulation of a *Prandtl's stress function*  $S$ . This approach is especially useful in relation to torsion of thin-walled profiles and will be used in the following derivations.

On figure 2.6 a cross-section of a prismatic beam is shown. The curve along the outer periphery is denoted as  $\Gamma_0$  while the interior boundary curves are determined as  $\Gamma_j$ ,  $j = 1, 2, \dots, N$ , for  $N$  number of holes. At the boundary curves arc-length coordinates  $s_0, s_1, \dots, s_N$  are defined. The arc-length coordinate  $s_0$  along  $\Gamma_0$  is orientated in an anti-clockwise direction, while the interior boundaries  $\Gamma_1, \Gamma_2, \dots, \Gamma_N$ , are orientated in a clock-wise direction. Each boundary curve has an outward directed unit vector denoted  $\mathbf{n}_j$ ,  $j = 0, 1, \dots, N$ . The unit tangential vector to a boundary curve is denoted  $\mathbf{s}_j$  and follows the same direction as the arc-length coordinate  $s_j$ . A local coordinate system is defined with the base unit vectors as  $\{\hat{i}, \mathbf{n}_j, \mathbf{s}_j\}$ . The exterior and interior arc-length coordinates insured that the related  $(x, n_j, s_j)$ -coordinate system forms a right-handed coordinate system.

The stresses in terms of Prandtl's stress function can be expressed as

$$\sigma_{xy} = \frac{\partial S}{\partial z}, \quad \sigma_{xz} = -\frac{\partial S}{\partial y}. \quad (2.17a-b)$$

Volume loads are ignored and the equilibrium equations read:

$$\frac{\partial \sigma_{xx}}{\partial x} + \frac{\partial \sigma_{xy}}{\partial y} + \frac{\partial \sigma_{xz}}{\partial z} = 0, \quad (2.18a)$$

$$\frac{\partial \sigma_{xy}}{\partial x} + \frac{\partial \sigma_{yy}}{\partial y} + \frac{\partial \sigma_{yz}}{\partial z} = 0, \quad (2.18b)$$

$$\frac{\partial \sigma_{xz}}{\partial x} + \frac{\partial \sigma_{yz}}{\partial y} + \frac{\partial \sigma_{zz}}{\partial z} = 0. \quad (2.18c)$$

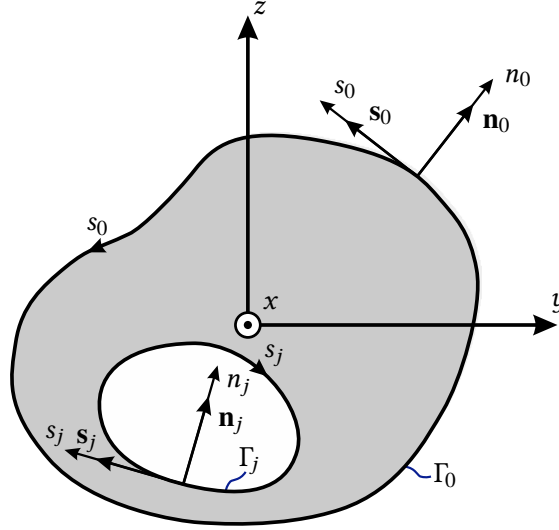


**Figure 2.6:** Cross-section with holes. Interior and exterior edges and definition of local  $(x, n_j, s_j)$ -coordinate.

With  $\sigma_{xx} = \sigma_{yy} = \sigma_{zz} = \sigma_{yz} = 0$ , and  $\sigma_{xy}$  and  $\sigma_{xz}$  only depends on  $y$  and  $z$ , (2.18b) and (2.18c) are fulfilled and (2.18a) reduces to

$$\frac{\partial \sigma_{xy}}{\partial y} + \frac{\partial \sigma_{xz}}{\partial z} = \frac{\partial^2 S}{\partial y \partial z} - \frac{\partial^2 S}{\partial z \partial y} = 0, \quad (2.19)$$

which can be seen as automatically fulfilled. From (2.11b) and (2.11c) it follows that

$$\frac{\partial \sigma_{xy}}{\partial z} - \frac{\partial \sigma_{xz}}{\partial y} = \left( \frac{\partial^2 \omega}{\partial z \partial y} - 1 \right) G \frac{d\theta_x}{dx} - \left( \frac{\partial^2 \omega}{\partial y \partial z} + 1 \right) G \frac{d\theta_x}{dx} = -2G \frac{d\theta_x}{dx}. \quad (2.20)$$

By insertion of (2.17) on the left hand side of (2.20) the differential equation for  $S$  is obtained:

$$\frac{\partial^2 S}{\partial y^2} + \frac{\partial^2 S}{\partial z^2} = -2G \frac{d\theta_x}{dx}, \quad (x, y) \in A. \quad (2.21)$$

(2.21) is a compatibility condition for the stress function  $S$  in the order that the kinematic conditions from (2.11) are fulfilled. On the boundary shear stresses can be expressed

along the local  $n$ - and  $s$ -axis, as  $\sigma_{xn}$  and  $\sigma_{xs}$  respectively. The boundary condition can be expressed as

$$\sigma_{xn} = \sigma_{xy}n_y + \sigma_{xz}n_z, \quad (2.22)$$

where  $n_y$  and  $n_z$  are the vector components of the unit normal vector  $\mathbf{n}$ . Since exterior and interior surfaces are considered free of surface traction it follows that

$$0 = \sigma_{xy}n_y + \sigma_{xz}n_z. \quad (2.23)$$

The boundary condition for  $S$  is obtained by insertion of (2.17) in (2.23)

$$\frac{\partial S}{\partial z}n_y - \frac{\partial S}{\partial y}n_z = 0. \quad (2.24)$$

It can be seen that the tangential unit vector can be expressed as  $\mathbf{s}^T = [s_y, s_z] = [-n_z, n_y]$  and (2.24) becomes

$$\frac{\partial S}{\partial y}s_y + \frac{\partial S}{\partial z}s_z = \frac{\partial S}{\partial s} = 0. \quad (2.25)$$

(2.25) implies that  $S$  is along exterior and interior boundary curves

$$S = S_j, \quad j = 0, 1, \dots, N, \quad (x, y) \in \Gamma_0 \cup \Gamma_1 \cup \dots \cup \Gamma_N. \quad (2.26)$$

For pure torsion the shear stresses  $\sigma_{xy}$  and  $\sigma_{xz}$  must be statically equivalent to the shear forces  $Q_y = Q_z = 0$  and the torsional moment  $M_x$ . By applying Green's theorem on the expression for the shear force, the relation between the integral over the plane region  $A$  and the line integral around the closed curves  $\Gamma_j$  is obtained:

$$Q_y = \int_A \sigma_{xy} dA = \int_A \frac{\partial S}{\partial z} dA = - \sum_{j=0}^N S_j \oint_{\Gamma_j} dy = 0 \quad (2.27a)$$

$$Q_z = \int_A \sigma_{xz} dA = - \int_A \frac{\partial S}{\partial y} dA = - \sum_{j=0}^N S_j \oint_{\Gamma_j} dz = 0 \quad (2.27b)$$

Since  $S_j$  is constant along the boundary curve it has been transferred outside the circular integral. Since  $\oint_{\Gamma_j} dy = \oint_{\Gamma_j} dz = 0$ , it follows that any solution to the boundary value problem from (2.21) and (2.26) automatically provides a solution fulfilling  $Q_y = Q_z = 0$ .

The torsional moment expressed by (2.14) and by substituting (2.17) in the expression, it is obtained

$$M_{x,s} = - \int_A \left( \frac{\partial S}{\partial y}y + \frac{\partial S}{\partial z}z \right) dA = - \int_A \left( \frac{\partial}{\partial y} (Sy) + \frac{\partial}{\partial z} (Sz) \right) dA + 2 \int_A S dA, \quad (2.28)$$

where the product rule by differentiation has been utilized. Green's theorem of the terms in the parenthesis gives:

$$\int_A \left( \frac{\partial}{\partial y} (Sy) + \frac{\partial}{\partial z} (Sz) \right) dA = \sum_{j=0}^N S_j \oint_{\Gamma_j} (ydz - zdy) = 2A_0S_0 - \sum_{j=1}^N 2A_jS_j. \quad (2.29)$$

Here it has been used that  $2A_j = \oint_{\Gamma_j} (ydz - zdy)$  and negative sign on clockwise circulation on interior boundaries. Since the shear stresses remain unchanged if an arbitrary constant

is added to  $S$ , it can be chosen that  $S_0 = 0$ , which is assumed in the following. The torsional constant  $I_x$  can be determined by comparing (2.15) and (2.29).

The warping function and Prandtl's stress function has the relation by comparing (2.11b), (2.11c) and (2.17):

$$\frac{\partial S}{\partial z} = G \left[ \frac{\partial \omega}{\partial y} - (z - z_s) \right] \frac{d\theta_x}{dx} \quad (2.30a)$$

$$-\frac{\partial S}{\partial y} = G \left[ \frac{\partial \omega}{\partial y} + (y - y_s) \right] \frac{d\theta_x}{dx} \quad (2.30b)$$

### Example 2.1: Homogeneous torsion of infinitely long rectangular cross-section

A torsional moment  $M_{x,s}$  is applied to an infinitely long rectangular cross-section as shown on figure 2.7. The torsional moment is carried by the shear stresses in the  $y$ -direction which makes  $S = S(z)$  independent of  $y$ , and the boundary value problem becomes:

$$\frac{d^2 S}{dz^2} = -2G \frac{d\theta_x}{dx}, \quad S(-t/2) = S(t/2) = 0, \quad (2.31a-b)$$

with the solution

$$S(z) = \frac{1}{4} (t^2 - 4z^2) G \frac{d\theta_x}{dx}. \quad (2.32)$$

The shear stresses follows from (2.17) as

$$\sigma_{xy} = \frac{\partial S}{\partial z} = -2zG \frac{d\theta_x}{dx}, \quad \sigma_{xz} = -\frac{\partial S}{\partial y} = 0. \quad (2.33a-b)$$

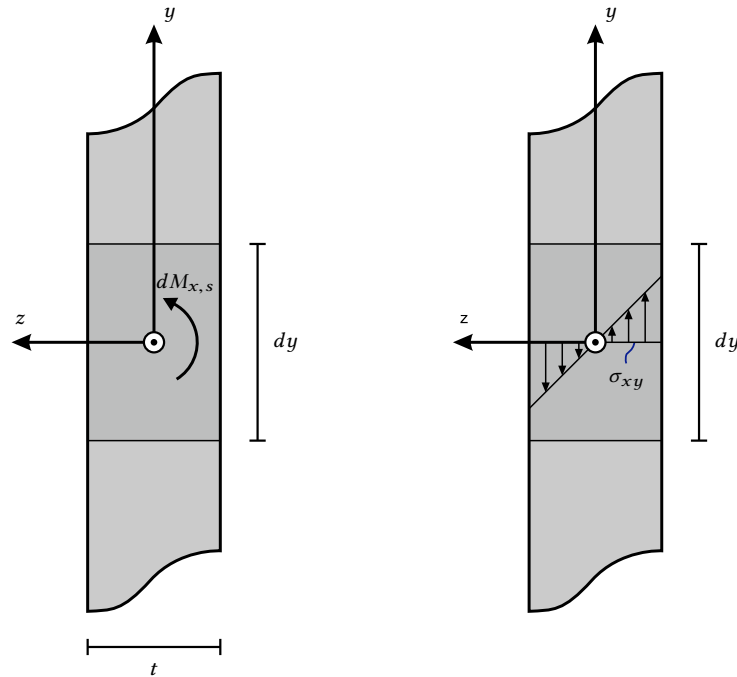


**Figure 2.7:** Infinitely long rectangular cross-section subjected to torsion.

Since the shear stresses are independent of  $y$ , a differential cross-sectional segment of the length  $dy$  can be analysed to be exposed to a torsional moment increment  $dM_{x,s}$ . From (2.29) the increment  $dM_{x,s}$  is related to the stress function:

$$dM_{x,s} = 2 \int_{-t/2}^{t/2} S(z) dy dz = \frac{1}{3} t^3 dy G \frac{d\theta_x}{dx}. \quad (2.34)$$

Furthermore  $dM_{x,s} = G dI_x d\theta_x/dx$ , where it can be seen that

$$dI_x = \frac{1}{3} t^3 dy, \quad (2.35)$$

where  $dI_x$  is the torsional constant for the differential segment and will be applied for the approximation of open thin-walled cross-sections.

### 2.5.2 Homogeneous Torsion of Open Thin-Walled Cross-Sections

It is desired to describe the warping function and stresses of thin-walled cross-section by approximating the governing formulas. An open cross-section of a prismatic beam is shown on figure 2.9. An arc-length coordinate  $s$  is defined along the midpoints of the profile wall, where the start position can be chosen arbitrarily. Here it has been chosen that the starting position  $s = 0$  is at one of the free ends, and that  $s$  follows the counter-clock wise direction of the local  $(s, n)$ -coordinate system until the other end located at  $s = L$ .  $L$  denotes the total length of the profile wall, and the wall thickness at the arc-length coordinate  $s$  is specified as  $t(s)$ . The moment arm  $r(s)$  is the distance between the tangent of the centre of the profile wall and the shear centre defined as

$$r(s) = (y - y_S) \frac{dz}{ds} - (z - z_S) \frac{dy}{ds}. \quad (2.36)$$

As mentioned before the cross-section will rotate as a rigid body around the shear centre with the angle  $\theta_x$ . A more detailed derivation of the displacement field due to torsion will be derived here and is illustrated on figure 2.8. Here a point lying in the middle of the profile wall is displaced by a length  $u_s$ . It can be seen that  $\tan(\theta_x/2) r(s) = u_s/2$  and a linearisation due to  $\theta_x$  is of small angles, reveals that  $u_s = \theta_x r(s)$ . Then the displacement in the  $y$ - and  $z$ -direction can be expressed when use of  $\sin \alpha = -(z - z_S)/r(s)$  and  $\cos \alpha = (y - y_S)/r(s)$ :

$$u_y = u_s \sin \alpha = -(z - z_S) \theta_x, \quad u_z = u_s \cos \alpha = (y - y_S) \theta_x. \quad (2.37a-b)$$

By considering the shear strain in the tangent plane ( $s$ -direction) is it assumed that  $\gamma_{xs}(x, s, 0) \approx 0$  (based on the shear stress is 0 here, which is implied in example 2.7).

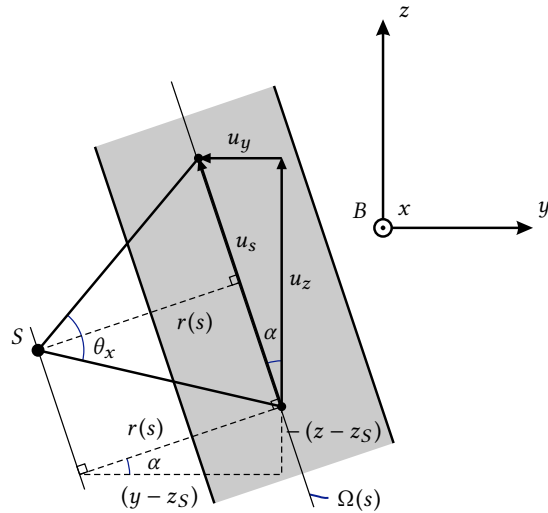


**Figure 2.8:** Torsional displacements due to the rotation  $\theta_x$  around the shear centre.

Then,

$$\gamma_{xs} = \frac{\partial u_x}{\partial s} + \frac{\partial u_s}{\partial x} = \frac{\partial u_x}{\partial s} + \frac{d\theta_x}{dx} r(s) = 0, \quad (2.38a)$$

↓

$$\frac{\partial u_x}{\partial s} = -\frac{d\theta_x}{dx} r(s) = -\frac{d\theta_x}{dx} \frac{d\omega_n(s)}{ds} \quad (2.38b)$$

↓

$$u_x = -\frac{d\theta_x}{dx} \int_{\Omega} r(s) ds + u_0(x) = -\frac{d\theta_x}{dx} \omega_n(s) + u_0(x), \quad (2.38c)$$

where it can be seen according to (2.7a) that  $\omega_n(s) = \int_{\Omega} r(s) ds$  and  $u_0(x)$  is an arbitrary function, which is simply set to 0. As seen the *sector-coordinate* (warping function) with respect to the shear centre  $S$  is defined as:

$$\frac{d\omega(s)}{ds} = r(s), \quad (2.39)$$

and the solution to (2.39) which gives

$$\int_{\Omega} \omega_n(s) t(s) ds = 0, \quad (2.40)$$

is called the *normalized sector-coordinate with respect to  $S$* . If  $\omega$  is an arbitrary solution to (2.39) as

$$\int_{\Omega} \omega(s) t(s) ds = \omega_0, \quad (2.41)$$

then the normalized sector-coordinate is determined by:

$$\omega_n(s) = \omega(s) - \frac{\omega_0}{A}. \quad (2.42)$$

The sector-coordinates can be seen on figure 2.9 where the two different locations of  $\omega_n$  and  $\omega$  are shown.

For thin-walled cross-sections it is further assumed that  $t(s) \ll L$ . Then the profile can be considered to be constructed by differential rectangles of the length  $ds$ , as those illustrated in example 2.1, where each has the torsional constant  $dI_x = 1/3 t^3 ds$ . Thus, the torsional constant for the whole profile is given as

$$I_x = \frac{1}{3} \int_{\Omega} t^3(s) ds. \quad (2.43)$$

The shear stresses are specified in the local  $(x, n, s)$ -coordinate system and (2.33) becomes

$$\sigma_{xs} = 2nG \frac{d\theta_x}{dx}, \quad \sigma_{xn} = 0. \quad (2.44a-b)$$

As  $Gd\theta_x/dx = M_{x,s}/I_x$ , the maximum shear stresses at  $n = t(s)/2$  becomes:

$$\tau = G \frac{d\theta_x}{dx} t(s) = \frac{M_{x,s}}{I_x} t(s). \quad (2.45)$$

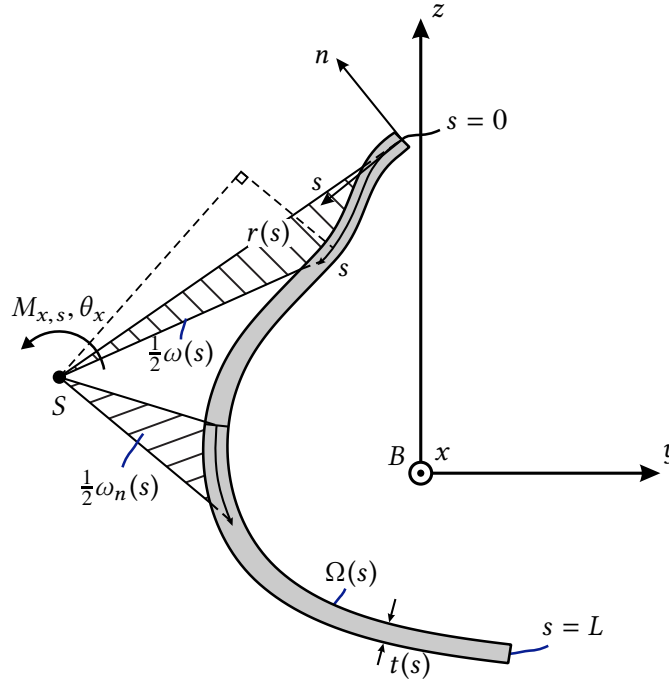


Figure 2.9: Thin-walled cross-section with defined sector-coordinates.

## 2.6 Non-homogeneous Torsion of Open Thin-Walled Cross-Sections

In this section the governing equations for non-homogeneous torsion for thin-walled cross-sections (also commonly referred to as Vlasov torsion).

The displacement field described in (2.38c) is considered and due to non-homogeneous torsion  $d\theta_x/dx$  is no longer a constant. This implies that the elongation strain becomes:

$$\epsilon_{xx} = \frac{\partial u_x}{\partial x} = -\frac{d^2\theta_x}{dx^2}\omega_n(s) \quad (2.46)$$

The normal stresses that stems from warping are found by means of Hookes law, as

$$\sigma_{xx} = -E\frac{d^2\theta_x}{dx^2}\omega_n(s). \quad (2.47)$$

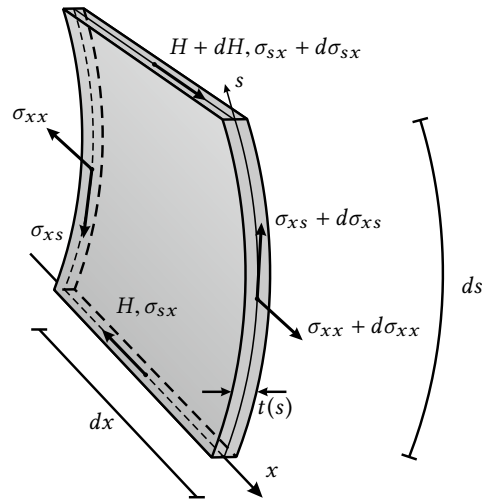


Figure 2.10: Differential element of a thin-walled cross-section.

These normal stresses will induce shear stresses due to equilibrium which will be considered in the following. The shear stress component  $\sigma_{xn}$  vanishes at the surfaces  $n = \pm 1/2t(s)$ , and since  $t \ll L$  it follows from continuity that  $\sigma_{xn}$  is ignorable in the interior of the wall, thus

$$\sigma_{xn} \simeq 0. \quad (2.48)$$

By looking at figure 2.10, a differential element with the side lengths  $dx$  and  $ds$  is cut free from the wall. The shear force per unit length  $H$  and  $H + dH$  acts at the sections with arc-length coordinates  $s$  and  $s + ds$ .

Furthermore due to symmetry of the stress tensor it is implied that  $\sigma_{sx} = \sigma_{xs}$ . Then it is assumed that  $\sigma_{sx}$  is evenly distributed over the wall thickness

$$H(x, s) = \int_{-t/2}^{t/2} \sigma_{sx}(x, n, s) \, dn \simeq \sigma_{xs}(x, s) t(s). \quad (2.49)$$

Equilibrium in the  $x$ -direction by use of figure 2.10 gives:

$$\begin{aligned} 0 &= (\sigma_{xx} + d\sigma_{xx}) t(s) \, ds - \sigma_{xx} t(s) \, ds + (H + dH) \, dx - H \, dx \\ &= d\sigma_{xx} t(s) \, ds + dH \, dx \\ &= \frac{\partial \sigma_{xx}}{\partial x} dx t(s) \, ds + \frac{\partial H}{\partial s} ds \, dx \\ \Downarrow \\ 0 &= \frac{\partial H}{\partial s} + \frac{\partial \sigma_{xx}}{\partial x} t(s) \end{aligned} \quad (2.50)$$

The shear force per unit length is then expressed in terms of the normalized sector coordinate as

$$\frac{\partial H}{\partial s} = -\frac{\partial \sigma_{xx}}{\partial x} t(s) = E \frac{d^3 \theta_x}{dx^3} \omega_n(s) t(s), \quad (2.51a)$$

$$\Downarrow \\ H(x, s) = E \frac{d^3 \theta_x}{dx^3} \int_{\Omega} \omega_n(s) t(s) \, ds + H_0(x), \quad (2.51b)$$

where  $H_0(x)$  represent an integration constant. In open thin-walled cross-sections the boundary condition  $\sigma_{xs} = 0$  applies at the ends of the profile, and to have (2.51b) obey this boundary condition requires that  $H_0(x) = 0$ . The shear stresses are assumed to be constant over the thickness, thus

$$\sigma_{xs} = \frac{1}{t(s)} H(x, s) = \frac{1}{t(s)} E \frac{d^3 \theta_x}{dx^3} \int_{\Omega} \omega_n(s) t(s) \, ds. \quad (2.52)$$

The internal forces that stems from the rotational displacement must only be equivalent to a torsional moment  $M_{x,v}$ . The other components as the normal force, shear forces and bending moments must be zero if the assumed displacement field is valid. The internal forces are related to the stresses by (2.5) and the normal force is:

$$N = \int_A \sigma_{xx} \, dA = -E \frac{d^2 \theta_x}{dx^2} \int_{\Omega} \omega_n(s) t(s) \, ds = 0, \quad (2.53)$$

where it can be seen that the normalized sector-coordinate is used in order to have the condition fulfilled since (2.40) must be true. Furthermore it is realised that the arbitrary function  $u_0(x)$  from (2.38c) must also be zero.

The shear force in the  $y$ -direction is found by projecting  $H(x, s)$  on the  $y$ -axis and integrating over the area as:

$$Q_y = \int_A \sigma_{xy} \, dA = \int_{\Omega} H(x, s) \frac{dy}{ds} \, ds, \quad (2.54)$$

and by integration by parts it is obtained that (2.54) becomes

$$\left[ H(x, s) y \right]_{\Omega} - \int_{\Omega} \frac{\partial H}{\partial s} y \, ds. \quad (2.55)$$

If the integration limits are to set to a profile similar to the one shown in 2.9, it is easy to see that the first term in (2.55) will be 0, due to the fact that  $H(x, s)$  is 0 at the integration limits. It is ensured by (2.51b) that  $H(x, s)$  is 0 at the free boundaries, also if there is branches leading up to multiples ends. Such a cross-section is shown on figure 2.11 and for that case the first term in (2.51a) is also 0. This can be explained by the sign convention as shown on figure 2.11. If the path  $s$  is following the paths as indicated by the figure  $H_i(x, s)$  can be projected on the  $x$ -axis and equilibrium states that

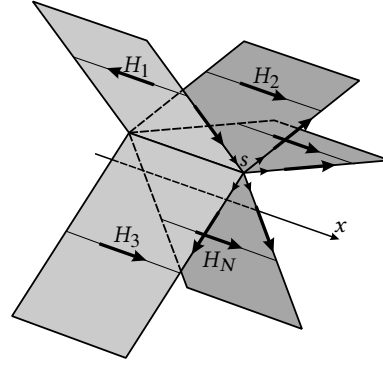


**Figure 2.11:** Equilibrium of shear flow with multiple branches in cross-section.

$$H_1(x, s) = \sum_{i=2}^N H_i(x, s), \quad (2.56)$$

where  $N$  is the total number of branches in the cross-section. With (2.56) inserted in the first term of (2.55) showing that the term must be 0.

Then

$$Q_y = \int_{\Omega} \frac{\partial H}{\partial s} y ds = -E \frac{d^3 \theta_x}{dx^3} \int_{\Omega} \omega_n(s) y t(s) ds = -E \frac{d^3 \theta_x}{dx^3} I_{\omega y}. \quad (2.57a)$$

Similar, with  $H(x, s)$  projected on the  $z$ -axis  $Q_z$  becomes

$$Q_z = \int_{\Omega} \frac{\partial H}{\partial s} z ds = -E \frac{d^3 \theta_x}{dx^3} \int_{\Omega} \omega_n(s) z t(s) ds = -E \frac{d^3 \theta_x}{dx^3} I_{\omega z}. \quad (2.57b)$$

The bending moments is also investigated, and it can be seen that

$$M_y = \int_A \sigma_{xx} z dA = -E \frac{d^2 \theta_x}{dx^2} \int_{\Omega} \omega_n(s) z t(s) ds = -E \frac{d^2 \theta_x}{dx^2} I_{\omega z}, \quad (2.57c)$$

$$M_z = - \int_A \sigma_{xx} y dA = -E \frac{d^2 \theta_x}{dx^2} \int_{\Omega} \omega_n(s) y t(s) ds = -E \frac{d^2 \theta_x}{dx^2} I_{\omega y}. \quad (2.57d)$$

It can be seen that in order to fulfil the conditions that  $Q_y = Q_z = M_y = M_z = 0$  it requires that  $I_{\omega y} = I_{\omega z} = 0$ , which is satisfied when the cross-section rotates about the shear centre  $S$ . The torsional moment must be statically equivalent to the shear force  $H$  acting at the distance  $h(s)$ , which can be expressed as

$$\begin{aligned} M_{x,v} &= \int_{\Omega} H(x, s) r(s) ds = - \int_{\Omega} \frac{\partial H}{\partial s} \omega_n(s) ds = -E \frac{d^2 \theta_x}{dx^2} \int_{\Omega} \omega_n^2(s) t(s) ds \\ &= -EI_{\omega} \frac{d^3 \theta_x}{dx^3}, \end{aligned} \quad (2.58)$$

then the shear stress can be expressed as

$$\sigma_{xs}(x, s) = - \frac{M_{x,v}}{t(s) I_{\omega}} S_{\omega}(s). \quad (2.59)$$

Thus, when a cross-section it subjected to a non-homogeneous torsional moment, the condition  $M_x = M_{x,s} + M_{x,v}$  is met, and with insertion of (2.15) and (2.58) in  $M_x$ , then

$$M_x = GI_x \frac{d\theta_x}{dx} - EI_{\omega} \frac{d^3 \theta_x}{dx^3}. \quad (2.60)$$

Some side notes are made for open thin-walled beams. It is in practical engineering often useful to define a “7<sup>th</sup> internal force”, the bimoment, which is defined as

$$\begin{aligned} B(x) &= \int_{\Omega} \sigma_{xx} \omega_n(s) t(s) ds = -E \frac{d^2 \theta_x}{dx^2} \int_{\Omega} \omega_n^2(s) t(s) ds \\ &= -EI_{\omega} \frac{d^2 \theta_x}{dx^2}. \end{aligned} \quad (2.61)$$

Then the normal stresses can be expressed as

$$\sigma_{xx}(x, s) = \frac{B}{I_{\omega}} \omega_n(s), \quad (2.62)$$

and the shear stresses as

$$\sigma_{xs}(x, s) = -\frac{1}{t(s) I_{\omega}} \frac{dB}{dx} S_{\omega}, \quad (2.63)$$

where  $S_{\omega} = \int_{\Omega} \omega_n(s) t(s) ds$ .

## 2.7 Shear stresses due to Bending in Open Thin-Walled Cross-sections

As seen in section 2.4 the shear forces (and shear stresses) cannot be derived from the kinematic conditions of the beam theory and therefore have to be determined from the static equations instead, which will be dealt with in this section. A thin-walled cross-section is shown on figure 2.12 and subjected to the bending moments  $M_y$  and  $M_z$  and the shear forces  $Q_y$  and  $Q_z$ . The shear stresses  $\sigma_{xs}$  and  $\sigma_{xn}$  are defined in the local  $(x, n, s)$ -coordinate system, which are caused by the shear forces.

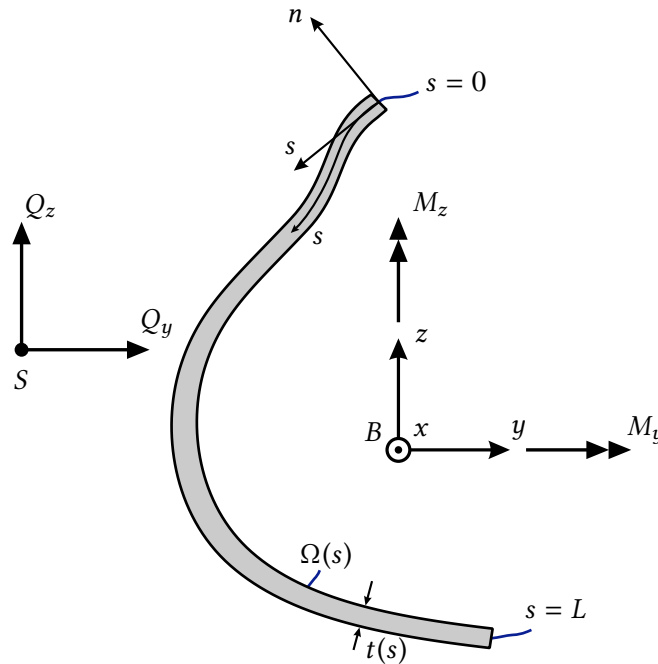


**Figure 2.12:** Thin-walled cross-section exposed to bending.

The normal stress from the bending components follows from (2.11a)

$$\sigma_{xx} = E \left( z \frac{d\theta_y}{dx} - y \frac{d\theta_z}{dx} \right) = \frac{M_y}{I_y} z - \frac{M_z}{I_z} y, \quad (2.64)$$

where  $I_y = \int_A z^2 dA$  and  $I_z = \int_A y^2 dA$  and the relations for  $M_y$  and  $M_z$  have been utilized from (2.5).

The same assumptions as stated in section 2.6 are made. It follows from (2.51b) that

$$\begin{aligned} \frac{\partial H}{\partial s} &= -\frac{\partial \sigma_{xx}}{\partial x} t(s) = -\left( \frac{dM_y}{I_y} z(s) - \frac{dM_z}{I_z} y(s) \right) t(s) \\ &= -\left( \frac{Q_y}{I_z} y(s) + \frac{Q_z}{I_y} z(s) \right) t(s) \end{aligned} \quad (2.65)$$

↓

$$H(x, s) = \int_{\Omega} \frac{\partial \sigma_{xx}}{\partial x} t(s) ds = -\frac{Q_y}{I_z} S_y - \frac{Q_z}{I_y} S_z,$$

where  $S_y = \int_{\Omega} z(s) t(s) ds$  and  $S_z = \int_{\Omega} y(s) t(s) ds$ . It is again used that the integration constant  $H_0(x)$  is 0, which also must be obeyed by the statical moments,  $S_y$  and  $S_z$ . Further, the equilibrium between the bending moment and shear force has been used from (2.4a–f).

The shear stress then becomes

$$\sigma_{xs}(x, s) = \frac{1}{t(s)} H(x, s) = -\frac{Q_y}{t(s) I_z} S_z(s) - \frac{Q_z}{t(s) I_y} S_y(s). \quad (2.66)$$

(2.66) is known as *Grashof's formula*. This equation is used to determine shear stresses in thin-walled beams and is derived from the static equations alone and therefore independent of any kinematic constraint which is known from the beam theory.

## 2.8 Generalised Internal Forces and Stresses

For three-dimensional beam elements the generalized internal forces are given in this section with their associated stresses. All the internal components from  $\mathbf{F}$  and  $\mathbf{M}$  are expressed in terms of  $\mathbf{w}$  and  $\theta_x$  with additional components that stems from the cross-sectional data.

The internal sectional forces and moments follows from (2.11a), (2.5), (2.4a–f), (2.14), and (2.58) and are summarized as

$$N(x) = EA \frac{dw_x}{dx}, \quad (2.67a) \quad Q_z(x) = -EI_y \frac{d^3 w_y}{dx^3}, \quad (2.67e)$$

$$M_y(x) = -EI_y \frac{d^2 w_z}{dx^2}, \quad (2.67b) \quad M_{x,s}(x) = GI_x \frac{d\theta_x}{dx}, \quad (2.67f)$$

$$M_z(x) = EI_z \frac{d^2 w_y}{dx^2}, \quad (2.67c) \quad M_{x,v}(x) = -EI_{\omega} \frac{d^3 \theta_x}{dx^3}, \quad (2.67g)$$

$$Q_y(x) = -EI_z \frac{d^3 w_z}{dx^3}, \quad (2.67d) \quad B(x) = -EI_{\omega} \frac{d^2 \theta_x}{dx^2}. \quad (2.67h)$$

The normal stresses follows from what is referred to as *Navier's generalised formula*:

$$\sigma_{xx} = \frac{N}{A} - \frac{M_z}{I_z} y + \frac{M_y}{I_y} z + \frac{B}{I_{\omega}} \omega_n \quad (2.68)$$

And the shear stresses follows from *Grashof's generalised formula*:

$$\sigma_{xs} = -\frac{1}{t} \left( \frac{Q_y}{I_z} S_z + \frac{Q_z}{I_y} S_y + \frac{M_{x,v}}{I_\omega} S_\omega \pm \frac{M_{x,s}}{I_x} t^2 \right) \quad (2.69)$$

### Example 2.2: Cross-Sectional Properties of a I/H-profile.

Until now the formulas have been derived for an arbitrary open thin-walled cross-section, and in this example the cross-sectional dependent variables are to be determined for a I/H-profile. This includes  $A$ ,  $S_y$ ,  $S_z$ ,  $S_\omega$ ,  $I_x$ ,  $I_y$ ,  $I_z$ ,  $I_\omega$  and  $\omega_n$ . The profile is shown on figure 1.3 with a height  $h$ , width  $b$ , flange thickness  $t_f$ , and web thickness  $t_w$ . Since the cross-section is double symmetric the principle axis are coincide with the lines of symmetry. This implies that the bending and shear centres are also coincide in the double symmetry point.

It is assumed that the thickness is  $t_f \ll b$  and  $t_w \ll h$ , which means that the thin-wall assumption applies. The cross-sectional area and the bending moments of inertia become

$$A = 2t_f b + t_w h, \quad I_y = \frac{1}{2} t_f b h^2 + \frac{1}{12} t_w h^3, \quad I_z = \frac{1}{6} t_f b^3. \quad (2.70a-c)$$

As can be seen on figure 2.13, arc-length coordinates  $s_j$  are defined by the local  $(n_j, s_j)$ -coordinate systems for each of the four branches and for the web of the profile. The statical moment of the area segment (defined by the line domain  $\Omega$ ) around the  $y$ -axis becomes:

$$\begin{aligned} S_y(s_1) &= \frac{1}{2} h t_f s_1, & S_y(s_2) &= \frac{h}{2} t_f s_2 \\ S_y(s_3) &= -\frac{1}{2} h t_f s_3, & S_y(s_4) &= -\frac{1}{2} h t_f s_4, \\ S_y(s_5) &= -\frac{1}{2} b h t_f - \frac{1}{2} t_w s_5 (h - s_5). \end{aligned} \quad (2.71a-e)$$

The statical moment around the  $z$ -axis becomes:

$$\begin{aligned} S_z(s_1) &= \frac{1}{2} t_f s_1 (s_1 - b) & S_z(s_2) &= -\frac{1}{2} t_f s_2 (s_2 - b) \\ S_z(s_3) &= \frac{1}{2} t_f s_3 (s_3 - b) & S_z(s_4) &= -\frac{1}{2} t_f s_4 (s_4 - b) \end{aligned} \quad (2.72a-d)$$

The distribution of these statical moments is visualised on figure 2.14.

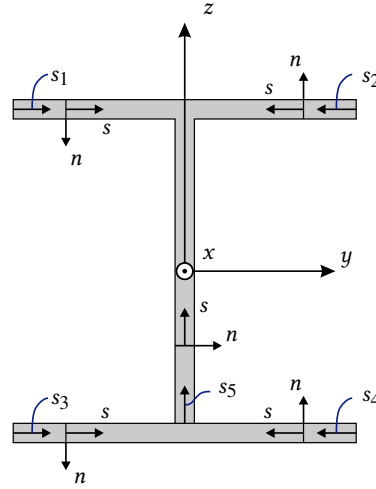


**Figure 2.13:** Definition of arc-length coordinates and local  $(n_j, s_j)$ -coordinate systems.

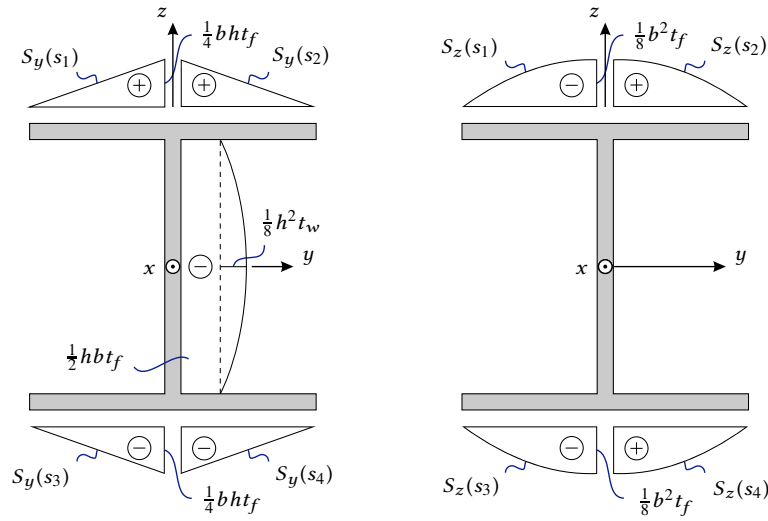


**Figure 2.14:** Distribution of  $S_y$  and  $S_z$  according to the  $(n_j, s_j)$ -coordinate systems.

Next, the normalized warping function  $\omega_n(s)$  is determined. Using the already defined arc-length coordinate  $s_1$  and  $s_2$ , (2.41) becomes

$$\begin{aligned} \omega(s_1) &= -\int_0^b \frac{1}{2} h t_f s_1 ds = -\frac{1}{4} h b^2 t_f \\ \omega(s_2) &= \int_0^b \frac{1}{2} h t_f s_1 ds = \frac{1}{4} h b^2 t_f \end{aligned} \quad (2.73a-b)$$

Then from (2.42) the normalized sector coordinate is found:

$$\begin{aligned} \omega_n(s_1) &= -\frac{1}{2} h s_1 + \frac{h b^2 t_f}{4 b t_f} = \frac{1}{4} h (b - 2s_1) \\ \omega_n(s_2) &= \frac{1}{2} h s_2 - \frac{h b^2 t_f}{4 b t_f} = -\frac{1}{4} (b - 2s_2) \end{aligned} \quad (2.73c-d)$$

Then the static moment of  $\omega_n$  becomes

$$\begin{aligned} S_\omega(s_1) &= \int_0^{s_1} \left( \frac{1}{4} b h - \frac{1}{2} h s_1 \right) t_f ds = \frac{1}{4} h t_f s_1 (b - s_1) \\ S_\omega(s_2) &= \int_0^{s_2} \left( \frac{1}{2} h s_2 - \frac{1}{4} b h \right) t_f ds = -\frac{1}{4} h s_1 t_f (b - s_2) \end{aligned} \quad (2.74a-b)$$

These distributions can be seen on figure 2.15. Finally, the sector moment of inertia becomes,

$$I_\omega = \int_0^b \left( \frac{1}{4} h (b - 2s_1) \right)^2 t_f ds + \int_0^b \left( -\frac{1}{4} (b - 2s_2) \right)^2 t_f ds = \frac{1}{24} h^2 b^3 t_f \quad (2.75)$$

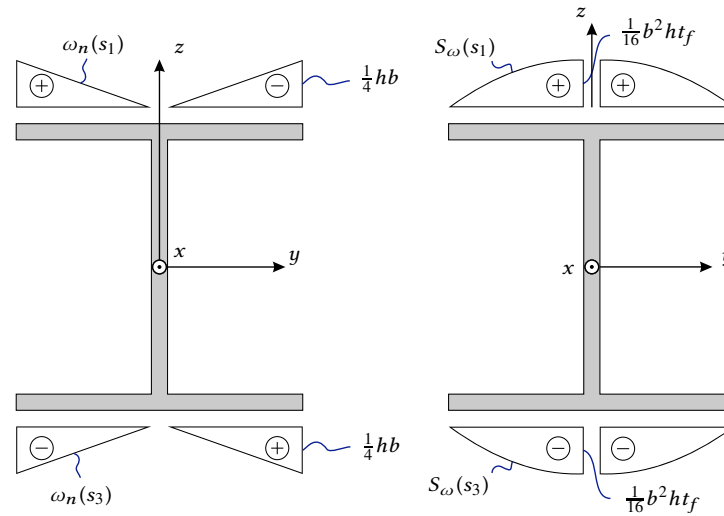


**Figure 2.15:** Distribution of  $S_y$  and  $S_z$  according to the  $(n_j, s_j)$ -coordinate systems.

It is important to notice that the calculated stresses from these cross-sectional dependent quantities are defined after their corresponding  $(n_j, s_j)$ -coordinate system, meaning that if  $\sigma_{x_s}(s_j) < 0$  the stress act in the opposite direction of  $s_j$ . The only  $n_j$ -dependent stress quantity are the shear stresses from St. Venant torsion that acts in both directions of  $s_j$ , which is the reason for the  $\pm$  sign in (2.69) for which the sign that gives the largest magnitude of  $\sigma_{x_s}$  is chosen.

Some final notes are made for torsion of I/H-profiles. As can be seen distribution of the static moment  $S_\omega$ , the shear stresses from Vlasov torsion  $\sigma_{x_s}$  induces opposite resulting shear forces  $Q_f$  in the flanges as shown on figure 2.16.

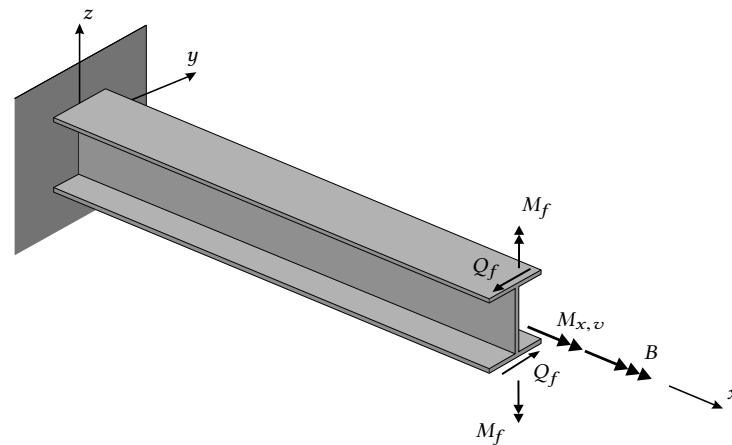


**Figure 2.16:** Vlasov torsional moment and bimoment for I/H profile.

The normal stresses  $\sigma_{x_x}$  follows the distribution of the sector coordinate  $\omega_n$ , which can be seen as a opposite resulting moments in the flanges  $M_f$ , similar to bending of beam cross-sections. The top flange rotates the angle  $\theta_z$  as indicated by figure 2.17.



**Figure 2.17:** Rotation of top flange.

For both flanges the work becomes

$$\delta W_e = 2M_f \delta \theta_z. \quad (2.76)$$

The rotation of the flange can be expressed in terms of the displacement  $u_s(s) = \theta_x r(s)$ . And the rotation angle  $\theta_z$  becomes:

$$\theta_z = -\frac{du_s}{dx} = -\frac{d\theta_x}{dx} r(s). \quad (2.77)$$

Thus, the external work done is

$$\begin{aligned} \delta W_e &= -2M_f r(s) \frac{d\delta\theta_x}{dx}, \\ &= -B(x) \frac{d\delta\theta_x}{dx}, \end{aligned} \quad (2.78)$$

meaning that the generalised virtual displacement work conjugated to  $B(x)$  is  $-\delta\theta'_x$ .

## 2.9 Differential Equations

In the following the governing differential equations to describe beam deformations are derived. These includes axial, bending and torsional deformation.

### Axial Deformation

(2.67a) may be recast from the axial equilibrium equation (2.4a–f) to the differential equation

$$\frac{d}{dx} \left( EA \frac{dw_x}{dx} \right) + q_x = 0. \quad (2.79)$$

This equation should be solved with proper boundary conditions. Let  $x_0$  denote the abscissa of any of the two end-section, then  $x_0$  is either  $x_0 = 0$  or  $x_0 = l$ . At  $x = x_0$  either kinematical or mechanical boundary conditions may be prescribed as:

$$\left. \begin{aligned} w_x(x_0) &= w_{x,0} \\ N(x_0) &= N_0 \end{aligned} \right\}, \quad \text{for } x_0 = 0, l. \quad (2.80)$$

### Bending Deformation

(2.67b) and (2.67c) are recast from the equilibrium equations expressed by (2.4a–f). The differential equations for bending deformations become:

$$\frac{d^2}{dx^2} \left( EI_z \frac{d^2 w_y}{dx^2} \right) - q_y + \frac{dm_z}{dx} = 0, \quad (2.81a)$$

$$\frac{d^2}{dx^2} \left( EI_y \frac{d^2 w_z}{dx^2} \right) - q_z - \frac{dm_y}{dx} = 0, \quad (2.81b)$$

with the boundary conditions

$$\left. \begin{aligned} w_y(x_0) &= w_{y,0} \\ w_z(x_0) &= w_{z,0} \\ w'_z(x_0) &= \theta_{y,0} \\ w'_y(x_0) &= \theta_{z,0} \\ M_y(x_0) &= M_{y,0} \\ M_z(x_0) &= M_{z,0} \end{aligned} \right\}, \quad \text{for } x_0 = 0, l. \quad (2.82)$$

### Homogeneous Torsion

Recasting (2.67f) with the equilibrium equations from (2.4a–f), the following differential equation is obtained

$$\frac{d}{dx} \left( GI_x \frac{d\theta_x}{dx} \right) + m_x = 0, \quad (2.83)$$

with the boundary conditions

$$\left. \begin{aligned} \theta_x(x_0) &= \theta_{x,0} \\ M_x(x_0) &= M_{x,0} \end{aligned} \right\}, \quad \text{for } x_0 = 0, l. \quad (2.84)$$

### Non-homogeneous Torsion

The total torsional moment is expressed as  $M_x = M_{x,s} + M_{x,v}$ , which is recast by the equilibrium equations from (2.4a–f) to

$$GI_x \frac{d^2\theta_x}{dx^2} - EI_\omega \frac{d^4\theta}{dx^4} + m_x = 0, \quad (2.85)$$

with the boundary conditions

$$\left. \begin{aligned} \theta_x(x_0) &= \theta_{x,0} \\ \theta'_x(x_0) &= \theta'_{x,0} \\ M_x(x_0) &= M_{x,0} \\ B(x_0) &= B_0 \end{aligned} \right\}, \quad \text{for } x_0 = 0, l. \quad (2.86)$$

**Example 2.3: Non-homogeneous Torsion of Cantilever I/H-beam Exposed to a Torsional Moment.**

A cantilever beam as shown on figure 1.3 is exposed to the torsional moment  $M_x = M_0$  at  $x = l$ .  $m_x = 0$  and the differential equation of (2.85) becomes

$$-EI_\omega \frac{d^4 \theta_x}{dx^4} + GI_x \frac{d^2 \theta_x}{dx^2} = 0, \quad (2.87a)$$

↓

$$\frac{d^4 \theta_x}{dx^4} - k^2 \frac{d^2 \theta_x}{dx^2} = 0, \quad (2.87b)$$

where  $k^2 = GI_x / (EI_\omega)$ . At  $x = 0$  both the rotation and warping is prevented, meaning that the kinematic boundary conditions become

$$\theta_x(0) = 0, \quad (2.88a)$$

$$u_x(0) = -\frac{d}{dx} \theta_x(0) \omega_n(s) = 0 \Rightarrow \frac{d}{dx} \theta_x(0) = 0. \quad (2.88b)$$

The mechanical boundary condition follows from (2.60) and (2.61) as

$$\begin{aligned} M_0 &= GI_x \frac{d}{dx} \theta_x(l) - EI_\omega \frac{d^3}{dx^3} \theta_x(l), \\ 0 &= -EI_\omega \frac{d^2}{dx^2} \theta_x(l). \end{aligned} \quad (2.89)$$

The general solution to (2.87b) has the form of

$$\theta_x(x) = c_0 + c_1 x + c_2 \cosh kx + c_3 \sinh kx. \quad (2.90)$$

From the kinematic boundary conditions at  $x = 0$  it is found that

$$\left. \begin{aligned} c_0 + c_2 &= 0 \\ c_1 + c_3 k &= 0 \end{aligned} \right\} \quad (2.91)$$

thus, the solution fulfilling the kinematic boundary conditions can be expressed with only the integration constants  $c_2$  and  $c_3$  as

$$\theta_x(x) = c_2 (\cosh kx - 1) + c_3 (\sinh kx - kx). \quad (2.92)$$

A unique solution for  $c_2$  and  $c_3$  is now sought. (2.89) can be expressed in another way as,

$$\frac{M_0}{GI_x} = \frac{d}{dx} \theta_x(l) - \frac{1}{k^2} \frac{d^3}{dx^3} \theta_x(l), \quad (2.93)$$

$$0 = \frac{d^2}{dx^2} \theta_x(l). \quad (2.94)$$

Insertion of (2.92) in (2.93) results in

$$\frac{M_0}{GI_x} = -c_3 k, \quad (2.95)$$

↓

$$-\frac{M_0}{GI_x k} = c_3. \quad (2.96)$$

Next,  $c_2$  is determined by insertion of (2.92) with  $c_3$  from (2.96) in (2.93). Then,

$$0 = c_2 \cosh(kl) k^2 - \frac{M_0}{GI_x} \sinh(kl) k, \quad (2.97)$$

↓

$$c_2 = \frac{M_0}{GI_x k} \tanh kl, \quad (2.98)$$

↓

$$\theta_x(x) = \frac{M_0}{GI_x k} (\tanh kl (\cosh kx - 1) - (\sinh kx - kx)) \quad (2.99)$$

Then  $M_{x,s}(x)$ ,  $M_{x,v}(x)$  and  $B(x)$  becomes from (2.15), (2.58) and (2.61):

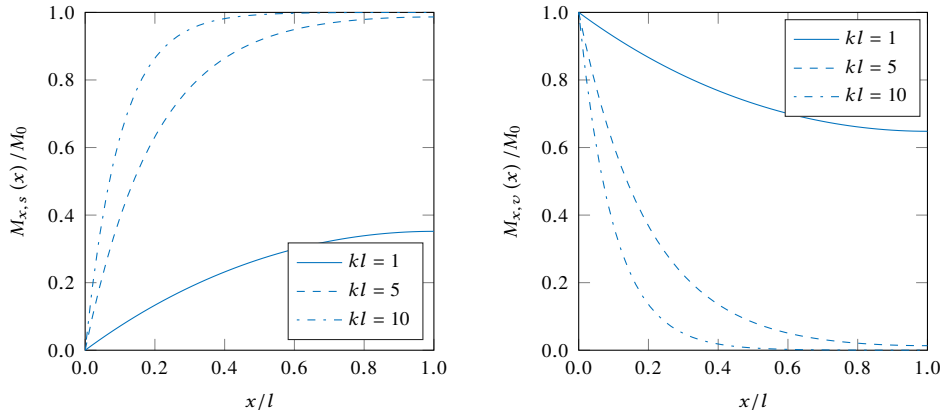
$$M_{x,s}(x) = M_0 + M_0 (\tanh kl \sinh kx - \cosh kx) \quad (2.100a)$$

$$M_{x,v}(x) = -M_0 (\tanh kl \sinh kx - \cosh kx) \quad (2.100b)$$

$$B(x) = -\frac{M_0}{k} (\tanh kl \cosh kx - \sinh kx) \quad (2.100c)$$

As expected  $M_{x,s}(x) + M_{x,v}(x) = M_0$ .

Figure 2.18 shows the variation of  $M_{x,s}(x)$  and  $M_{x,v}(x)$  for  $kl = 1, 5$  and  $10$ . Close to the support at  $x = 0$  the torsional moment  $M_0$  is primarily carried by the Vlasov moment, whereas the St. Venant moment is small. For  $kl = 1$  both torsion mechanisms contribute to  $M_0$  throughout the beam. However, for  $kl = 10$  the influence of the Vlasov moment reduces fast, and the torsional moment  $M_0$  is carried by St. Venant in the major part of the beam. The variation of  $B(x)$  shows the largest values at the fixed support where the warping is prevented and induces the largest normal stresses. At the free end the beam can warp freely which means the normal stresses is zero, thus  $B(l) = 0$ .



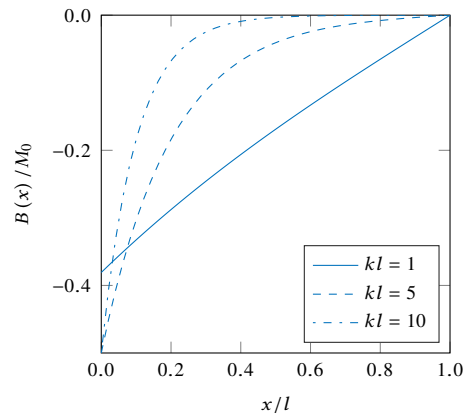


**Figure 2.18:** Variation of  $M_{x,s}/M_0$ ,  $M_{x,v}/M_0$  and  $B(x)/M_0$  along the beam for  $kl = 1, 5$  and  $10$ . For  $B(x)$   $k$  is set to  $2$ .

If one were to calculate  $\theta_x$  by homogeneous torsion it is obtained that  $\theta_x(l) = M_0 / (GI_x) l$ , and by non-homogeneous torsion

$$\theta_x(l) = \frac{M_0}{GI_x k} (kl - \tanh kl) = \frac{M_0}{GI_x} l \left( 1 - \frac{1}{kl} \tanh kl \right), \quad (2.101)$$

where it can be seen that the torsional angle is less than for homogeneous torsion. For increasing values of  $l$  it can be seen that

$$\lim_{l \rightarrow \infty} \left( \frac{M_0}{GI_x} l \left( 1 - \frac{1}{kl} \tanh kl \right) \right) = \frac{M_0}{GI_x} l. \quad (2.102)$$



# 3 Basics of the Finite Element Method

---

The basic theory of the finite element method will be outlined in this chapter. The idea is to make discretization of a structural system into a number of beam elements, each with two nodal points. Subsequently, displacement, internal forces and moments can be determined by cutting free a beam element at the nodes and formulate equilibrium at the nodes with help from the principle of virtual displacements, which is used to derive the stiffness matrix and nodal load vector for a beam element, such that these are connected to the corresponding deformation at the beam ends. Sources for the following derivations are [Andersen and Nielsen, 2008] and [Kindmann and Kraus, 2011].

## 3.1 The Principle of Virtual Displacements

In the principle of virtual displacements the actual sectional forces and moments are assumed to be in equilibrium with the loads and the reaction forces applied at the end sections. The virtual displacements (and rotations) are considered as arbitrary increments to the actual displacements and they only need to fulfil homogeneous kinematic boundary conditions, so that the combined field of the actual forces and virtual displacement always fulfils the actual non-homogeneous boundary conditions.

The virtual work for linear beam theory becomes:

$$\begin{aligned} \delta W_i &= \int_V \delta \varepsilon_{xx} \sigma_{xx} + \delta \gamma_{xs} \sigma_{xs} dV \\ &= \int_0^l \frac{d\delta w_u}{dx} EA \frac{dw_u}{dx} + \frac{d^2 \delta w_y}{dx^2} EI_z \frac{d^2 w_y}{dx^2} + \frac{d^2 \delta w_z}{dx^2} EI_y \frac{d^2 w_z}{dx^2} \\ &\quad + \frac{d\delta \theta_x}{dx} GI_x \frac{d\theta_x}{dx} + \frac{d^2 \delta \theta_x}{dx^2} EI_\omega \frac{d^2 \theta_x}{dx^2} dx \end{aligned} \quad (3.1)$$

The external virtual work due to concentrated forces follows as:

$$\begin{aligned} \delta W_e &= \delta w_x N_x + \delta w_y Q_y + \delta w_z Q_z + \delta \theta_z M_z \\ &\quad + \delta \theta_y M_y + \delta \theta_x M_x - \frac{d\delta \theta_x}{dx} B \end{aligned} \quad (3.2)$$

And the external virtual work for distributed loads per unit length is:

$$\begin{aligned} \delta \omega_e &= \delta w_x q_x + \delta w_y q_y + \delta w_z q_z \\ &\quad + \delta \theta_y m_y + \delta \theta_z m_z + \delta \theta_x m_x \end{aligned} \quad (3.3)$$

### 3.2 Basic Deformation and Shape Functions

On figure 3.1 a beam element with the length  $l$  and the stiffness constants  $EA$ ,  $GI_x$  and  $EI_\omega$  are shown. The sign convention for FEM differs from the derived theory as both end-nodes have same sign convention as illustrated on the figure. The element has 7 degrees of freedom defining the displacements, rotations and the extra nodal degree of freedom introduced, denoted as the rotation gradient  $-\theta'_{x,j}$ , at both ends.

$$\mathbf{w}_e = \begin{bmatrix} \mathbf{w}_{e,1} \\ \mathbf{w}_{e,2} \end{bmatrix} = \begin{bmatrix} w_{x,1} & w_{y,1} & w_{z,1} & \theta_{x,1} & \theta_{y,1} & \theta_{z,1} & -\theta'_{x,1} \\ w_{x,2} & w_{y,2} & w_{z,2} & \theta_{x,2} & \theta_{y,2} & \theta_{z,2} & -\theta'_{x,2} \end{bmatrix}^T \quad (3.4)$$

The rotation gradient is chosen as negative, since the bimoment  $B$  is work conjugated to the rotation gradient by the relation  $\delta W = -B\delta\theta'_x$ . The opposite sign convention could have been chosen for the rotation gradient, but since it is often the applied loads which are known and displacement only known at supports, the chosen sign convention seems more appropriate.

The nodal forces are assembled in the vector:

$$\mathbf{r}_e = \begin{bmatrix} \mathbf{r}_{e,1} \\ \mathbf{r}_{e,2} \end{bmatrix} = \begin{bmatrix} N_1 & Q_{y,1} & Q_{z,1} & M_{x,1} & M_{y,1} & M_{z,1} & B_1 \\ N_2 & Q_{y,2} & Q_{z,2} & M_{x,2} & M_{y,2} & M_{z,2} & B_2 \end{bmatrix}^T \quad (3.5)$$

The idea is to use appropriate shape functions to describe the displacement field through-

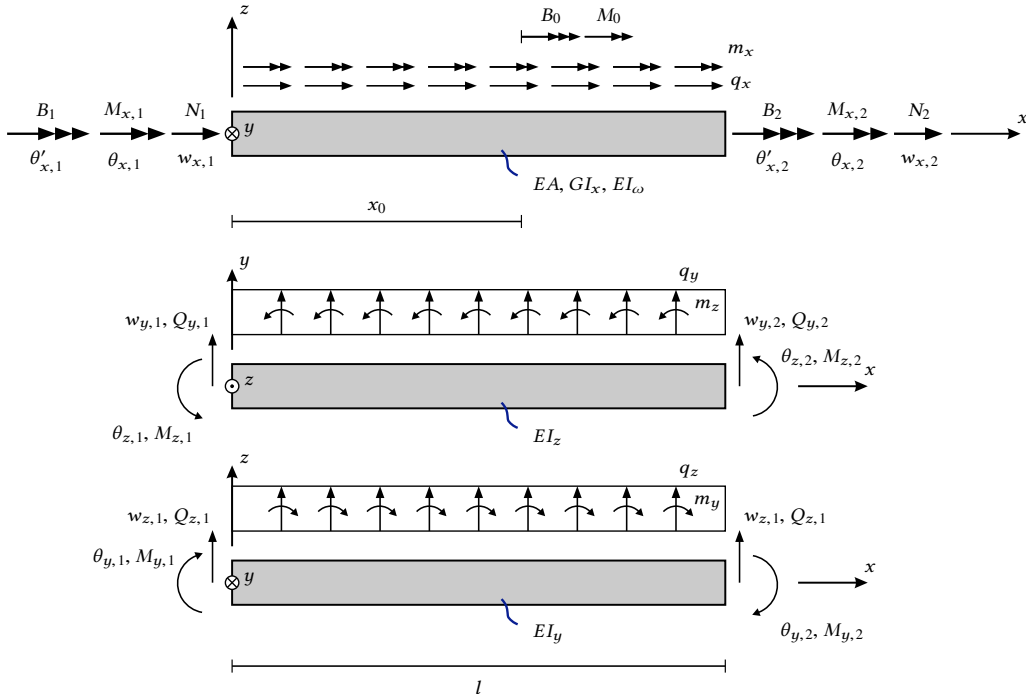


**Figure 3.1:** Beam element with definition of degrees of freedom and nodal reaction forces.

out the beam by interpolating the nodal displacement values, expressed as:

$$\mathbf{u}_e(x) = \Phi(x) \mathbf{w}_e, \quad (3.6)$$

and the virtual displacement field in the element,

$$\delta \mathbf{u}_e(x) = \mathbf{\Psi}(x) \delta \mathbf{w}_e. \quad (3.7)$$

### Deformation by Axial Force

The differential equation for this case is described by (2.79). Ignoring the term of  $q_x$  double integration leads to solution

$$w_x(x) = c_0 + c_1 x, \quad (3.8)$$

and with the boundary conditions  $w_x(0) = w_{x,1}$  and  $w_x(l) = w_{x,2}$  the function for the longitudinal displacement becomes a first degree polynomial,

$$w_x(x) = \left(1 - \frac{x}{l}\right) w_{x,1} + \frac{x}{l} w_{x,2}, \quad (3.9)$$

and can be expressed in terms of linear shape functions  $\phi_1(x)$  and  $\phi_2(x)$ :

$$w_x(x) = \begin{bmatrix} \phi_1(x) & \phi_2(x) \end{bmatrix} \begin{bmatrix} w_{x,1} \\ w_{x,2} \end{bmatrix}, \quad (3.10)$$

where  $\phi_1(x) = 1 - x/l$  and  $\phi_2(x) = x/l$ . These correspond to the deformation at the given node by adopting the value 1, while the deformation at the other node describes the value 0.

### Deformation by Bending

The differential equation describing the bending deformation around the  $z$ -axis is given by (2.81a). Ignoring the term of  $q_y$  and integration four times leads to

$$w_y(x) = c_0 + c_1 x + c_2 x^2 + c_3 x^3. \quad (3.11)$$

With the boundary condition  $w_y(0) = w_{y,1}$ ,  $w_y(l) = w_{y,2}$ ,  $w'_y(0) = \theta_{z,1}$  and  $w'_y(l) = \theta_{z,2}$  it follows that

$$\begin{aligned} w_y(x) = & \left(1 - 3\frac{x^2}{l^2} + 2\frac{x^3}{l^3}\right) w_{y,1} + \left(x - 2\frac{x^2}{l} + \frac{x^3}{l^2}\right) \theta_{z,1} \\ & + \left(3\frac{x^2}{l^2} - 2\frac{x^3}{l^3}\right) w_{y,2} + \left(\frac{x^3}{l^2} - \frac{x^2}{l}\right) \theta_{z,2}, \end{aligned} \quad (3.12)$$

or more compactly:

$$w_y(x) = \begin{bmatrix} \phi_3(x) & \phi_4(x) & \phi_5(x) & \phi_6(x) \end{bmatrix} \begin{bmatrix} w_{y,1} \\ \theta_{z,1} \\ w_{y,2} \\ \theta_{z,2} \end{bmatrix}, \quad (3.13)$$

The same is now done with bending around the  $y$ -axis.  $w_z(x)$  is described with the same polynomial as (3.11) but with the change of the boundary conditions as,  $w'_z(0) = -\theta_{y,1}$  and  $w'_z(l) = -\theta_{y,2}$ , which stems from (2.8). This means that

$$w_z(x) = \begin{bmatrix} \phi_3(x) & -\phi_4(x) & \phi_5(x) & -\phi_6(x) \end{bmatrix} \begin{bmatrix} w_{z,1} \\ \theta_{y,1} \\ w_{z,2} \\ \theta_{y,2} \end{bmatrix}. \quad (3.14)$$

### Deformation by Homogeneous Torsion

Integration twice of (2.83) leads to the equation

$$\theta_x(x) = c_0 + c_1x \quad (3.15)$$

which is similar to the case with axial displacement, which means that a first degree polynomial for the shape function is suitable. With the boundary conditions  $\theta'_x(0) = \theta_{x,1}$  and  $\theta'_x(l) = \theta_{x,2}$ , then

$$\theta_x(x) = \left(1 - \frac{x}{l}\right) \theta_{x,1} + \frac{x}{l} \theta_{x,2}, \quad (3.16)$$

or

$$\theta_x(x) = \begin{bmatrix} \phi_1(x) & \phi_2(x) \end{bmatrix} \begin{bmatrix} \theta_{x,1} \\ \theta_{x,2} \end{bmatrix}. \quad (3.17)$$

### Deformation by Non-Homogeneous Torsion

The general solution to (2.85) takes the form of (2.90). As it can be seen, if one were to derive the shape functions based on hyperbolic functions, these will be included in the stiffness matrix which can lead to numerical difficulties for small or large values of  $kl$  implied by the sources [Damkilde, 1999] and [Kindmann and Kraus, 2011]. Instead other suitable shape functions are sought. The functions must be at least three times differential, and the cubic functions from (3.13) is used, which results in

$$\begin{aligned} \theta_x(x) = & \left(1 - 3\frac{x^2}{l^2} + 2\frac{x^3}{l^3}\right) \theta_{x,1} + \left(x - 2\frac{x^2}{l} + \frac{x^3}{l^2}\right) \theta'_{x,1} \\ & + \left(3\frac{x^2}{l^2} - 2\frac{x^3}{l^3}\right) \theta_{x,2} + \left(\frac{x^3}{l^2} - \frac{x^2}{l}\right) \theta'_{x,2}, \end{aligned} \quad (3.18)$$

or more compactly:

$$\theta_x(x) = \begin{bmatrix} \phi_3(x) & -\phi_4(x) & \phi_5(x) & -\phi_6(x) \end{bmatrix} \begin{bmatrix} \theta_{x,1} \\ -\theta'_{x,1} \\ \theta_{x,2} \\ -\theta'_{x,2} \end{bmatrix}. \quad (3.19)$$

The shape functions describing the exact displacement from (2.90) is obtained by solving the integration constants for the boundary conditions  $\theta_x(0) = \theta_{x,1}$ ,  $\theta'_x(0) = \theta'_{x,1}$ ,  $\theta_x(l) = \theta_{x,2}$  and  $\theta'_x(l) = \theta'_{x,2}$ . Then the shape functions  $\phi_7$ ,  $\phi_8$ ,  $\phi_9$  and  $\phi_{10}$  can be found in Appendix D, and the torsional rotation expressed in terms of the nodal values is expressed as

$$\theta_x(x) = \begin{bmatrix} \phi_7(x) & -\phi_8(x) & \phi_9(x) & -\phi_{10}(x) \end{bmatrix} \begin{bmatrix} \theta_{x,1} \\ -\theta'_{x,1} \\ \theta_{x,2} \\ -\theta'_{x,2} \end{bmatrix}. \quad (3.20)$$

## 3.3 Stiffness Matrix for a Beam Element

In this section the stiffness matrix will be derived for a beam element by use of the principle of virtual work.

### Axial Stiffness

The weak form of the differential equation from (2.79), with a virtual (variation) field  $\delta w_y$  and afterwards integrated by parts with respect to  $x$ :

$$\begin{aligned} & \int_0^l \delta w_x EA \frac{d^2 w_x}{dx^2} dx + \int_0^l \delta w_x q_x dx = 0 \\ \Downarrow & \\ & \int_0^l \frac{d\delta w_x}{dx} EA \frac{du}{dx} dx = \left[ \delta w_x N \right]_0^l + \int_0^l \delta w_x q_x dx \end{aligned} \quad (3.21)$$

The physical displacement field is here denoted as  $w_x(x) = \Phi(x) \mathbf{w}_e$ , which includes the values from (3.10). The weight function is used in the virtual field as  $\delta w_x(x) = \Psi(x) \delta \mathbf{w}_e$ , and by use of the *Galerkin approach* it is known that  $\Psi(x) = \Phi(x)$ . These are substituted in (3.21) and it is obtained that

$$\begin{aligned} & \delta \mathbf{w}_e^T \int_0^l \frac{d\Phi^T}{dx} EA \frac{d\Phi}{dx} dx \mathbf{w}_e = \delta \mathbf{w}_e^T \left[ \Phi^T N \right]_0^l + \delta \mathbf{w}_e^T \int_0^l \Phi^T q_x dx, \\ \Downarrow & \\ & \underbrace{\int_0^l \frac{d\Phi^T}{dx} EA \frac{d\Phi}{dx} dx}_{\mathbf{K}_e} \mathbf{w}_e = \underbrace{\left[ \Phi^T N \right]_0^l + \int_0^l \Phi^T q_x dx}_{\mathbf{f}_e = \mathbf{r}_e + \mathbf{q}_e}, \end{aligned} \quad (3.22)$$

$$\Downarrow \quad \frac{EA}{l} \begin{bmatrix} 1 & -1 \\ -1 & 1 \end{bmatrix} \begin{bmatrix} w_{x,1} \\ w_{x,2} \end{bmatrix} = \begin{bmatrix} N_1 \\ N_2 \end{bmatrix} + \frac{l}{2} \begin{bmatrix} q_x \\ q_x \end{bmatrix}, \quad (3.23)$$

where  $\mathbf{K}_e$  is the element stiffness matrix and  $\mathbf{f}_e$  is the total load vector composed of the vector  $\mathbf{r}_e$ , which is the reaction forces and  $\mathbf{q}_e$  is the element load vector. It can be seen that the weak form of (3.21) corresponds to the internal and external virtual work as stated in (3.1), (3.2) and (3.3).

### Bending Stiffness

The bending stiffness will be derived from the strong form of (2.81a). The weak form is obtained by multiplication of  $\delta w_y(x)$  and the moment per unit length is multiplied by  $\delta \theta_z = \delta w'_y$  as follows.

$$\begin{aligned} & \int_0^l \delta w_y EI_z \frac{d^4 w_y}{dx^4} dx = \int_0^l \delta w_y q_y dx + \int_0^l \delta \theta_z m_z dx \\ \Downarrow & \\ & \int_0^l \frac{d^2 \delta w_y}{dx^2} EI_z \frac{d^2 w_y}{dx^2} dx = \left[ \frac{d\delta w_y}{dx} M_z \right]_0^l - \left[ \delta w_y Q_y \right]_0^l \\ & \quad + \int_0^l \delta w_y q_y dx + \int_0^l \frac{d\delta w_y}{dx} m_z dx \end{aligned} \quad (3.24)$$

By again using Galerkin's approach and using the same weight functions as shape function, which is described by (3.13), the weak form becomes:

$$\begin{aligned} \delta \mathbf{w}_e^\top \int_0^l \frac{d^2 \Phi^\top}{dx^2} EI_z \frac{d^2 \Phi}{dx^2} dx \mathbf{w}_e &= \delta \mathbf{w}_e^\top \left( \left[ \frac{d\Phi^\top}{dx} M_z \right]_0^l - \left[ \Phi^\top Q_y \right]_0^l + \int_0^l \Phi^\top q_y + \frac{d\Phi^\top}{dx} m_z dx \right) \\ \Downarrow \\ \int_0^l \frac{d^2 \Phi^\top}{dx^2} EI_z \frac{d^2 \Phi}{dx^2} dx \mathbf{w}_e &= \left[ \frac{d\Phi^\top}{dx} M_z \right]_0^l - \left[ \Phi^\top Q_y \right]_0^l + \int_0^l \Phi^\top q_y + \frac{d\Phi^\top}{dx} m_z dx \end{aligned} \quad (3.25)$$

$$\Downarrow \frac{EI_z}{l^3} \begin{bmatrix} 12 & 6l & -12 & 6l \\ 6l & 4l^2 & -6l & 2l^2 \\ -12 & -6l & 12 & -6l \\ 6l & 2l^2 & -6l & 4l^2 \end{bmatrix} \begin{bmatrix} w_{y,1} \\ \theta_{z,1} \\ w_{y,2} \\ \theta_{z,2} \end{bmatrix} = \begin{bmatrix} Q_{y,1} \\ M_{z,1} \\ Q_{y,2} \\ M_{z,2} \end{bmatrix} + \begin{bmatrix} q_y l/2 - m_z \\ q_y l^2/12 \\ q_y l/2 + m_z \\ -q_y l^2/12 \end{bmatrix} \quad (3.26)$$

The same can be done for bending around the  $y$ -axis, which will not be shown fully here, but the finite element form obtains the form with the shape functions from (3.14):

$$\int_0^l \frac{d^2 \Phi^\top}{dx^2} EI_y \frac{d^2 \Phi}{dx^2} dx \mathbf{w}_e = \left[ \frac{d\Phi^\top}{dx} M_y \right]_0^l - \left[ \Phi^\top Q_z \right]_0^l + \int_0^l \Phi^\top q_z - \frac{d\Phi^\top}{dx} m_y dx \quad (3.27)$$

$$\Downarrow \frac{EI_y}{l^3} \begin{bmatrix} 12 & -6l & -12 & -6l \\ -6l & 4l^2 & 6l & 2l^2 \\ -12 & 6l & 12 & 6l \\ -6l & 2l^2 & 6l & 4l^2 \end{bmatrix} \begin{bmatrix} w_{z,1} \\ \theta_{y,1} \\ w_{z,2} \\ \theta_{y,2} \end{bmatrix} = \begin{bmatrix} Q_{z,1} \\ M_{y,1} \\ Q_{z,2} \\ M_{y,2} \end{bmatrix} + \begin{bmatrix} q_z l/2 + m_y \\ -q_z l^2/12 \\ q_z l/2 - m_y \\ q_z l^2/12 \end{bmatrix} \quad (3.28)$$

### Homogeneous Torsion Stiffness

The weak form of (2.83) is obtained by multiplying with the virtual displacement  $\delta\theta_x$  and integrating over the domain:

$$\int_0^l \delta\theta_x GI_x \frac{d^2 \theta_x}{dx^2} dx + \int_0^l \delta\theta_x m_x dx = 0 \quad (3.29)$$

$$\Downarrow \int_0^l \frac{d\delta\theta_x}{dx} GI_x \frac{d\theta_x}{dx} dx = \left[ \delta\theta_x M_x \right]_0^l + \int_0^l \delta\theta_x m_x dx \quad (3.30)$$

Using the relation  $\theta_x(x) = \Phi(x) \mathbf{w}_e$  from (3.17) and assuming the Galerkin approach it is provided that

$$\begin{aligned} \delta \mathbf{w}_e^\top \int_0^l \frac{d\Phi^\top}{dx} GI_x \frac{d\Phi}{dx} dx \mathbf{w}_e &= \delta \mathbf{w}_e^\top \left( \left[ \Phi^\top M_x \right]_0^l + \int_0^l \Phi^\top m_x dx \right) \\ \Downarrow \\ \int_0^l \frac{d\Phi^\top}{dx} GI_x \frac{d\Phi}{dx} dx \mathbf{w}_e &= \left[ \Phi^\top M_x \right]_0^l + \int_0^l \Phi^\top m_x dx \end{aligned} \quad (3.31)$$

$$\Downarrow \frac{GI_x}{l} \begin{bmatrix} 1 & -1 \\ -1 & 1 \end{bmatrix} \begin{bmatrix} \theta_{x,1} \\ \theta_{x,2} \end{bmatrix} = \begin{bmatrix} M_{x,1} \\ M_{x,2} \end{bmatrix} + \frac{l}{2} \begin{bmatrix} m_x \\ m_x \end{bmatrix}, \quad (3.32)$$

### Non-Homogeneous Torsion Stiffness

The differential equation describing the phenomenon of non-homogeneous torsion was derived and described by (2.85). Multiplying the strong form by the virtual displacement  $\delta\theta_x$  and integrating over the domain, the weak form is obtained:

$$\int_0^l \delta\theta_x GI_x \frac{d^2\theta_x}{dx^2} dx - \int_0^l \delta\theta_x EI_\omega \frac{d^4\theta_x}{dx^4} dx + \int_0^l \delta\theta_x m_x dx = 0$$

$$\Downarrow$$

$$\int_0^l \frac{d\delta\theta_x}{dx} GI_x \frac{d\theta_x}{dx} + \frac{d^2\delta\theta_x}{dx^2} EI_\omega \frac{d^2\theta_x}{dx^2} dx = \left[ \delta\theta_x M_x \right]_0^l + \left[ -\frac{d\delta\theta_x}{dx} B \right]_0^l + \int_0^l \delta\theta_x m_x dx \quad (3.33)$$

Furthermore, it is desired to distribute a concentrated torsion moment  $M_0$  and bimoment  $B_0$  at the abscisse  $x_0$ . By use of the virtual work, the following is added to the right side of (3.33),

$$\delta W_e = \delta\theta_x(x_0) M_0 - \delta\theta'_x(x_0) B_0. \quad (3.34)$$

Then by Galerkin's approach the finite element form of (3.33) is described by inserting the relation from (3.19):

$$\int_0^l \left( \frac{d\Phi^\top}{dx} GI_x \frac{d\Phi}{dx} + \frac{d^2\Phi^\top}{dx^2} EI_\omega \frac{d^2\Phi}{dx^2} \right) dx \mathbf{w}_e = \left[ \Phi^\top M_x - \frac{d\Phi^\top}{dx} B \right]_0^l + \int_0^l \Phi^\top m_x dx$$

$$+ \Phi^\top(x_0) M_0 - \frac{d}{dx} \Phi^\top(x_0) B_0$$

$$\Updownarrow$$

$$\left( \frac{GI_x}{30l} \begin{bmatrix} 36 & -3l & -36 & -3l \\ -3l & 4l^2 & 3l & -l^2 \\ -36 & 3l & 36 & 3l \\ -3l & -l^2 & 3l & 4l^2 \end{bmatrix} + \frac{EI_\omega}{l^3} \begin{bmatrix} 12 & -6l & -12 & -6l \\ -6l & 4l^2 & 6l & 2l^2 \\ -12 & 6l & 12 & 6l \\ -6l & 2l^2 & 6l & 4l^2 \end{bmatrix} \right) \begin{bmatrix} \theta_{x,1} \\ -\theta'_{x,1} \\ \theta_{x,2} \\ -\theta'_{x,2} \end{bmatrix}$$

$$= \begin{bmatrix} M_{x,1} \\ B_1 \\ M_{x,2} \\ B_2 \end{bmatrix} + \begin{bmatrix} m_x + \frac{M_0}{l^3} (l + 2x_0) (l - x_0)^2 + \frac{6B_0x_0}{l^3} (l - x_0) \\ \frac{M_0x_0}{l^2} (2lx_0 - x_0^2 - l^2) + \frac{B_0}{l^2} (l^2 + 3x_0^2 - 4lx_0) \\ m_x + \frac{M_0x_0^2}{l^3} (3l - 2x_0) - \frac{6B_0x_0}{l^3} (l - x_0) \\ \frac{M_0x_0^2}{l^2} (l - x_0) - \frac{B_0x_0}{l^2} (2l - 3x_0) \end{bmatrix} \quad (3.35)$$

Using the hyperbolic shape functions instead, the stiffness matrix will look like

$$\mathbf{K}_e = \frac{EI_\omega}{l^3} \begin{bmatrix} \delta_T & -\gamma_T l & -\delta_T & -\gamma_T l \\ -\gamma_T l & \alpha_T l^2 & \gamma_T l & \beta_T l^2 \\ -\delta_T & \gamma_T l & \delta_T & \gamma_T l \\ -\gamma_T l & \beta_T l^2 & \gamma_T l & \alpha_T l^2 \end{bmatrix}, \quad (3.36)$$

where

$$\alpha_T = \frac{kl (\sinh kl - kl \cosh kl)}{2 (\cosh kl - 1) - kl \sinh kl}, \quad \beta_T = \frac{kl (kl - \sinh kl)}{2 (\cosh kl - 1) - kl \sinh kl},$$

$$\gamma_T = \alpha_T + \beta_T, \quad \delta_T = -\frac{(kl)^3 \sinh kl}{2 (\cosh kl - 1) - kl \sinh kl}. \quad (3.37a-d)$$

The distribution of the concentrated torsion moment  $M_0$  and bimoment  $B_0$  at the abscisse  $x_0$  changes its extrapolated values to the nodal points and can be calculated by the terms

$$\mathbf{q}_e = \int_0^l \Phi^\top m_x dx \Phi^\top(x_0) M_0 - \frac{d}{dx} \Phi^\top(x_0) B_0. \quad (3.38)$$

The total  $\mathbf{K}_e$  matrix for an element has the size  $14 \times 14$ , and is assembled by having the correct values at the right places corresponding to how both  $\mathbf{w}_e$  and  $\mathbf{r}_e$  are constructed from (3.4) and (3.5). The element stiffness matrix is divided into four  $7 \times 7$  submatrices, corresponding to

$$\mathbf{K}_e = \begin{bmatrix} \mathbf{K}_{e,11} & \mathbf{K}_{e,12} \\ \mathbf{K}_{e,21} & \mathbf{K}_{e,22} \end{bmatrix}. \quad (3.39)$$

### 3.4 System of Equations

For a system with multiple nodal points and elements as shown on figure 3.2, the equilibrium for element  $e = j$  is referred to as

$$\mathbf{K}_j \mathbf{w}_j = \mathbf{r}_j + \mathbf{q}_j \quad \text{for } j = 1, 2, \dots, N. \quad (3.40)$$

The slightly bold notation for  $(\cdot)_j$  refers to element  $j$ , while  $(\cdot)_j$  refers to nodal point  $j$ . At

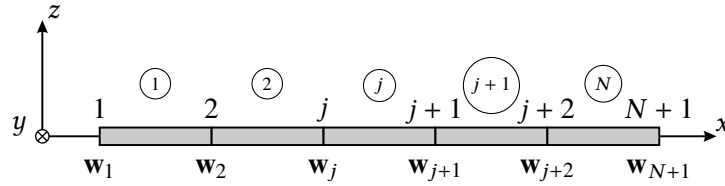


**Figure 3.2:** Element discretization over space with node, element and degree of freedom numbering.

a shared node between element  $j$  and element  $j + 1$  the reaction forces  $\mathbf{r}_{j,2}$  and  $\mathbf{r}_{j+1,1}$  are acting. Both reaction forces belonging to the right end of element  $j$  and the left end of element  $j + 1$  contribute to the node  $j + 1$ . The corresponding element loads are denoted as  $\mathbf{q}_{j,2}$  and  $\mathbf{q}_{j+1,1}$ . For the whole system the global system of equations for equilibrium are formulated on the form

$$\mathbf{K} \mathbf{w} = \mathbf{r} + \mathbf{q}, \quad (3.41)$$

where

$$\mathbf{w} = \begin{bmatrix} \mathbf{w}_1 \\ \mathbf{w}_2 \\ \vdots \\ \mathbf{w}_j \\ \mathbf{w}_{j+1} \\ \mathbf{w}_{j+2} \\ \vdots \\ \mathbf{w}_{N+1} \end{bmatrix}, \quad \mathbf{r} = \begin{bmatrix} \mathbf{r}_{1,1} \\ \mathbf{r}_{1,2} + \mathbf{r}_{2,1} \\ \vdots \\ \mathbf{r}_{j-1,2} + \mathbf{r}_{j,1} \\ \mathbf{r}_{j,2} + \mathbf{r}_{j+1,1} \\ \mathbf{r}_{j+1,2} + \mathbf{r}_{j+2,1} \\ \vdots \\ \mathbf{r}_{N,2} \end{bmatrix}, \quad \mathbf{q} = \begin{bmatrix} \mathbf{q}_{1,1} \\ \mathbf{q}_{1,2} + \mathbf{q}_{2,1} \\ \vdots \\ \mathbf{q}_{j-1,2} + \mathbf{q}_{j,1} \\ \mathbf{q}_{j,2} + \mathbf{q}_{j+1,1} \\ \mathbf{q}_{j+1,2} + \mathbf{q}_{j+2,1} \\ \vdots \\ \mathbf{q}_{N,2} \end{bmatrix}, \quad (3.42a-c)$$



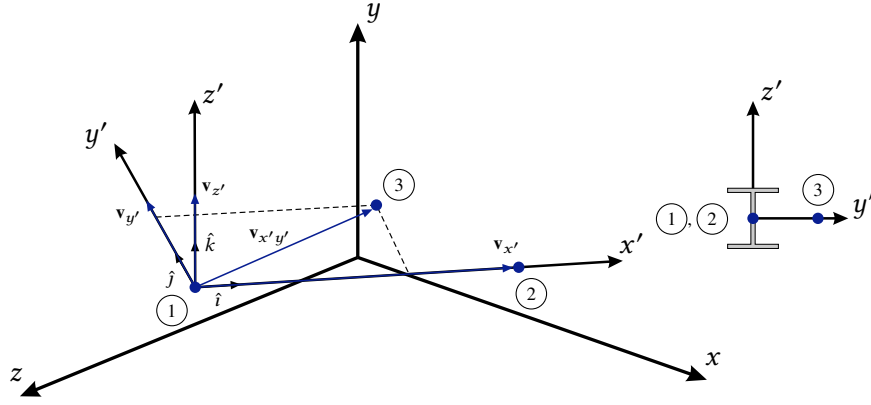


**Figure 3.3:** Spatial beam element in global and local coordinate system.

Then the vectors in  $z'$  and  $y'$  direction are

$$\mathbf{v}_{z'} = \mathbf{v}_{x'} \times \mathbf{v}_{x'y'}, \quad \mathbf{v}_{y'} = \mathbf{v}_{z'} \times \mathbf{v}_{x'}. \quad (3.49a-b)$$

The unit vectors of the system can be calculated as

$$\hat{\mathbf{i}} = \frac{\mathbf{v}_{x'}}{|\mathbf{v}_{x'}|}, \quad \hat{\mathbf{j}} = \frac{\mathbf{v}_{y'}}{|\mathbf{v}_{y'}|}, \quad \hat{\mathbf{k}} = \frac{\mathbf{v}_{z'}}{|\mathbf{v}_{z'}|}. \quad (3.50a-c)$$

Defining the transformation matrix  $\mathbf{T}_e$  as

$$\mathbf{T}_e = \begin{bmatrix} \hat{\mathbf{i}} & \hat{\mathbf{j}} & \hat{\mathbf{k}} \end{bmatrix}, \quad (3.51)$$

The nodal coordinates in the local coordinate system can be found as

$$\mathbf{x}'_e = \mathbf{x}_e \mathbf{T}_e, \quad (3.52)$$

where

$$\mathbf{x}_e = \begin{bmatrix} \mathbf{0} \\ \mathbf{v}_{x'}^\top \\ \mathbf{v}_{y'}^\top \end{bmatrix}, \quad \mathbf{x}'_e = \begin{bmatrix} 0 & 0 & 0 \\ x'_2 & 0 & 0 \\ x'_3 & y'_3 & 0 \end{bmatrix}. \quad (3.53a-b)$$

This transformation matrix also holds for displacement, rotations, forces and moments. With beam elements with the additional degree of freedom for rate of twist this can be seen as a scalar quantity and does not need to be converted during coordinate transformation [Damkilde, 1999]. Defining the full  $14 \times 14$  transformation matrix, this becomes

$$\mathbf{T} = \begin{bmatrix} \mathbf{T}_e & & & \mathbf{0} \\ & \mathbf{T}_e & & \\ & & 1 & \\ & & & \mathbf{T}_e \\ \mathbf{0} & & & & \mathbf{T}_e \\ & & & & & 1 \end{bmatrix}. \quad (3.54)$$

Then the vector containing the degrees of freedom and the element load vector can be transformed as

$$\mathbf{w}'_e = \mathbf{T}^\top \mathbf{w}_e, \quad \mathbf{q}'_e = \mathbf{T}^\top \mathbf{q}_e, \quad (3.55a-b)$$

and the stiffness matrix as

$$\mathbf{K}_e = \mathbf{T} \mathbf{K}'_e \mathbf{T}^\top. \quad (3.56)$$

# 4 Numerical Results and Comparison

---

Within the following a comparison different aspects of the MATLAB code is investigated, hereunder the changes of the accuracy due to more elements and results from both cubic and exact shape functions. A comparison with the advanced numerical program ABAQUS is furthermore performed, shown in section 4.1.

Firstly the torsional rotation  $\theta_x$  and the rate of torsional rotation  $\theta'_x$  are investigated, as these parameters are key components to describe the internal forces,  $M_x$  and  $B$ . Quadratic shape functions are used in this case and results from one and two elements are investigated. At the fixed end of the cantilever beam,  $\theta_x$  starts by having the value

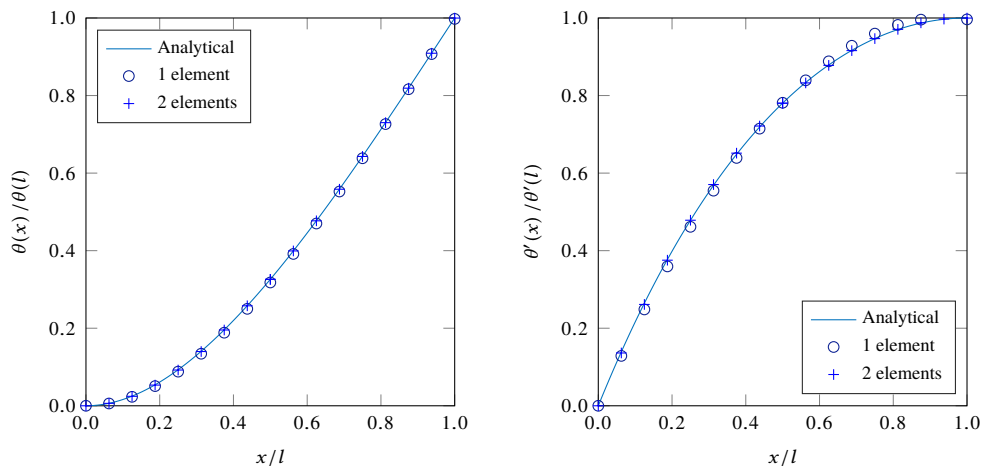


**Figure 4.1:** Deformation variables  $\theta_x(x)$  and  $\theta'_x(x)$  due to non-homogeneous torsion of cantilever beam subjected to  $M_0$  and quadratic shape functions.

zero, as the beam is prevented from moving in any direction nor rotate. When being at a location of about half way through the beam length, the effects from the fixed support is drastically reduced and  $\theta_x$  starts to increase more or less linearly with a steep slope. As  $\theta'_x$  is showing the rate of change, the reverse of the  $\theta_x$  is therefore present in figure 4.1 to the right. When having one element only, the results are deviating by a small amount at the midspan of the beam and when having two elements, the results are somewhat in line with the analytical result.

Despite  $\theta_x$  and  $\theta'_x$ , the St. Venant- and Vlasov moment along with the bimoment are investigated as these are dominating factors in the stress evaluation. Figure 4.2a and 4.2b shows the variation of  $M_{x,s}(x)$  and  $M_{x,v}(x)$  for the chosen beam. At  $x = 0$  the torsional moment  $M_0$  is fully carried by the Vlasov moment, whereas the St. Venant moment is 0. As  $x$  increases, so does the St. Venant moment and the Vlasov moment reduces until

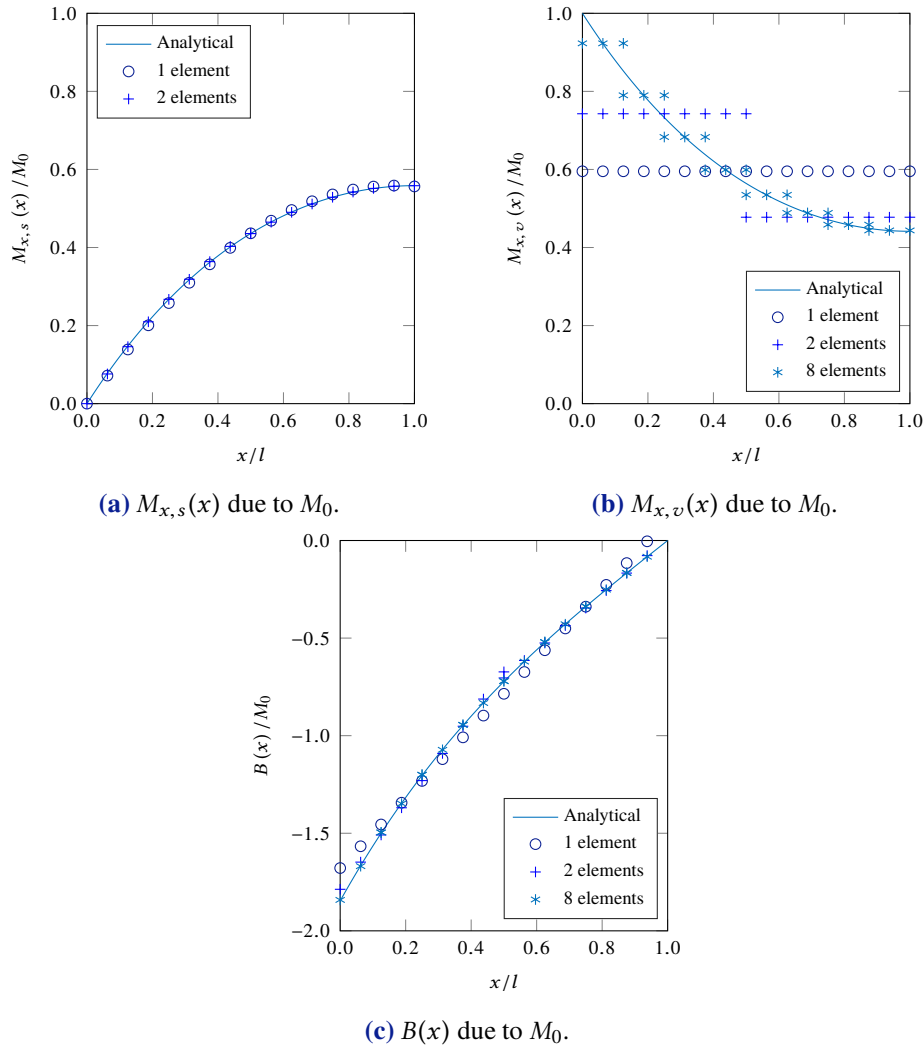


**Figure 4.2:** Internal forces due to non-homogeneous torsion of cantilever beam subjected to  $M_0$ .

the end, where both mechanisms reaches values that are approximately the same. The bimoment  $B$  shows the largest values at the fixed support where the warping is prevented and induces the largest normal stresses. At the free end the beam can warp freely which means the normal stresses is zero, thus  $B(l) = 0$ .

Rather small deviations are observed when looking at one element describing  $M_{x,s}(x)$ , and nearly identical results compared to the analytical solution are obtained when using two elements. An important aspect is observed, when looking at  $M_{x,v}(x)$  as it can be seen in figure 4.2b, a lot of elements are needed in order to get near the analytical solution. This is because  $M_{x,v}$  is calculated from the third derivative of  $\theta_x$ . With the shape functions being cubic, this gives constant values, which tries to fit the curve. The bimoment also requires a few more elements in order to obtain something near the analytical solution compared to  $M_{x,s}(x)$ .

As mentioned in chapter 2 numerical problems can occur when using hyperbolic shape functions. Despite this, the exact shape functions are investigated and the results for each of the above analysed parameters are shown in the figures below. As it can be seen from figure 4.4 it was possible to obtain exact values to describe the internal forces

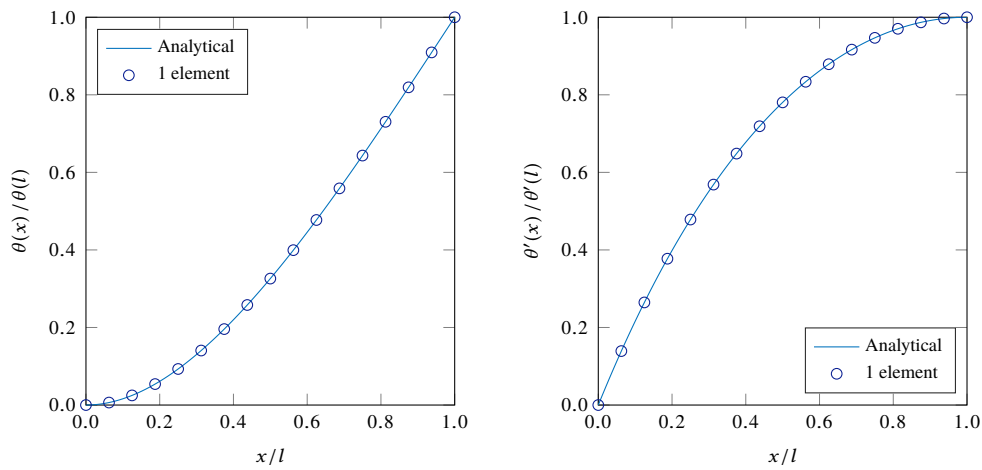
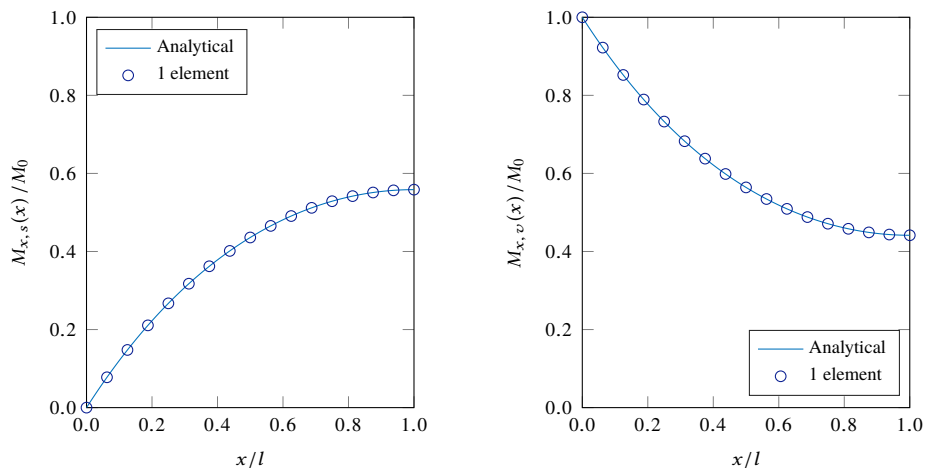
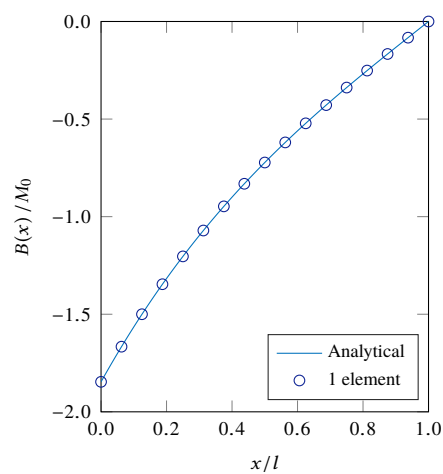


**Figure 4.3:** Deformation variables  $\theta_x(x)$  and  $\theta'_x(x)$  due to non-homogeneous torsion of cantilever beam subjected to  $M_0$  with exact shape functions.



**(a)**  $M_{x,s}(x)$  due to  $M_0$ .

**(b)**  $M_{x,v}(x)$  due to  $M_0$ .



**(c)**  $B(x)$  due to  $M_0$ .

**Figure 4.4:** Internal forces due to non-homogeneous torsion of cantilever beam subjected to  $M_0$  with exact shape functions.

based on the derivatives of the exact shape functions without any numerical problems. Due to the previous, a thought experiment is made with a cantilever beam and the rotation  $\theta_x(l)$  is calculated for different values of  $kl$ , which can be seen on figure 4.5. Numerical problems occur when  $kl$  is very small (below  $10^{-3}$ ), which can be observed on the left figure. One point is missing since it was calculated as negative and cannot be plotted on

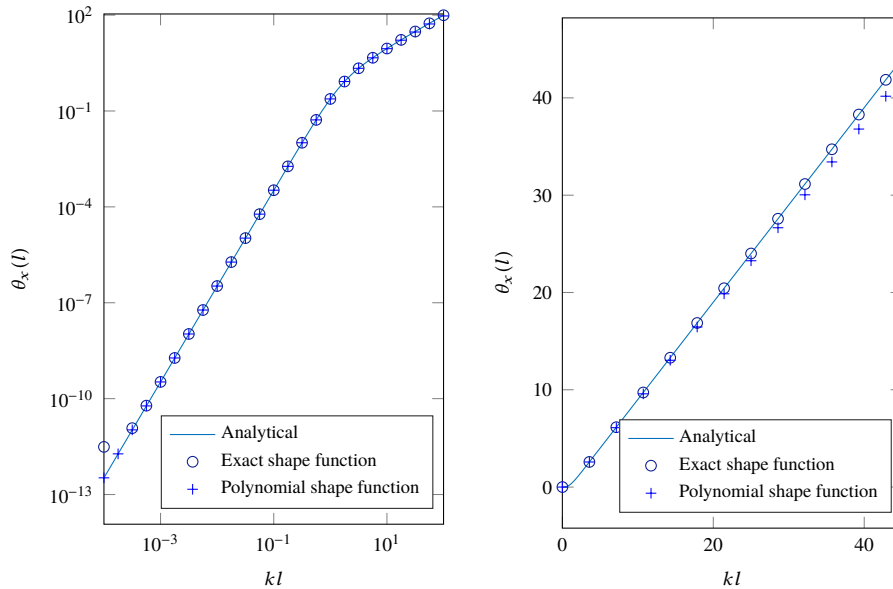


**Figure 4.5:**  $\theta_x(l)$  with different values of  $kl$ .

a log-diagram, which again implies the numerical problems in that range.

The computational power has drastically increased over the last few decades and numerical difficulties in MATLAB does not seem to be an issue in the case of a prismatic beam subjected to torsion, since the values of  $kl$  that leads to difficulties seems unreasonable small. Furthermore when looking at the right figure the polynomial shape function starts to give adequate results for increasing values of  $kl$ . This is also implied by [Kindmann and Kraus, 2011], where it is stated that the condition  $kl < 1$  should be met in order to give reasonable results when using polynomial shape functions. Numerical instability may occur with beams having varying cross-section constants and non-linear problems like buckling, but this has not been investigated.

Cross-sectional stress variation is investigated at the fixed- and free end of the cantilever beam. Normal stress- and shear stress variation throughout the cross-section are shown in figure 4.6. Red indicates positive stresses and blue negative. The normal and shear stress at the fixed end of the cantilever beam is investigated along with the two shear stress contributions at the free end of the beam, as the normal stress in this section equals zero. As it can be seen in figure 4.6c, the blue line does not form a horizontal line, as the Vlasov shear stress contribution is functional and zero at the edge of the flange from where it develops to a maximum at the middle of the flange. It should be noticed, the shear stress from Vlasov gives a much smaller contribution to the total shear stress compared to the St. Venant shear stress. At the web negative shear stresses also occur since the St. Venant shear stresses varies linearly over the thickness and is 0 in the middle of the web.

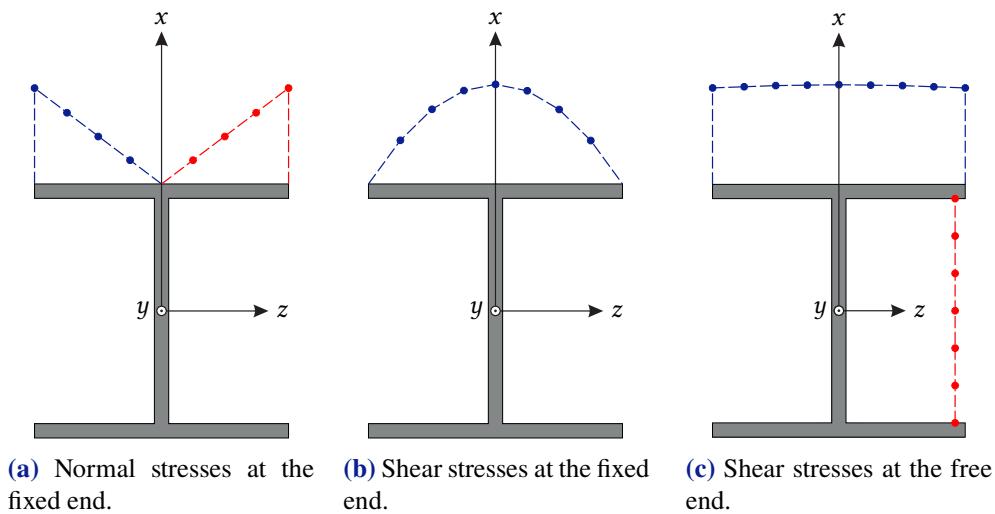


**Figure 4.6:** Cross sectional normal- and shear stresses at the fixed and free end of the cantilever beam.

## 4.1 ABAQUS Comparison

Non-homogeneous torsion is evaluated in ABAQUS by use of a shell model. A shell model is used because a thin-walled spatial beam is investigated. It is furthermore beneficial to use a shell model with respect to computational time compared to a solid model, because shell model work with a reduced number of finite elements meaning less equations to solve. When it is possible to reduce the problem to a planar problem and neglect what happens at the thickness of the element, a shell model should be chosen prior to a solid model. Shell elements are therefore used to model structures in which one dimension is significantly smaller than the other dimensions in this case  $t \ll b, h$  and  $l$  [SIMULIA, 2013].

A comparison between normal stresses in a shell- and solid model along with normal stresses from the home-made MATLAB program are showed in appendix B. Quadratic hexahedrons are used in the shell model as twisting and bending occurs due to the loading of the beam. The boundary- and load condition of the cantilever beam shell element model is shown on figure 4.7. As the cross-section rotates around the shear centre as a

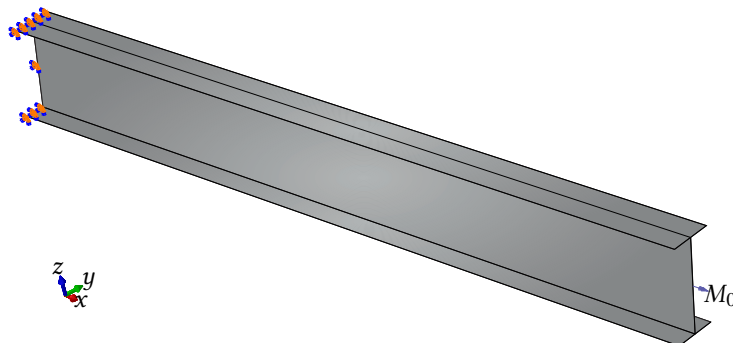


**Figure 4.7:** Boundary- and load condition of the shell model in Abaqus.

rigid body, the point of investigation of the cross-section is chosen to be the outer edge of the top flange. Here the greatest normal stresses occur due to the highest values of  $\omega_n$

in the edges of the flanges. Either outer edges of the two flanges could have been chosen. The chosen points of investigation are seen on figure 4.8. In order to secure enough

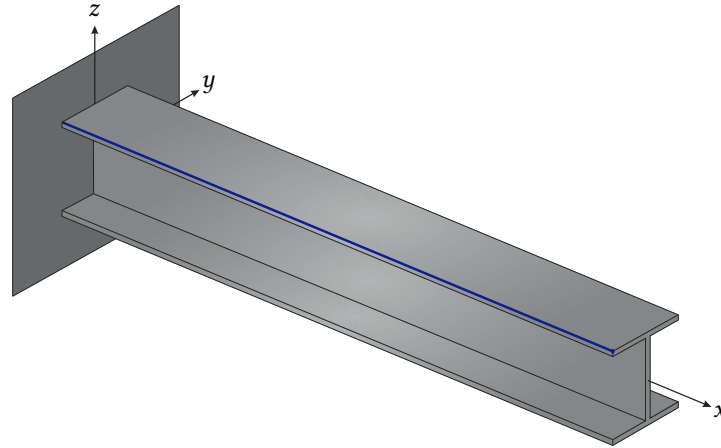


**Figure 4.8:** Presentation of investigation point displayed with a blue line.

elements are used when simulating results, a convergence analysis is performed for the shell model. The convergence analysis is shown in figure 4.9. Looking at the figure, it

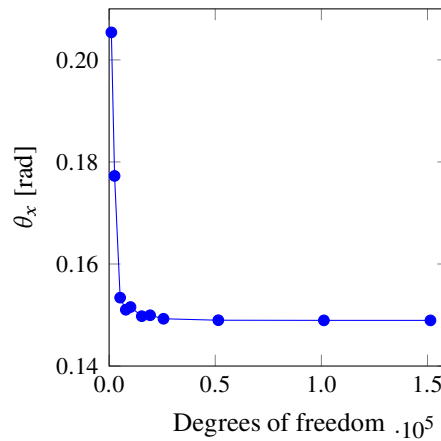


**Figure 4.9:** Convergence analysis of the shell model with respect to a IPE 450 steel profile.

can be stated that using a mesh with more than 20 000 degrees of freedom equivalent to more or less 3250 elements is reasonable for the IPE 450 steel profile shell model, as the data starts to converge from this amount of degrees of freedom. A model with 150 000 degrees of freedom equivalent to around 24 500 elements should be avoided as the result is only corrected by a significantly small amount but the computational time is drastically increased and in no way advantageous.

The convergence analysis is investigated at the free end of the cantilever beam and the rotational angle of the cross-section  $\theta_x$  is chosen as the convergence parameter subjected to a torsional moment of  $M_0 = 7$  kNm. The rotational angle equals zero at the support, from which the shell model starts to deviate by a small amount but increases until the free end is reached, where the deviation reaches 20%. Despite comparing  $\theta_x$ , the normal stresses  $\sigma_{xx}$  are investigated in shell model, see figure 4.11. The normal stresses at each end of the beam gets close to the results from the MATLAB model but undergoes rather large deviations throughout the beam length.

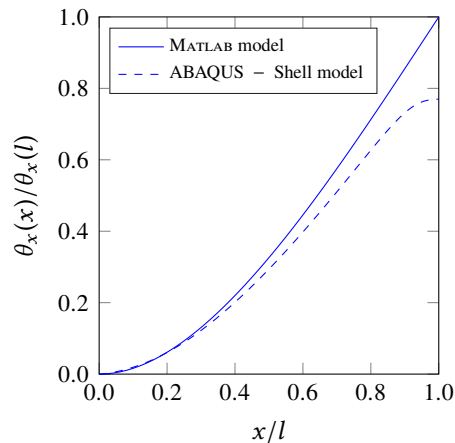


**Figure 4.10:** Variation of  $\theta_x$  through the beam length. The torsional rotation has been normalized with respect to the analytical rotation at the end.

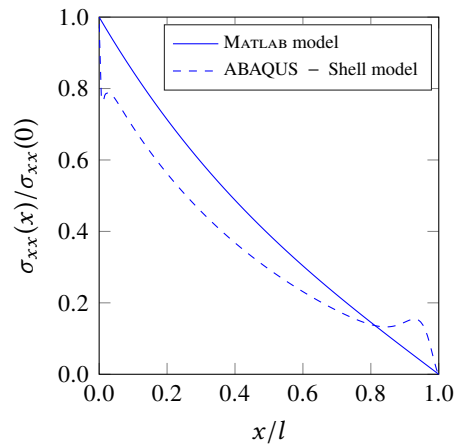


**Figure 4.11:** Variation of  $\sigma_{xx}$  through the blue line. The stresses has been normalized with the maximum normal stress obtain from analytical calculation.

An additional comparison with a solid model from ABAQUS is included in appendix B, from where it can be seen, the solid model actually follows the MATLAB model normal stresses within the range  $0.2l-0.7l$ , see figure B.1. At the fixed end of the cantilever beam, nearly the same normal stresses can be observed, as the shell model and the solid model deviates with 2% and 4% respectively. The variation of  $\theta_x$  throughout the beam length is shown on figure 4.12. At the fixed end of the cantilever beam,  $\theta_x = -2.477 \cdot 10^{-5}$  rad which can be seen as zero. By moving further along the beam and therefore closing in on the free end of the cantilever beam,  $\theta_x$  starts to accelerate and ends up with a magnitude of 0.159 rad. Despite  $\theta_x$ , normal stresses along the beam length is also investigated as shown on figure 4.13. It can clearly be seen, that the stresses are equal to zero at the free end of the cantilever beam and starts to develop when approaching the fixed end. As the beam can not warp freely at the fixed end, normal stresses are build up at the flanges as these are tightened to the support and therefore can't move in the  $x$ -direction. As the flanges would warp in different directions on each side of the connecting point to the web of the profile, positive stresses are build up on one side and negative on the other. A maximum of 355 MPa is reached as this is the maximum capacity of chosen the steel

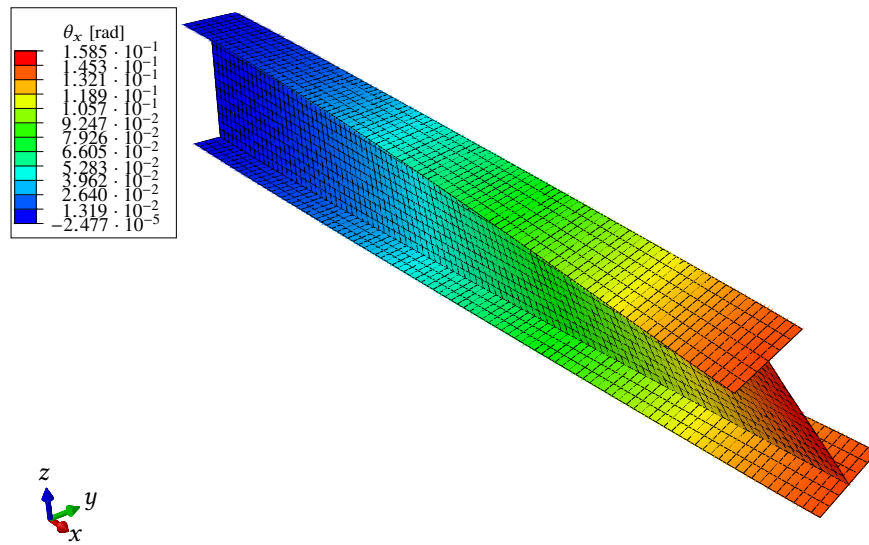


**Figure 4.12:** Non-homogeneous torsion resulting in rotational angle variation along the beam.

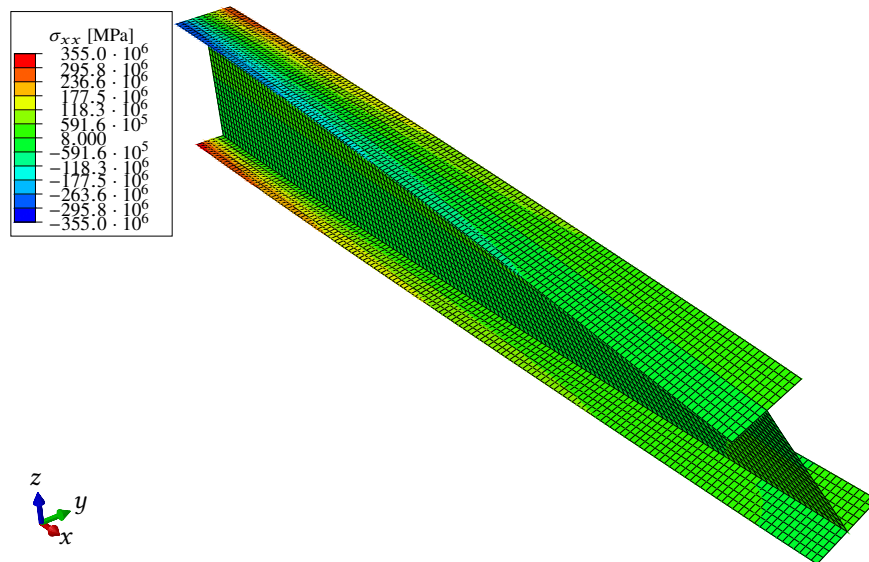


**Figure 4.13:** Non-homogeneous torsion resulting in normal stress variation along the beam.

type.

## 5 Conclusion

---

The severity of the torsional problem were stated within the introduction. Looking at figure 1.4, it can clearly be stated, when having fixed support conditions as shown in figure 1.3 and A.9, that Vlasov torsion must be accounted for. All sizes of both steel profile types I/H presented in [Teknisk Ståbi, 2011] were investigated and the linear behaviour for St. Venant and Vlasov torsion were present for both types, with Vlasov torsion showing a much steeper slope.

A thorough presentation of spatial beam theory was presented, leading to the analytical solutions and working as the foundation for the finite element method. Within the spatial beam theory, homogeneous and non-homogeneous torsion were derived generally to fit all types of thin-walled open profiles. By means of a few examples the general formulas are written to fit I/H profiles, giving the possibility to discuss results across the different objectives, analytical and FEM both with respect to the home-made MATLAB program and the shell model in ABAQUS.

A gathering of all the numerical results were made in chapter 4, from where it can be concluded a beam finite element model with the hyperbolic shape functions gave the exact results as the analytical. Moreover solutions with respect to polynomial shape functions came close to the analytical solution when more than eight elements were used despite the Vlasov moment  $M_{x,v}$  would require alot more elements in order to obtain a result near the analytical solution. Using polynomial shape functions would therefore require the use of multiple finite elements. It was stated in [Damkilde, 1999] and [Kindmann and Kraus, 2011] that use of hyperbolic shape functions could lead to numerical calculations difficulties. Therefore it was tested for which values of  $kl$  it could give problems for MATLAB to obtain reasonable results. With values for  $kl < 10^{-3}$  numerical issues occurred. It is however doubtful, that values so small would to be a problem for prismatic beams. It has not been tested for which values of  $kl$  it would occur when dealing with numerical integration of beams with varying cross-sectional quantities and non-linear behaviour as buckling.

It was of interest to observe the stress development in the cross section as presented in figure 4.6. It can be concluded that the utilization ratio of the investigated cantilever beam should be checked for shear stresses dominating the free end, and at the fixed end. Here normal stresses dominate because the cross-section is prevented from warping. As the Vlasov shear stresses are very small, the worst case is obtained at the point where the normal stress has its maximum value, which means  $s_1 = 0$ , resulting in the shear stresses from Vlasov torsion disappears. Additionally no contribution from the St. Venant shear stress is present, as  $M_{x,s}(0) = 0$ .

Contradictory to this, only shear stresses are present at the free end, dominated by St. Venant shear stresses. The maximum value is obtained at the middle of the flange, where both St. Venant and Vlasov stresses are present, though the last mentioned are of minor magnitude.

An additional comparison were made between the `MATLAB` model with exact shape functions and the shell- and solid model in `ABAQUS`. This yielded some large deviations just after the start and before the end of the beam, meaning the result values at the ends and the middle of the beam were reasonable. It should be noticed from figure B.1, the results from the solid model were closer to the `MATLAB` model at the middle of the beam. The solid model still showed the large deviations when looking at the normal stresses closer to the ends of the beam as the shell model did.

# Bibliography

---

- Andersen and Nielsen, 2008.** Lars Andersen and Søren R.K. Nielsen. *Elastic Beams in Three Dimensions*. ISSN: 1901-7286. Aalborg University, 2008. DCE Lecture Notes No. 23.
- Autodesk, 2015a.** Autodesk. *Robot Structural Analysis Professional*. URL: <http://www.autodesk.com/products/robot-structural-analysis/features/all/list-view>, 2015.
- Autodesk, 2015b.** Autodesk. *Troubleshooting*. URL: <http://knowledge.autodesk.com/support/robot-structural-analysis-products/troubleshooting/caas/sfdcarticles/sfdcarticles/ROBOT-is-warping-torsion-considered-for-bar-elements.html>, 2015.
- Damkilde, 1999.** Lars Damkilde. *Elementmetodeformulering af tyndvæggede bjælker*. URL: <http://homes.civil.aau.dk/lda/Notes/TH22.pdf>, 1999.
- Eurocode 3, 2007.** Eurocode 3. *Eurocode 3: Design of steel structures - Part 1-1: General rules and rules for buildings*. ISBN: 978-3-433-03091-2, 1. edition. Ernst and Sohn, 2007.
- Kindmann and Kraus, 2011.** Rolf Kindmann and Matthias Kraus. *Steel Structures Design using FEM*. ISBN: 978-3-433-02978-7. Ernst & Sohn - A Wiley Company, 2011. DCE Lecture Notes No. 23.
- Mathworks, 2015.** Mathworks. *MATLAB R2015a*. URL: <http://se.mathworks.com/products/matlab>, 2015.
- Nielsen and Hansen, 1978.** M.P. Nielsen and L. Pilegaard Hansen. *Mekanik 3.3 del 1 - Spændinger og deformation i rumbjælker*. ISBN: 87-87245-62-0. Den private Ingeniørfond ved Danmarks tekniske Højskole, 1978. Aalborg/København.
- Ottosen and Ristinmaa, 2005.** Niels Saabye Ottosen and Matti Ristinmaa. *The Mechanics of Constitutive Modeling*. ISBN: 978-0080446066, 1. edition. Elsevier Inc., 2005.
- SIMULIA, 2015.** SIMULIA. *Abaqus 6.14*. URL: <http://www.3ds.com/products-services/simulia/products/abaqus>, 2015.
- SIMULIA, 2013.** SIMULIA. *Abaqus 6.13 Theory Guide*. 1. edition. Dassault Systèmes, 2013.
- Stærdahl, 2009.** Jesper W. Stærdahl. *Structural Element Method II - Strucutral elements, 3D beam element*. URL: [http://www.wind.civil.aau.dk/lecture/7sem\\_finite\\_element/lecture\\_notes/Lecture\\_6\\_7.pdf](http://www.wind.civil.aau.dk/lecture/7sem_finite_element/lecture_notes/Lecture_6_7.pdf), 2009.

**Strusoft, 2015.** Strusoft. *FEM-Design*. URL: <http://www.strusoft.com/products/fem-design>, 2015.

**Teknisk Ståbi, 2011.** Teknisk Ståbi. *Teknisk Ståbi*. ISBN: 978-87-571-2729-4, 21. edition. Nyt Teknisk Forlag, 2011.

# Appendix



# A Analysis of torsional behaviour of I/H-profiles

---

The steel profiles of type HEM, is fully displayed in chapter 1. Results from steel HEA-, HEB-, INP- and IPE-profiles are presented below:

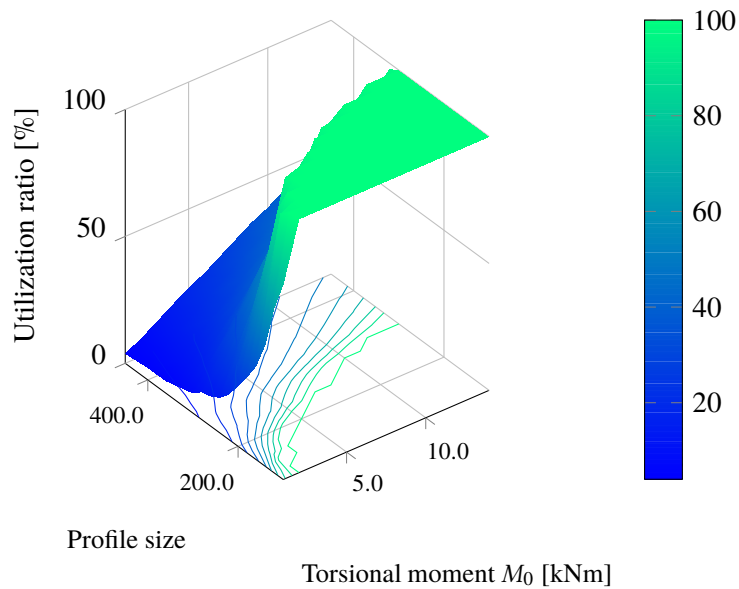


**Figure A.1:** Utilization ratios of HEA profiles exposed to St. Venant torsion presented in surface plot combined with contour lines.

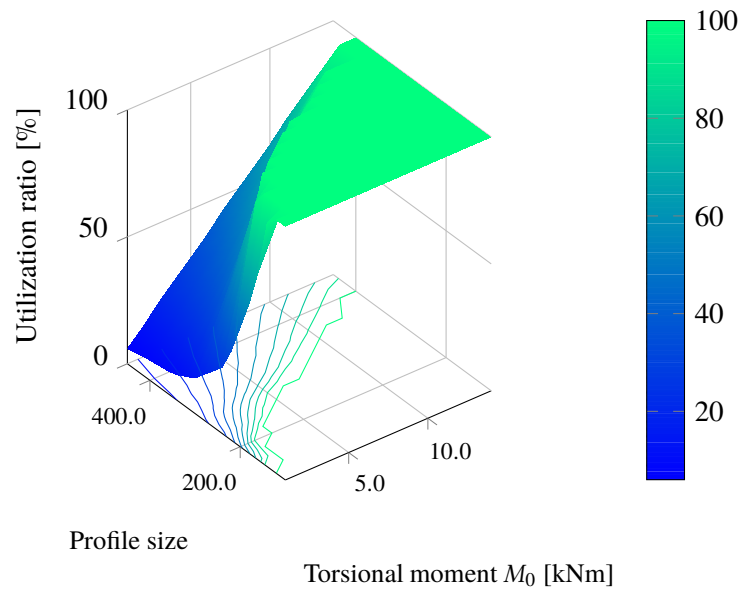


**Figure A.2:** Utilization ratios of HEA profiles exposed to Vlasov torsion presented in surface plot combined with contour lines.

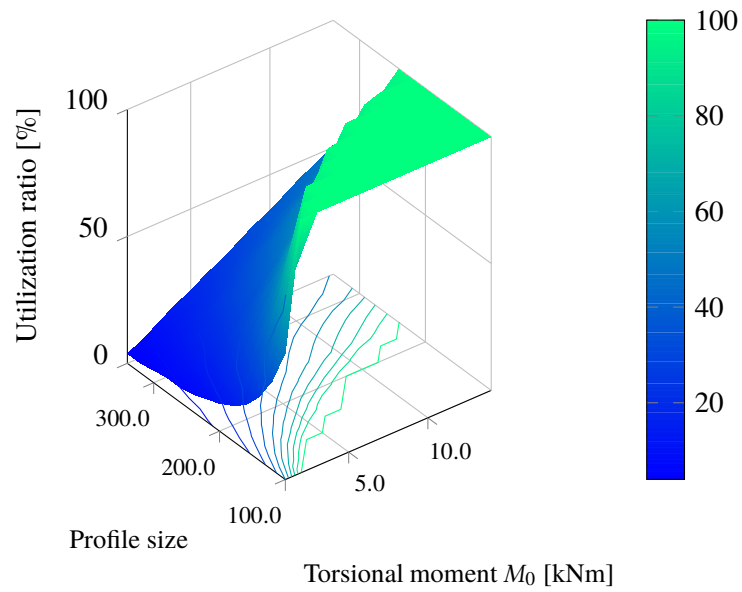


**Figure A.3:** Utilization ratios of HEB profiles exposed to St. Venant torsion presented in surface plot combined with contour lines.

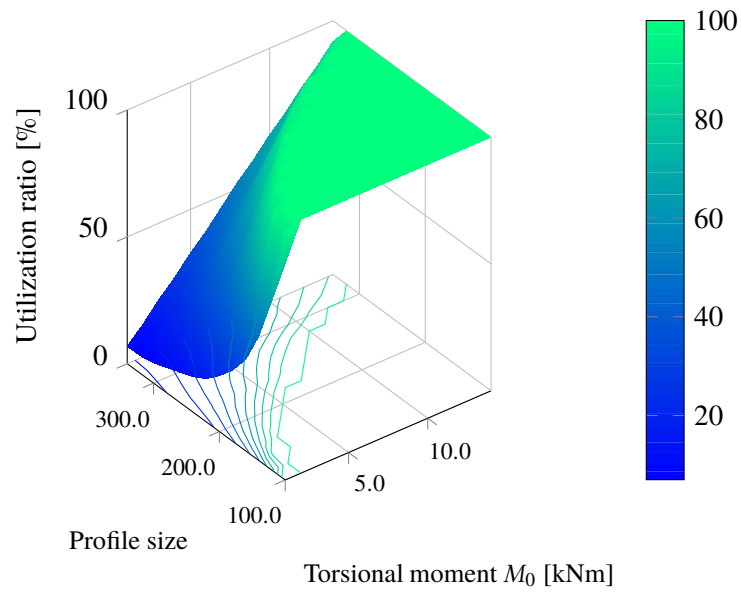


**Figure A.4:** Utilization ratios of HEB profiles exposed to Vlasov torsion presented in surface plot combined with contour lines.

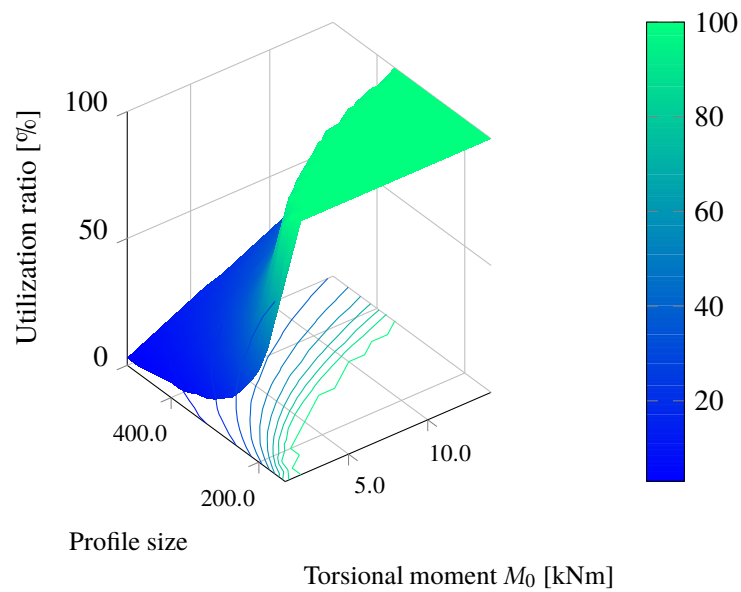


**Figure A.5:** Utilization ratios of INP profiles exposed to St. Venant torsion presented in surface plot combined with contour lines.

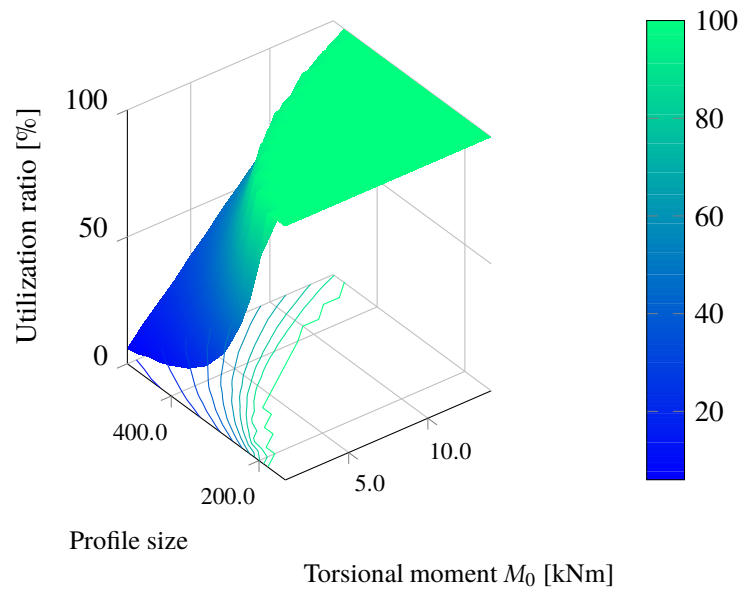


**Figure A.6:** Utilization ratios of INP profiles exposed to Vlasov torsion presented in surface plot combined with contour lines.

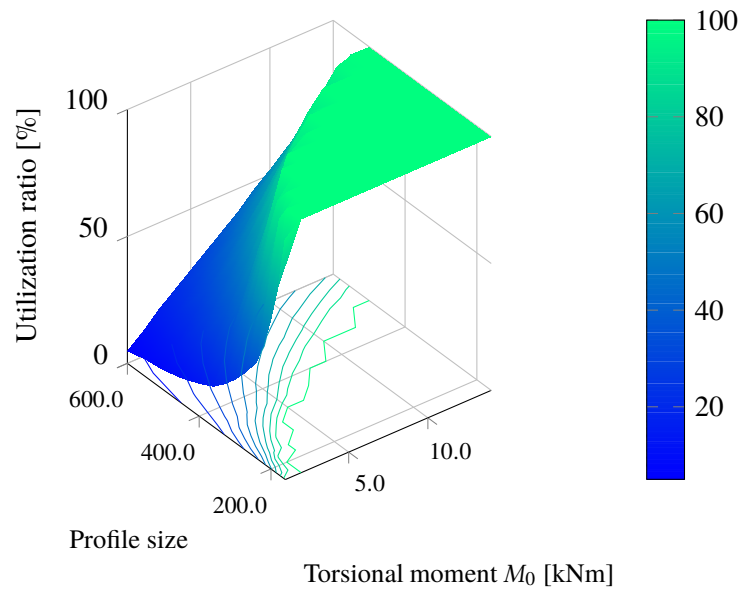


**Figure A.7:** Utilization ratios of IPE profiles exposed to St. Venant torsion presented in surface plot combined with contour lines.

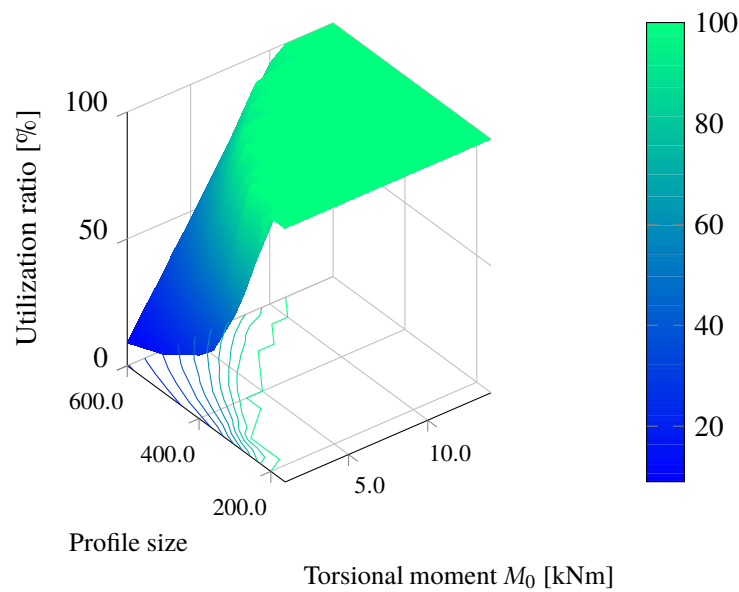


**Figure A.8:** Utilization ratios of IPE profiles exposed to Vlasov torsion presented in surface plot combined with contour lines.

The commercial software program: “Autodesk Robot Structural Analysis Professional” adhere to the steel eurocode to some extent, meaning when dealing with torsion, the software only accounts for St. Venant torsion as shown in the following detailed calculation results from Autodesk Robot, see figure A.11 and A.12.

The model is fixed in both ends and subjected to a torsional moment in the midspan in the non-homogeneous torsion case, see figure A.9 and simply supported in both ends in the other case, meaning the beam is able to warp freely. A torsional moment of exactly half of what the beam is subjected to in the non-homogeneous torsion case is inflicted in both ends of the beam in the simply supported case and these moments are acting in the opposite direction of one another, see figure A.10. The boundary and load condition for both models are shown below:

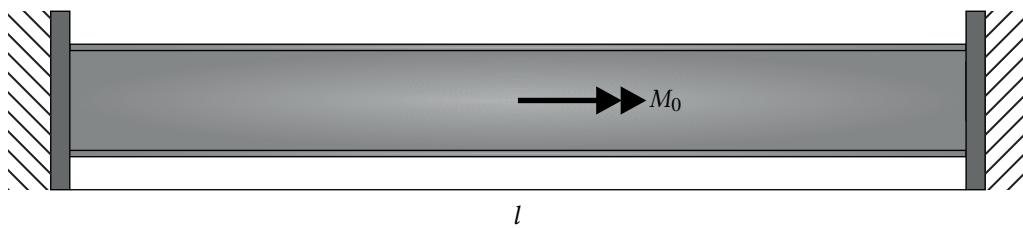


**Figure A.9:** Boundary- and load condition for the fixed supported beam seen from the side.

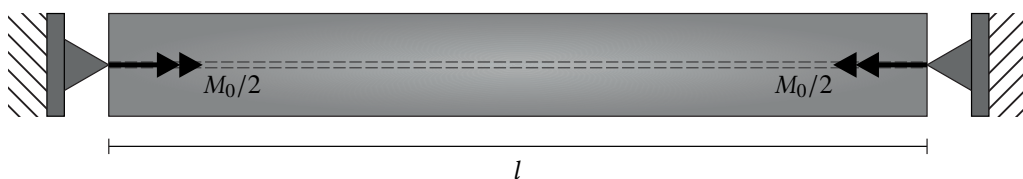


**Figure A.10:** Boundary- and load condition for a torsionally simply supported beam seen from above.

## [Autodesk Robot - Detailed results - Torsionally simply supported beam - Page 1]

Autodesk Robot Structural Analysis Professional 2015

Author:

File: **St. Venant torsion.rtd**

Address:

Project: Structure

Symbol	Values	Unit	Symbol description	Section
<b>MEMBER: 1 Simple bar_1 ; COORDINATE: x = 0.00 L= 0.00 m</b>				
<b>Cross-section properties: IPE 500</b>				
Ax	11552	mm <sup>2</sup>	Cross-section area	
Ay	7207	mm <sup>2</sup>	Shear area - y-axis	
Az	5987	mm <sup>2</sup>	Shear area - z-axis	
Ix	890000	mm <sup>4</sup>	Torsional constant	
Iy	481985000	mm <sup>4</sup>	Moment of inertia of a section about the y-axis	
Iz	21416900	mm <sup>4</sup>	Moment of inertia of a section about the z-axis	
Wply	2194260	mm <sup>3</sup>	Plastic section modulus about the y (major) axis	
Wplz	335887	mm <sup>3</sup>	Plastic section modulus about the z (minor) axis	
h	500	mm	Height of cross-section	
b	200	mm	Width of cross-section	
tf	16	mm	Flange thickness	
tw	10	mm	Web thickness	
ry	204	mm	Radius of gyration - y-axis	
rz	43	mm	Radius of gyration - z-axis	
Anb	1.00		Net area to gross area ratio	(6.2.2.2)
Eta	1.00		Factor for Av calculation	(6.2.6.(3))
<b>Material:</b>				
Name	Steel ( S235 )			
fy	235.00	MPa	Design yield strength of material	(3.2)
fu	360.00	MPa	limit tensile stress - characteristic value	(3.2)
gM0	1.10		Partial safety factor	(6.1.(1))
gM1	1.20		Partial safety factor	(6.1.(1))
gM2	1.35		Partial safety factor	(6.1.(1))
<b>Designations of additional codes:</b>				
EN112	EN 1991-1-2:2003 - Fire loads on a structure			
EN312	EN 1993-1-2:2005 - Steel structures - fire design			
EN313	EN 1993-1-3:2005 - Steel structures from cold-formed sections			
EN315	EN 1993-1-5:2005 - Steel structures - plated elements			
EC111	ECCS No111:2001 - Guidebook with recommendations for fire			
ENV311	ENV 1993-1-1:1992 - Steel structures - general code			
<b>Class of section</b>				
KLF	1		Flange class	(5.5.2)
KLW	1		Web class	(5.5.2)
(hw/tw)lim	72.00		limit slenderness of a web for shear	EN315(5.1)
hw/tw	45.88		web slenderness for shear	EN315(5.1)
KLSZ	Plastic		Web class (shear)	EN315(5.1)
KL	1		Section type	(5.5.2)
<b>Parameters of lateral-torsional buckling analysis:</b>				
XLT	1.00		Reduction factor for lateral-torsional buckling	(6.3.2.2.(1))

Date : 24/03/15

Page : 1

Figure A.11: Autodesk Robot - Detailed results of a torsionally simply supported beam.

## [Autodesk Robot - Detailed results - Torsionally simply supported beam - Page 2]

Autodesk Robot Structural Analysis Professional 2015

Author:

File: **St. Venant torsion.rtd**

Address:

Project: Structure

Symbol	Values	Unit	Symbol description	Section
<b>Internal forces at characteristic points of cross section</b>				
Tt,Ed	3.50	kN*m	torsional moment	
<b>Stresses at characteristic points of cross-section:</b>				
Tau,ty,Ed	62.92	MPa	shear stress due to torsional moment Tt,Ed	(6.2.7)
Tau,tz,Ed	40.11	MPa	shear stress due to torsional moment Tt,Ed	(6.2.7)
<b>Design forces:</b>				
<b>Verification formulas:</b>				
<b>Section strength check:</b>				
UFS[VyT]	0.51		$Tau,ty,Ed/(fy/(\sqrt{3}*gM0))$	(6.2.6)
UFS[VzT]	0.33		$Tau,tz,Ed/(fy/(\sqrt{3}*gM0))$	(6.2.6)

## [Autodesk Robot - Detailed results - Fixed supported beam - Page 1]

Autodesk Robot Structural Analysis Professional 2015	File: <b>Restrained torsion.rtd</b>
Author:	Project: Structure
Address:	

Symbol	Values	Unit	Symbol description	Section
<b>MEMBER: 1 Simple bar_1 ; COORDINATE: x = 0.00 L = 0.00 m</b>				
<b>Cross-section properties: IPE 500</b>				
Ax	11552	mm <sup>2</sup>	Cross-section area	
Ay	7207	mm <sup>2</sup>	Shear area - y-axis	
Az	5987	mm <sup>2</sup>	Shear area - z-axis	
Ix	890000	mm <sup>4</sup>	Torsional constant	
Iy	481985000	mm <sup>4</sup>	Moment of inertia of a section about the y-axis	
Iz	21416900	mm <sup>4</sup>	Moment of inertia of a section about the z-axis	
Wply	2194260	mm <sup>3</sup>	Plastic section modulus about the y (major) axis	
Wplz	335887	mm <sup>3</sup>	Plastic section modulus about the z (minor) axis	
h	500	mm	Height of cross-section	
b	200	mm	Width of cross-section	
tf	16	mm	Flange thickness	
tw	10	mm	Web thickness	
ry	204	mm	Radius of gyration - y-axis	
rz	43	mm	Radius of gyration - z-axis	
Anb	1.00		Net area to gross area ratio	(6.2.2.2)
Eta	1.00		Factor for Av calculation	(6.2.6.(3))
<b>Material:</b>				
Name			Steel ( S235 )	
fy	235.00	MPa	Design yield strength of material	(3.2)
fu	360.00	MPa	limit tensile stress - characteristic value	(3.2)
gM0	1.10		Partial safety factor	(6.1.(1))
gM1	1.20		Partial safety factor	(6.1.(1))
gM2	1.35		Partial safety factor	(6.1.(1))
<b>Designations of additional codes:</b>				
EN112			EN 1991-1-2:2003 - Fire loads on a structure	
EN312			EN 1993-1-2:2005 - Steel structures - fire design	
EN313			EN 1993-1-3:2005 - Steel structures from cold-formed sections	
EN315			EN 1993-1-5:2005 - Steel structures - plated elements	
EC111			ECCS No111:2001 - Guidebook with recommendations for fire	
ENV311			ENV 1993-1-1:1992 - Steel structures - general code	
<b>Class of section</b>				
KLF	1		Flange class	(5.5.2)
KLW	1		Web class	(5.5.2)
(hw/tw)lim	72.00		limit slenderness of a web for shear	EN315(5.1)
hw/tw	45.88		web slenderness for shear	EN315(5.1)
KLSZ	Plastic		Web class (shear)	EN315(5.1)
KL	1		Section type	(5.5.2)
<b>Parameters of lateral-torsional buckling analysis:</b>				
XLT	1.00		Reduction factor for lateral-torsional buckling	(6.3.2.2.(1))

Figure A.12: Autodesk Robot - Detailed results of a fixed supported beam.

## [Autodesk Robot - Detailed results - Fixed supported beam - Page 2]

Autodesk Robot Structural Analysis Professional 2015

Author:

File: **Restrained torsion.rtd**

Address:

Project: Structure

Symbol	Values	Unit	Symbol description	Section
<b>Internal forces at characteristic points of cross section</b>				
Tt,Ed	-3.50	kN*m	torsional moment	
<b>Stresses at characteristic points of cross-section:</b>				
Tau,ty,Ed	62.92	MPa	shear stress due to torsional moment Tt,Ed	(6.2.7)
Tau,tz,Ed	40.11	MPa	shear stress due to torsional moment Tt,Ed	(6.2.7)
<b>Design forces:</b>				
<b>Verification formulas:</b>				
<b>Section strength check:</b>				
UFS[VyT]	0.51		Tau,ty,Ed/(fy/(sqrt(3)*gM0))	(6.2.6)
UFS[VzT]	0.33		Tau,tz,Ed/(fy/(sqrt(3)*gM0))	(6.2.6)

Date : 24/03/15

Page : 2

As it can be seen,  $\tau_{ty,Ed} = 62.92$  MPa which is equivalent to a utilization of  $0.51 \leq 1.0$  in the IPE 450 steel profile, see figure A.11, which is exactly the same as in figure A.12, meaning Autodesk Robot does not account for warping effects.

If Autodesk Robot did account for warping effects, the utilization in the non-homogeneous torsion case would be  $\neq 0.51$  and therefore different from the homogeneous case.

The same statement is valid for the commercial software program FEM-Design where two situations again were compared with respect to homogeneous torsion and non-homogeneous torsion, and therefore the same support conditions, but the calculations yet again ends up with the same result, respectively  $\frac{T_{Ed}}{T_{Rd}} = 0.81 \leq 1.0$  in figure A.13, and the same in figure A.14 containing results from a fixed supported beam, where it again can be concluded, nor does FEM-design account for warping effects else, as previous mentioned, the results would be different from each other and not  $0.81 \leq 1.0$  in both cases.

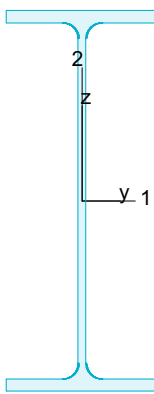
[FEM-Design detailed results - Torsionally simply supported beam - Page 1]

### B.1.1 Maximum of load combinations

#### S 235

E	=	210000 N/mm <sup>2</sup>		
G	=	80769 N/mm <sup>2</sup>		
Y <sub>M0,ult</sub>	=	1.10	Y <sub>M0,acc./seis</sub>	= 1.00
Y <sub>M1,ult</sub>	=	1.20	Y <sub>M1,acc./seis</sub>	= 1.00
Y <sub>M2,ult</sub>	=	1.35	Y <sub>M2,acc./seis</sub>	= 1.00

#### IPE 500

	A	=	11552 mm <sup>2</sup>	f <sub>y</sub>	=	235 N/mm <sup>2</sup>
	I <sub>y</sub>	=	4.820e+08 mm <sup>4</sup>	ε	=	1.00
	I <sub>z</sub>	=	2.142e+07 mm <sup>4</sup>	λ <sub>1</sub>	=	93.90
	I <sub>1</sub>	=	4.820e+08 mm <sup>4</sup>			
	I <sub>2</sub>	=	2.142e+07 mm <sup>4</sup>			
	W <sub>pl,y</sub>	=	2.194e+06 mm <sup>3</sup>			
	W <sub>pl,z</sub>	=	3.361e+05 mm <sup>3</sup>			
	W <sub>el,min,y</sub>	=	1.928e+06 mm <sup>3</sup>			
	W <sub>el,min,z</sub>	=	2.142e+05 mm <sup>3</sup>			
	i <sub>1</sub>	=	204 mm			
	i <sub>2</sub>	=	43 mm			
	I <sub>t</sub>	=	8.863e+05 mm <sup>4</sup>			
I <sub>w</sub>	=	1.235e+12 mm <sup>6</sup>				

#### Shear resistance, y-y - Part 1-1:6.2.6, 6.2.8

LC: egon, x = 0 mm

Class<sub>N</sub> = 3; Class<sub>My</sub> = 1; Class<sub>Mz</sub> = 1;

$$V_{y,pl,Rd} = \frac{A_{y,v} f_y}{\sqrt{3} V_{M0}} = \frac{6779 \cdot 235}{1.73 \cdot 1.10} = 836.09 \text{ kN} \quad (6.18)$$

$$V_{y,pl,T,Rd} = \sqrt{1 - \frac{T_{t,Ed}}{1.25 (f_y \sqrt{3}) / V_{M0}}} V_{y,pl,Rd} = \sqrt{1 - \frac{100.18}{1.25 \cdot (235/1.73)/1.10}} \cdot 836.09 = 494.80 \text{ kN} \quad (6.26)$$

$$\frac{V_{y,Ed}}{V_{y,pl,T,Rd}} = \frac{0.00}{494.80} = 0.00 \leq 1.0 \quad (6.25) - \text{OK}$$

Project		Scale	
Description		File name	
Designer		Date/Time	
Signature		Comments	
FEM-Design Educational Version. For non-commercial use only! FEM-Design 14 Educational version - © StruSoft			page : 1

Figure A.13: FEM-Design - Detailed results - Torsionally simply supported beam

## [FEM-Design detailed results - Torsionally simply supported beam - Page 2]

**Shear resistance, z-z - Part 1-1:6.2.6, 6.2.8**

LC: egon, x = 0 mm

Class<sub>N</sub> = 3; Class<sub>My</sub> = 1; Class<sub>Mz</sub> = 1;

$$V_{z,pl,Rd} = \frac{A_z v_f}{\sqrt{3} V_{MO}} = \frac{5987 \cdot 235}{1.73 \cdot 1.10} = 738.50 \text{ kN} \quad (6.18)$$

$$V_{z,pl,T,Rd} = \sqrt{1 - \frac{T_{t,Ed}}{1.25(f_y/\sqrt{3})/V_{MO}}} V_{z,pl,Rd} = \sqrt{1 - \frac{100.18}{1.25 \cdot (235/1.73)/1.10}} \cdot 738.50 = 437.05 \text{ kN} \quad (6.26)$$

$$\frac{V_{z,Ed}}{V_{z,pl,T,Rd}} = \frac{0.00}{437.05} = 0.00 \leq 1.0 \quad (6.25) - \text{OK}$$

**Torsional resistance - Part 1-1:6.2.7**

LC: egon, x = 0 mm

Class<sub>N</sub> = 3; Class<sub>My</sub> = 1; Class<sub>Mz</sub> = 1;

$$\frac{T_{Ed}}{T_{Rd}} = \frac{3.50}{4.31} = 0.81 \leq 1.0 \quad (6.23) - \text{OK}$$

**Shear stress - Part 1-1:6.2.6**

Not relevant

**Normal stress - Part 1-1:6.2.1**

Not relevant

**Normal capacity - Part 1-1:6.2.1**

LC: egon, x = 0 mm

Class<sub>N</sub> = 3; Class<sub>My</sub> = 1; Class<sub>Mz</sub> = 1;

$$V_{y,Ed} \leq 0.5V_{y,pl,T,Rd} \rightarrow \rho_y = 0.0$$

$$V_{z,Ed} \leq 0.5V_{z,pl,T,Rd} \rightarrow \rho_z = 0.0$$

$$\frac{N_{Ed}}{N_{Rd}} + \frac{M_{y,Ed}}{M_{y,Rd}} + \frac{M_{z,Ed}}{M_{z,Rd}} = \frac{0.00}{2467.96} + \frac{0.00}{468.74} + \frac{0.00}{71.81} = 0.00 \leq 1.0 \quad (6.2) - \text{OK}$$

Project		Scale	
Description		File name	
Designer		Date/Time	
Signature		Comments	
FEM-Design Educational Version. For non-commercial use only! FEM-Design 14 Educational version - © StruSoft			page : 2

## [FEM-Design detailed results - Torsionally simply supported beam - Page 3]

**Flexural buckling, 1-1 - Part 1-1:6.3.1**

LC: egon, x = 0 mm

Class<sub>N</sub> = 3; Class<sub>My</sub> = 1; Class<sub>Mz</sub> = 1;

$$\bar{\lambda}_1 = \frac{L_{cr,1}}{i_1 \lambda_1} = \frac{6000}{204 \cdot 93.90} = 0.31 \quad (6.50)$$

 $\alpha_1 = 0.21$  (Buckling curve: a)

$$\varphi_1 = 0.5 \left[ 1 + \alpha_1 (\bar{\lambda}_1 - 0.2) + \bar{\lambda}_1^2 \right] = 0.5 \left[ 1 + 0.21 (0.31 - 0.2) + 0.31^2 \right] = 0.56$$

$$\chi_1 = \min \left( \frac{1}{\varphi_1 + \sqrt{\varphi_1^2 - \bar{\lambda}_1^2}}, 1.0 \right) = \min \left( \frac{1}{0.56 + \sqrt{0.56^2 - 0.31^2}}, 1.0 \right) = 0.97 \quad (6.49)$$

$$N_{b,Rd,1} = \frac{\chi_1 A f_y}{\gamma_{M1}} = \frac{0.97 \cdot 11552 \cdot 235}{1.20} = 2204.56 \text{ kN} \quad (6.47)$$

$$\frac{N_{Ed}}{N_{b,Rd,1}} = \frac{0.00}{2204.56} = 0.00 \leq 1.0 \quad (6.46) \text{ - OK}$$

**Flexural buckling, 2-2 - Part 1-1:6.3.1**

LC: egon, x = 0 mm

Class<sub>N</sub> = 3; Class<sub>My</sub> = 1; Class<sub>Mz</sub> = 1;

$$\bar{\lambda}_2 = \frac{L_{cr,2}}{i_2 \lambda_1} = \frac{6000}{43 \cdot 93.90} = 1.48 \quad (6.50)$$

 $\alpha_2 = 0.34$  (Buckling curve: b)

$$\varphi_2 = 0.5 \left[ 1 + \alpha_2 (\bar{\lambda}_2 - 0.2) + \bar{\lambda}_2^2 \right] = 0.5 \left[ 1 + 0.34 (1.48 - 0.2) + 1.48^2 \right] = 1.82$$

$$\chi_2 = \min \left( \frac{1}{\varphi_2 + \sqrt{\varphi_2^2 - \bar{\lambda}_2^2}}, 1.0 \right) = \min \left( \frac{1}{1.82 + \sqrt{1.82^2 - 1.48^2}}, 1.0 \right) = 0.35 \quad (6.49)$$

$$N_{b,Rd,2} = \frac{\chi_2 A f_y}{\gamma_{M1}} = \frac{0.35 \cdot 11552 \cdot 235}{1.20} = 787.69 \text{ kN} \quad (6.47)$$

$$\frac{N_{Ed}}{N_{b,Rd,2}} = \frac{0.00}{787.69} = 0.00 \leq 1.0 \quad (6.46) \text{ - OK}$$

Project		Scale	
Description		File name	
Designer		Date/Time	
Signature		Comments	
FEM-Design Educational Version. For non-commercial use only! FEM-Design 14 Educational version - © StruSoft			page : 3

## [FEM-Design detailed results - Torsionally simply supported beam - Page 4]

**Torsional-flexural buckling - Part 1-1:6.3.1**

LC: egon, x = 0 mm

Class<sub>N</sub> = 3; Class<sub>My</sub> = 1; Class<sub>Mz</sub> = 1;

$$i_0^2 = i_1^2 + i_2^2 + y_0^2 + z_0^2 = 204^2 + 43^2 + 0^2 + 0^2 = 43576 \text{ mm}^2$$

$$N_{cr,T} = \frac{1}{i_0^2} \left( G I_t + \frac{\pi^2 E I_w}{l_T^2} \right) = \frac{1}{43576} \left( 80769 \cdot 8.863e+05 + \frac{\pi^2 210000 \cdot 1.235e+12}{6.00^2} \right) = 3274.90 \text{ kN}$$

$$i_0^2 (N - N_{b,Rd,1}) (N - N_{b,Rd,2}) (N - N_{cr,T}) - N^2 y_0^2 (N - N_{b,Rd,2}) - N^2 z_0^2 (N - N_{b,Rd,1}) = 0$$

Smallest root of the above equation:  $N_{cr,TF} = 3274.90 \text{ kN}$ 

$$N_{cr} = \min(N_{cr,T}, N_{cr,TF}) = \min(3274.90, 3274.90) = 3274.90 \text{ kN}$$

$$\bar{\lambda}_T = \sqrt{\frac{A \lambda_T}{N_{cr}}} = \sqrt{\frac{11552 \cdot 93.90}{3274.90}} = 0.91 \quad (6.53)$$

$$\alpha_T = 0.34 \quad (\text{Buckling curve: b})$$

$$\varphi_T = 0.5 \left[ 1 + \alpha_T (\bar{\lambda}_T - 0.2) + \bar{\lambda}_T^2 \right] = 0.5 \left[ 1 + 0.34 (0.91 - 0.2) + 0.91^2 \right] = 1.04$$

$$\chi_T = \min \left( \frac{1}{\varphi_T + \sqrt{\varphi_T^2 - \bar{\lambda}_T^2}}, 1.0 \right) = \min \left( \frac{1}{1.04 + \sqrt{1.04^2 - 0.91^2}}, 1.0 \right) = 0.65 \quad (6.49)$$

$$N_{b,Rd,T} = \frac{\chi_T A f_y}{\gamma_{M1}} = \frac{0.65 \cdot 11552 \cdot 235}{1.20} = 1480.55 \text{ kN} \quad (6.47)$$

$$\frac{N_{Ed}}{N_{b,Rd,T}} = \frac{0.00}{1480.55} = -0.00 \leq 1.0 \quad (6.46) - \text{OK}$$

**Lateral torsional buckling, y-y - Part 1-1:6.3.2.4**

LC: egon, x = 0 mm

Class<sub>N</sub> = 3; Class<sub>My</sub> = 1; Class<sub>Mz</sub> = 1;

$$\bar{\lambda}_{f,y} = \frac{k_c L_c}{i_{f,2} \lambda_1} = \frac{0.94 \cdot 6000}{52 \cdot 93.90} = 1.15 \quad (6.59)$$

$$\alpha_y = 0.49 \quad (\text{Buckling curve: c})$$

$$\varphi_y = 0.5 \left[ 1 + \alpha_y (\bar{\lambda}_{f,y} - 0.2) + \bar{\lambda}_{f,y}^2 \right] = 0.5 \left[ 1 + 0.49 (1.15 - 0.2) + 1.15^2 \right] = 1.40$$

$$\chi_y = \min \left( \frac{1}{\varphi_y + \sqrt{\varphi_y^2 - \bar{\lambda}_{f,y}^2}}, 1.0 \right) = \min \left( \frac{1}{1.40 + \sqrt{1.40^2 - 1.15^2}}, 1.0 \right) = 0.46 \quad (6.49)$$

$$M_{y,c,Rd} = W_{yy} \frac{f_y}{\gamma_{M1}} = 2194113 \cdot \frac{235}{1.20} = 429.68 \text{ kNm}$$

$$M_{y,b,Rd} = \min(k_{\eta} \chi_y M_{y,c,Rd}, M_{y,c,Rd}) = \min(1.10 \cdot 0.46 \cdot 429.68, 429.68) = 216.22 \text{ kNm} \quad (6.60)$$

$$\frac{M_{y,Ed}}{M_{y,b,Rd}} = \frac{0.00}{216.22} = 0.00 \leq 1.0 \quad (6.54) - \text{OK}$$

Project		Scale	
Description		File name	
Designer		Date/Time	
Signature		Comments	
FEM-Design Educational Version. For non-commercial use only! FEM-Design 14 Educational version - © StruSoft			page : 4

[FEM-Design detailed results - Torsionally simply supported beam - Page 5]

**Lateral torsional buckling, z-z - Part 1-1:6.3.2.4**

Not relevant

**Interaction between normal force and bending 1. - Part 1-1:6.3.3**

Not relevant

**Interaction between normal force and bending 2. - Part 1-1:6.3.3**

Not relevant

**Interaction between normal force and bending, 2nd order - Part 1-1:6.3.3**

Not relevant

**Shear buckling - Part 1-5:5**

Not relevant

**Summary**



Project		Scale	
Description		File name	
Designer		Date/Time	
Signature		Comments	
FEM-Design Educational Version. For non-commercial use only! FEM-Design 14 Educational version - © StruSoft			page : 5

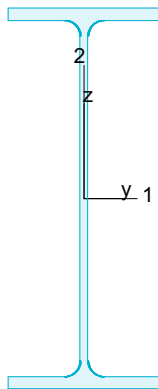
[FEM-Design detailed results - Fixed supported beam - Page 1]

### B.1.1 Maximum of load combinations

#### S 235

E	=	210000 N/mm <sup>2</sup>		
G	=	80769 N/mm <sup>2</sup>		
Y <sub>M0,ult</sub>	=	1.10	Y <sub>M0,acc./seis</sub>	= 1.00
Y <sub>M1,ult</sub>	=	1.20	Y <sub>M1,acc./seis</sub>	= 1.00
Y <sub>M2,ult</sub>	=	1.35	Y <sub>M2,acc./seis</sub>	= 1.00

#### IPE 500



A	=	11552 mm <sup>2</sup>	f <sub>y</sub>	= 235 N/mm <sup>2</sup>
I <sub>y</sub>	=	4.820e+08 mm <sup>4</sup>	ε	= 1.00
I <sub>z</sub>	=	2.142e+07 mm <sup>4</sup>	λ <sub>1</sub>	= 93.90
I <sub>1</sub>	=	4.820e+08 mm <sup>4</sup>		
I <sub>2</sub>	=	2.142e+07 mm <sup>4</sup>		
W <sub>pl,y</sub>	=	2.194e+06 mm <sup>3</sup>		
W <sub>pl,z</sub>	=	3.361e+05 mm <sup>3</sup>		
W <sub>el,min,y</sub>	=	1.928e+06 mm <sup>3</sup>		
W <sub>el,min,z</sub>	=	2.142e+05 mm <sup>3</sup>		
i <sub>1</sub>	=	204 mm		
i <sub>2</sub>	=	43 mm		
I <sub>t</sub>	=	8.863e+05 mm <sup>4</sup>		
I <sub>w</sub>	=	1.235e+12 mm <sup>6</sup>		

#### Shear resistance, y-y - Part 1-1:6.2.6, 6.2.8

LC: egon, x = 0 mm

Class<sub>N</sub> = 3; Class<sub>My</sub> = 1; Class<sub>Mz</sub> = 1;

$$V_{y,pl,Rd} = \frac{A_{y,v} f_y}{\sqrt{3} Y_{M0}} = \frac{6779 \cdot 235}{1.73 \cdot 1.10} = 836.09 \text{ kN} \quad (6.18)$$

$$V_{y,pl,T,Rd} = \sqrt{1 - \frac{T_{t,Ed}}{1.25 (f_y / \sqrt{3}) / Y_{M0}}} V_{y,pl,Rd} = \sqrt{1 - \frac{100.18}{1.25 \cdot (235/1.73)/1.10}} \cdot 836.09 = 494.80 \text{ kN} \quad (6.26)$$

$$\frac{V_{y,Ed}}{V_{y,pl,T,Rd}} = \frac{0.00}{494.80} = 0.00 \leq 1.0 \quad (6.25) - \text{OK}$$

Project		Scale	
Description		File name	
Designer		Date/Time	
Signature		Comments	
FEM-Design Educational Version. For non-commercial use only! FEM-Design 14 Educational version - © StruSoft			page : 1

Figure A.14: FEM-Design - Detailed results of fixed supported beam.

## [FEM-Design detailed results - Fixed supported beam - Page 2]

**Shear resistance, z-z - Part 1-1:6.2.6, 6.2.8**

LC: egon, x = 0 mm

Class<sub>N</sub> = 3; Class<sub>My</sub> = 1; Class<sub>Mz</sub> = 1;

$$V_{z,pl,Rd} = \frac{A_{z,v} f_v}{\sqrt{3} Y_{M0}} = \frac{5987 \cdot 235}{1.73 \cdot 1.10} = 738.50 \text{ kN} \quad (6.18)$$

$$V_{z,pl,T,Rd} = \sqrt{1 - \frac{T_{f,Ed}}{1.25 (f_y / \sqrt{3}) / Y_{M0}}} V_{z,pl,Rd} = \sqrt{1 - \frac{100.18}{1.25 \cdot (235 / 1.73) / 1.10}} \cdot 738.50 = 437.05 \text{ kN} \quad (6.26)$$

$$\frac{V_{z,Ed}}{V_{z,pl,T,Rd}} = \frac{0.00}{437.05} = 0.00 \leq 1.0 \quad (6.25) - \text{OK}$$

**Torsional resistance - Part 1-1:6.2.7**

LC: egon, x = 0 mm

Class<sub>N</sub> = 3; Class<sub>My</sub> = 1; Class<sub>Mz</sub> = 1;

$$\frac{T_{Ed}}{T_{Rd}} = \frac{3.50}{4.31} = 0.81 \leq 1.0 \quad (6.23) - \text{OK}$$

**Shear stress - Part 1-1:6.2.6**

Not relevant

**Normal stress - Part 1-1:6.2.1**

Not relevant

**Normal capacity - Part 1-1:6.2.1**

LC: egon, x = 0 mm

Class<sub>N</sub> = 3; Class<sub>My</sub> = 1; Class<sub>Mz</sub> = 1;

$$V_{y,Ed} \leq 0.5 V_{y,pl,T,Rd} \rightarrow \rho_y = 0.0$$

$$V_{z,Ed} \leq 0.5 V_{z,pl,T,Rd} \rightarrow \rho_z = 0.0$$

$$\frac{N_{Ed}}{N_{Rd}} + \frac{M_{y,Ed}}{M_{y,Rd}} + \frac{M_{z,Ed}}{M_{z,Rd}} = \frac{0.00}{2467.96} + \frac{0.00}{468.74} + \frac{0.00}{71.81} = 0.00 \leq 1.0 \quad (6.2) - \text{OK}$$

Project		Scale	
Description		File name	
Designer		Date/Time	
Signature		Comments	
FEM-Design Educational Version. For non-commercial use only! FEM-Design 14 Educational version - © StruSoft			page : 2

## [FEM-Design detailed results - Fixed supported beam - Page 3]

**Flexural buckling, 1-1 - Part 1-1:6.3.1**

LC: egon, x = 0 mm

Class<sub>N</sub> = 3; Class<sub>M<sub>y</sub></sub> = 1; Class<sub>M<sub>z</sub></sub> = 1;

$$\bar{\lambda}_1 = \frac{L_{cr,1}}{i_1 \lambda_1} = \frac{6000}{204 \cdot 93.90} = 0.31 \quad (6.50)$$

 $\alpha_1 = 0.21$  (Buckling curve: a)

$$\varphi_1 = 0.5 \left[ 1 + \alpha_1 (\bar{\lambda}_1 - 0.2) + \bar{\lambda}_1^2 \right] = 0.5 \left[ 1 + 0.21 (0.31 - 0.2) + 0.31^2 \right] = 0.56$$

$$\chi_1 = \min \left( \frac{1}{\varphi_1 + \sqrt{\varphi_1^2 - \bar{\lambda}_1^2}}, 1.0 \right) = \min \left( \frac{1}{0.56 + \sqrt{0.56^2 - 0.31^2}}, 1.0 \right) = 0.97 \quad (6.49)$$

$$N_{b,Rd,1} = \frac{\chi_1 A_f}{Y_{M1}} = \frac{0.97 \cdot 11552 \cdot 235}{1.20} = 2204.56 \text{ kN} \quad (6.47)$$

$$\frac{N_{Ed}}{N_{b,Rd,1}} = \frac{0.00}{2204.56} = 0.00 \leq 1.0 \quad (6.46) - \text{OK}$$

**Flexural buckling, 2-2 - Part 1-1:6.3.1**

LC: egon, x = 0 mm

Class<sub>N</sub> = 3; Class<sub>M<sub>y</sub></sub> = 1; Class<sub>M<sub>z</sub></sub> = 1;

$$\bar{\lambda}_2 = \frac{L_{cr,2}}{i_2 \lambda_1} = \frac{6000}{43 \cdot 93.90} = 1.48 \quad (6.50)$$

 $\alpha_2 = 0.34$  (Buckling curve: b)

$$\varphi_2 = 0.5 \left[ 1 + \alpha_2 (\bar{\lambda}_2 - 0.2) + \bar{\lambda}_2^2 \right] = 0.5 \left[ 1 + 0.34 (1.48 - 0.2) + 1.48^2 \right] = 1.82$$

$$\chi_2 = \min \left( \frac{1}{\varphi_2 + \sqrt{\varphi_2^2 - \bar{\lambda}_2^2}}, 1.0 \right) = \min \left( \frac{1}{1.82 + \sqrt{1.82^2 - 1.48^2}}, 1.0 \right) = 0.35 \quad (6.49)$$

$$N_{b,Rd,2} = \frac{\chi_2 A_f}{Y_{M1}} = \frac{0.35 \cdot 11552 \cdot 235}{1.20} = 787.69 \text{ kN} \quad (6.47)$$

$$\frac{N_{Ed}}{N_{b,Rd,2}} = \frac{0.00}{787.69} = 0.00 \leq 1.0 \quad (6.46) - \text{OK}$$

Project		Scale	
Description		File name	
Designer		Date/Time	
Signature		Comments	

## [FEM-Design detailed results - Fixed supported beam - Page 4]

**Torsional-flexural buckling - Part 1-1:6.3.1**

LC: egon, x = 0 mm

Class<sub>N</sub> = 3; Class<sub>M<sub>y</sub></sub> = 1; Class<sub>M<sub>z</sub></sub> = 1;

$$i_0^2 = i_1^2 + i_2^2 + y_0^2 + z_0^2 = 204^2 + 43^2 + 0^2 + 0^2 = 43576 \text{ mm}^2$$

$$N_{cr,T} = \frac{1}{i_0^2} \left( G I_t + \frac{\pi^2 E I_w}{l_T^2} \right) = \frac{1}{43576} \left( 80769 \cdot 8.863e+05 + \frac{\pi^2 210000 \cdot 1.235e+12}{6.00^2} \right) = 3274.90 \text{ kN}$$

$$i_0^2 (N - N_{b,Rd,1}) (N - N_{b,Rd,2}) (N - N_{cr,T}) - N^2 y_0^2 (N - N_{b,Rd,2}) - N^2 z_0^2 (N - N_{b,Rd,1}) = 0$$

Smallest root of the above equation:  $N_{cr,TF} = 3274.90$  kN

$$N_{cr} = \min(N_{cr,T}, N_{cr,TF}) = \min(3274.90, 3274.90) = 3274.90 \text{ kN}$$

$$\bar{\lambda}_T = \sqrt{\frac{A \lambda_1}{N_{cr}}} = \sqrt{\frac{11552 \cdot 93.90}{3274.90}} = 0.91 \quad (6.53)$$

 $\alpha_T = 0.34$  (Buckling curve: b)

$$\varphi_T = 0.5 \left[ 1 + \alpha_T (\bar{\lambda}_T - 0.2) + \bar{\lambda}_T^2 \right] = 0.5 \left[ 1 + 0.34 (0.91 - 0.2) + 0.91^2 \right] = 1.04$$

$$\chi_T = \min \left( \frac{1}{\varphi_T + \sqrt{\varphi_T^2 - \bar{\lambda}_T^2}}, 1.0 \right) = \min \left( \frac{1}{1.04 + \sqrt{1.04^2 - 0.91^2}}, 1.0 \right) = 0.65 \quad (6.49)$$

$$N_{b,Rd,T} = \frac{\chi_T A f_y}{\gamma_{M1}} = \frac{0.65 \cdot 11552 \cdot 235}{1.20} = 1480.55 \text{ kN} \quad (6.47)$$

$$\frac{N_{Ed}}{N_{b,Rd,T}} = \frac{0.00}{1480.55} = -0.00 \leq 1.0 \quad (6.46) - \text{OK}$$

**Lateral torsional buckling, y-y - Part 1-1:6.3.2.4**

LC: egon, x = 0 mm

Class<sub>N</sub> = 3; Class<sub>M<sub>y</sub></sub> = 1; Class<sub>M<sub>z</sub></sub> = 1;

$$\bar{\lambda}_{f,y} = \frac{k_c L_c}{i_{f,z} \lambda_1} = \frac{0.94 \cdot 6000}{52 \cdot 93.90} = 1.15 \quad (6.59)$$

 $\alpha_y = 0.49$  (Buckling curve: c)

$$\varphi_y = 0.5 \left[ 1 + \alpha_y (\bar{\lambda}_{f,y} - 0.2) + \bar{\lambda}_{f,y}^2 \right] = 0.5 \left[ 1 + 0.49 (1.15 - 0.2) + 1.15^2 \right] = 1.40$$

$$\chi_y = \min \left( \frac{1}{\varphi_y + \sqrt{\varphi_y^2 - \bar{\lambda}_{f,y}^2}}, 1.0 \right) = \min \left( \frac{1}{1.40 + \sqrt{1.40^2 - 1.15^2}}, 1.0 \right) = 0.46 \quad (6.49)$$

$$M_{y,c,Rd} = W_{yM1} \frac{f_y}{\gamma_{M1}} = 2194113 \cdot \frac{235}{1.20} = 429.68 \text{ kNm}$$

$$M_{y,b,Rd} = \min(k_{fl} \chi_y M_{y,c,Rd}, M_{y,c,Rd}) = \min(1.10 \cdot 0.46 \cdot 429.68, 429.68) = 216.22 \text{ kNm} \quad (6.60)$$

$$\frac{M_{y,Ed}}{M_{y,b,Rd}} = \frac{0.00}{216.22} = 0.00 \leq 1.0 \quad (6.54) - \text{OK}$$

Project		Scale	
Description		File name	
Designer		Date/Time	
Signature		Comments	
FEM-Design Educational Version. For non-commercial use only! FEM-Design 14 Educational version - © StruSoft			page : 4

[FEM-Design detailed results - Fixed supported beam - Page 5]

**Lateral torsional buckling, z-z - Part 1-1:6.3.2.4**

Not relevant

**Interaction between normal force and bending 1. - Part 1-1:6.3.3**

Not relevant

**Interaction between normal force and bending 2. - Part 1-1:6.3.3**

Not relevant

**Interaction between normal force and bending, 2nd order - Part 1-1:6.3.3**

Not relevant

**Shear buckling - Part 1-5:5**

Not relevant

**Summary**



Project		Scale	
Description		File name	
Designer		Date/Time	
Signature		Comments	

## B Shell- and solid model comparison

---

Despite the shell model presented in the main report, a solid model is established and the normal stresses are compared in order to clarify, no errors are made by neglecting the third dimension. The results are very similar and both the shell and the solid model results deviate from the home-made MATLAB program results of the normal stresses, as seen in figure B.1.

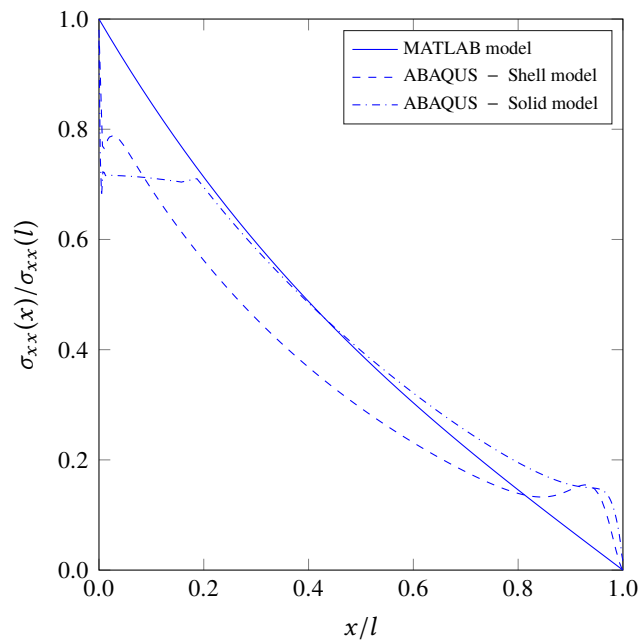


**Figure B.1:** Comparison of normal stresses in a shell and solid model along with the home-made MATLAB program.

It should be noticed, the normal stresses from the solid model actually follows the home-made MATLAB program normal stresses in the range  $0.2l - 0.7l$  but deviates a lot at the fixed support and just before the free end of the cantilever beam, similar to the shell model.



# C von Mises Criterion

---

The von Mises criterion is a very often used material model to describe the stress state of metals and steel [Ottosen and Ristinmaa, 2005]. The hydrostatic stress  $I_1$  has no influence on the yielding and a general expression for the yield criteria can be summarized as

$$\sqrt{3J_2} - f_y = 0, \quad (\text{C.1})$$

where  $J_2$  is the second deviatoric stress invariant and  $f_y$  is the yield strength of steel in uniaxial tension. In terms of principle stresses (C.1) becomes

$$\sqrt{\frac{1}{2} \left( (\sigma_1 - \sigma_2)^2 + (\sigma_2 - \sigma_3)^2 + (\sigma_3 - \sigma_1)^2 \right)} - f_y = 0, \quad (\text{C.2})$$

or in the general case as

$$\sqrt{\frac{1}{2} \left( (\sigma_{xx} - \sigma_{yy})^2 + (\sigma_{yy} - \sigma_{zz})^2 + (\sigma_{zz} - \sigma_{xx})^2 \right) + 6 \left( \sigma_{xy}^2 + \sigma_{yz}^2 + \sigma_{xz}^2 \right)} - f_y = 0. \quad (\text{C.3})$$



# D Exact Non-Homogeneous Shape Functions

---

The exact shape functions describing the rotation  $\theta_x(x)$  throughout the beam length by interpolating nodal values of  $\theta_{x,j}$  and  $\theta'_{x,j}$  for  $j = 1, 2$  are:

$$\phi_7(x) = \frac{k(x-l)\sinh kl + \cosh(k(l-x)) + \cosh kl - \cosh kx - 1}{2(1 - \cosh kl) + kl \sinh kl} \quad (\text{D.1a})$$

$$\phi_8(x) = \frac{1}{k(2(1 - \cosh kl) + kl \sinh kl)} \left( ((l-x)k - kl \cosh kx - \sinh kx) \cdot \cosh kl + (\cosh kx + kl \sinh kx - 1) \sinh kl + \sinh kx + kx \right) \quad (\text{D.1b})$$

$$\phi_9(x) = \frac{(\cosh kx - 1) \cosh kl + (kx - \sinh kx) \sinh kl - \cosh kx + 1}{2(1 - \cosh kl) + kl \sinh kl} \quad (\text{D.1c})$$

$$\phi_{10}(x) = \frac{1}{k(2(1 - \cosh kl) + kl \sinh kl)} \left( (\sinh kx - kx) \cosh kl + (kl - \sinh kl) \cosh kx + \sinh kl - \sinh kx + (x-l)k \right) \quad (\text{D.1d})$$